AMRL-TR-64-117

MEASUREMENTS AND MODELS FOR RELATING THE PHYSICAL CHARACTERISTICS OF IMAGES TO TARGET DETECTION

DONALD G. CORBETT
N. D. DIAMANTIDES
R. H. KAUSE

GOODYEAR AEROSPACE CORPORATION

DECEMBER 1964

BEHAVIORAL SCIENCES LABORATORY
AEROSPACE MEDICAL RESEARCH LABORATORIES
AEROSPACE MEDICAL DIVISION
AIR FORCE SYSTEMS COMMAND
WRIGHT-PATTERSON AIR FORCE BASE, OHIO

NOTICES

When US Government drawings, specifications, or other data are used for any purpose other than a definitely related Government procurement operation, the Government thereby incurs no responsibility nor any obligation whatsoever, and the fact that the Government may have formulated, furnished, or in any way supplied the said drawings, specifications, or other data, is not to be regarded by implication or otherwise, as in any manner licensing the holder or any other person or corporation, or conveying any rights or permission to manufacture, use, or sell any patented invention that may in any way be related thereto.

Qualified requesters may obtain copies from the Defense Documentation Center (DDC), Cameron Station, Alexandria, Virginia 22314. Orders will be expedited if placed through the librarian or other person designated to request documents from DDC (formerly ASTIA).

Stock quantities available, for sale to the public, from:

Chief, Input Section
Clearinghouse for Federal Scientific and Technical Information, CFSTI
Sills Building
5285 Port Royal Road
Springfield, Virginia 22151

Change of Address

Organizations and individuals receiving reports via the Aerospace Medical Research Laboratories' automatic mailing lists should submit the addressograph plate stamp on the report envelope or refer to the code number when corresponding about change of address or cancellation.

Do not return this copy. Retain or destroy.

900 - January 1965 - 448-24-546

MEASUREMENTS AND MODELS FOR RELATING THE PHYSICAL CHARACTERISTICS OF IMAGES TO TARGET DETECTION

DONALD G. CORBETT
N. D. DIAMANTIDES
R. H. KAUSE

FOREWORD

This study was initiated by the Behavioral Sciences Laboratory of the Aerospace Medical Research Laboratories, Aerospace Medical Division, Wright-Patterson Air Force Base, Ohio, and conducted by Goodyear Aerospace Corporation of Akron, Ohio, under Contract AF33(657)-9476. Donald G. Corbett, N. D. Diamantides and R. H. Kause were the principal investigators for Goodyear Aerospace. Dr. H. C. Self of the Performance Requirements Branch, Human Engineering Division, was the contract monitor for the Behavioral Sciences Laboratory. The work was initiated by M. Rudov of the Behavioral Sciences Laboratory and was performed in support of the Advanced Technology Program 665A Reconnaissance/Strike. Research sponsored by this contract was started in July 1962 and was completed in September 1963.

This technical report has been reviewed and is approved.

WALTER F. GRETHER, PhD
Technical Director
Behavioral Sciences Laboratory

ABSTRACT

Three metrics for predicting the time required to identify targets in high-resolution radar pictures were developed. One metric, based on four automatically measured variables related to transmissivity of positive transparencies, was tested. Through multiple-regression analysis, a correlation of 0.69 between observed and predicted identification times was obtained. When these relationships were applied to a new set of radar pictures and new test subjects, the correlation coefficient was too low to be significantly different from zero with the number of pictures used. A principal reason for the low correlation was the unexpected correlation between the four transmissivity variables. The metric also had an insignificant correlation coefficient when applied to optical and infrared photographs (0.07 and 0.04, respectively). It is hypothesized that, if additional variables are utilized, the metric examined in this study may be useful as a base to develop a more effective prediction equation.

TABLE OF CONTENTS

LIST OF ILLUSTRATIONS

LIST OF TABLES

SECTION I

INTRODUCTION

The relationship of certain physical characteristics of radar pictures to the time required for humans to identify designated targets in these pictures was investigated. As used here, "target" means the radar return from a single object or combination of objects making up a small part of a relatively large radar picture containing many returns. The purpose was to express the relationship in a metric that would make it possible to predict target-identification times for similar radar pictures. A secondary purpose was to determine if the metric could be used to predict the time required for identification of targets in infrared and optical photographs.

This was an exploratory effort supporting the continuing research into the larger field of image interpretation. Eventually, establishment of the complete psychophysical relationship between quantitative measurements of picture content and human response could aid in the planning of reconnaissance-strike missions, and could contribute to the development of automatic equipment for identifying targets. However, the exploratory effort reported here was limited essentially to consideration of only the relative lightness and darkness, detail, and size of targets and their backgrounds. It did not include such target features as shapes and patterns or inferential cues that would be present in an operational reconnaissance-strike situation.

The departure from a more realistic situation was influenced in part by a requirement that the selected characteristics be measured automatically. To a large extent, these characteristics were chosen to reflect the stimulus complexity of the radar pictures. In this way, the experiment was not confounded by parameters of lesser interest to this particular study, or by those that could not be measured with state-of-the-art equipment.

The emphasis was on high-resolution (side-looking) radar pictures. All had the same general resolution, graininess, acutance, etc. The experiment consisted of the following general steps:

> Measurement of human target-identification times for a series of high-resolution radar pictures (section II)
>
> Measurement of certain physical characteristics of these pictures (section III)
>
> Relating these two sets of data mathematically in a metric to permit prediction of target-recognition times for similar pictures (section IV)
>
> Checking the validity of this metric with new pictures and new subjects (section V)
>
> Checking the applicability of the metric to infrared and optical photographs (section V)

The task required construction of a combined slide projector and viewer and of a flying spot scanner, programming of an analog computer to measure the

variations of the selected physical characteristics of the pictures, and use of a digital computer for data analysis.

Three prediction metrics were developed; only one was evaluated.

SECTION II

MEASUREMENT OF HUMAN PERFORMANCE

INTRODUCTION

The human response data required for generation of the prediction metric were recorded in identical experiments with 30 Strategic Air Command bomb-navigators, as discussed below. The other data required for the metric - measurements of physical characteristics of the pictures - are discussed in section III. To obtain sufficient subjects to make the data significant, the human response experiments were conducted at two SAC bases, Griffiss in New York (11 subjects) and Pease in New Hampshire (19 subjects).

The experiments were somewhat artificial, in that they were neither reconnaissance-strike nor image-interpretation tasks. In an operational situation, more information about a target, its surroundings, and its location would be given to the subject and thus he could use associational and inferential cues. For example, if a subject knew that the target were a dam, he would infer the presence of a lake and roads. However, the experiments did involve some of the perceptual factors inherent in reconnaissance-strike and image-interpretation tasks, such as target size and detail, and contrast with the background.

GENERAL PROCEDURE

The slide projector-viewer built under the contract was transported first to Griffiss and then to Pease. The subjects were trained to bring all to the same level of familiarity with high-resolution radar pictures to prevent contamination of the scores by learning acquired during the experiments. Each subject was trained individually for 1 hour. High-resolution and ppi radar pictures of the same areas recorded simultaneously by the same airplane on Air Force Quick-Check flights were used. Operational navigation charts of the same areas aided the interpretations. The increased resolution and different reflectance properties of the high-resolution radar pictures were emphasized. The differences between high-resolution and ppi displays of the following were cited: large cities, land-water boundaries, communication and transportation links in various terrains, geologic features and drainage patterns in mountainous areas, and small towns in flat and hilly terrain and in terrain confounded by the texture of vegetation. High-resolution radar pictures similar to those to be used in the tests were shown, and typical targets were pointed out.

Thirty targets and the 30 high-resolution pictures from which they had been extracted were used in the tests. These pictures also were obtained in Quick-Check flights. They were taken from 20,000-ft altitude; each covered an 18- by 18-nautical-mile ground area. Seven other similar targets and pictures were supplied for practice trials. All the test targets and pictures containing them were prepared on positive slides for use with the projector-viewer.

EXTRACTION OF TARGETS

One entity in each picture was designated a target. These were limited to airfields, industrial complexes, oil tank "farms," small towns, and military camps. The targets had the same size, pattern, orientation, and approximate

density as in the complete pictures. As such, they were pictorial briefing cues requiring no mental adjustments for locating them in the pictures. Human-dynamic and cybernetic studies suggest that a human is at his best when he functions in this way as a simple comparator (reference 1).

The targets were prepared by projecting a complete scene and tracing the selected target image on white paper. This drawing was transferred to a sheet of clear plastic and inked black or white depending on the predominant polarity of the target. The transparency was photographed against a neutral gray background at a distance calculated to make the projected target the same size as in the projection of the complete picture, and prepared on a 70-mm slide.

The targets were selected at random in respect to their positions within the pictures to prevent any display-position pattern that would have invalidated the results of the psychophysical experiments..

SLIDE PROJECTOR AND VIEWER

As shown in figure 1, the projector-viewer had three 12- by 12-in. screens arranged side by side. It contained two 70-mm slide projectors. One projected the target image on the left-hand screen at a magnification of 5.5. The other projected the slide of the entire radar scene on the center screen at the same 5.5 magnification, and a portion of the same slide on the right-hand screen at a magnification of 25; this was done through two channels as shown in figure 2.

The center image was formed at a set of cross hairs on a translating plate through a 127-mm f/5.6 lens, and projected onto the screen through a 180-mm f/4.5 lens. The right-hand image was formed at another set of cross hairs on the same translating plate, and projected onto the screen through a 50-mm f/2.3 lens. The plate was driven in the X and Y directions by servomechanisms controlled through an ASQ-28 tracking handle operated by the subject. When the plate was moved, the center-screen radar image remained stationary and the cross-hair image moved over it; on the right-hand screen, the cross-hair image remained stationary and the radar image moved. The center-screen cross hairs were used by the subject to indicate the target; the magnified image on the right-hand screen simplified the checking of the accuracy of the target identification. The cross-hair images were inserted in this fashion to ensure sharp focus and reduce parallax.

The projector-viewer was equipped with three electrical clocks to record the times consumed in studying the target, locating the target in the complete scene, and positioning the cross hairs over the target. A fourth clock measured the total time.

TEST SEQUENCE

The experimenter seated the subject at the projector-viewer in front of the three screens. The experimenter read a standard set of instructions to the subject (see appendix V). Seven practice trials were run. Then the experimenter projected the first test target on the left-hand screen, automatically starting the first clock.

Figure 1 - Slide Projector-Viewer

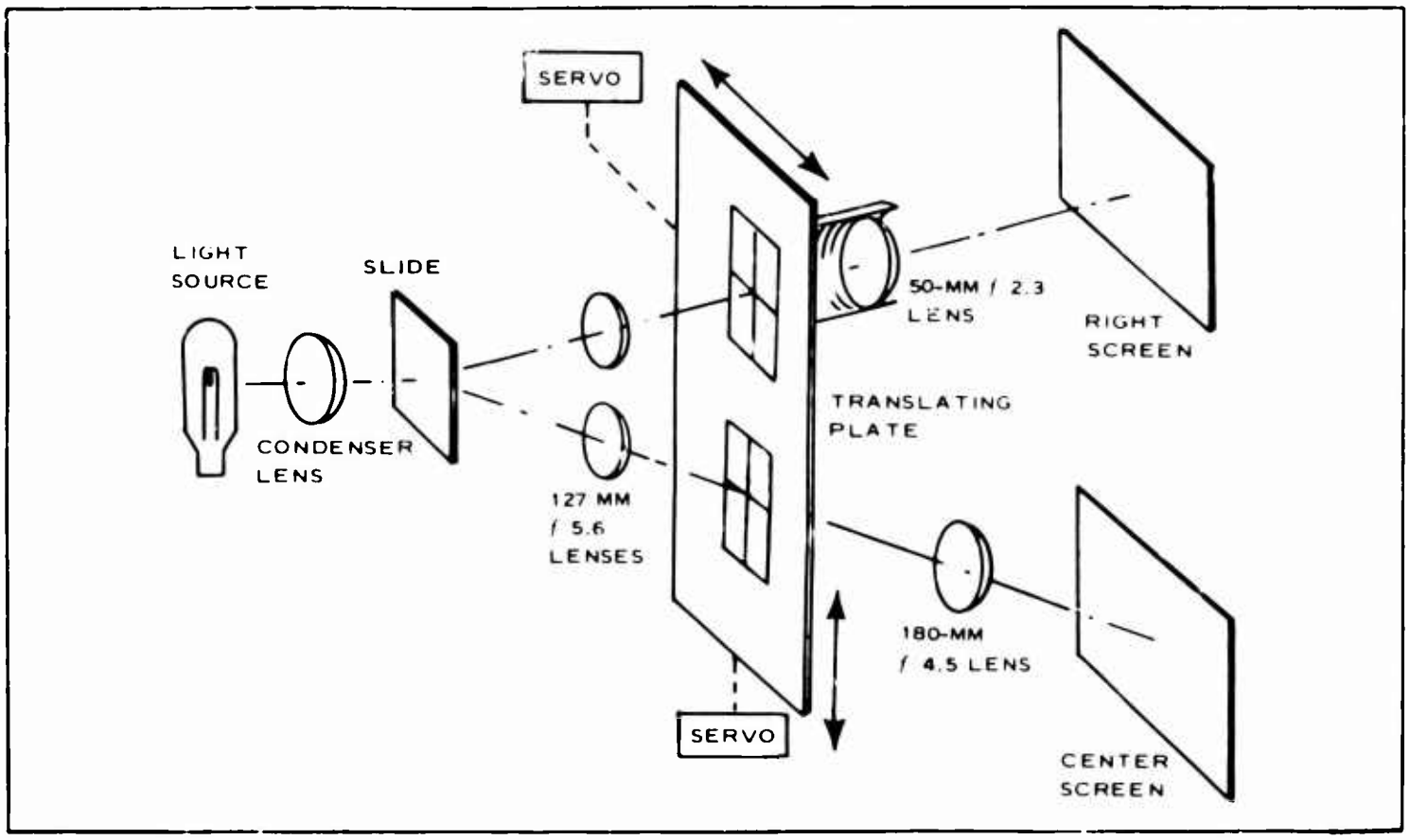

Figure 2 - Schematic of Projector-Viewer Center and Right-Hand Channels

The subject studied the target for as long as he desired. When he decided that he had memorized it, he said "Ready." The experimenter then projected the complete picture on the center screen, an action that simultaneously stopped the first clock and started the second. The target remained on the left-hand screen. The subject scanned the picture, and when he decided that he had found the target, he pressed a button. This stopped the second clock and illuminated the right-hand screen. The original target and complete picture remained on their respective screens. The subject positioned the center-screen cross hairs over the target he had identified and pressed a second button, stopping the third clock and completing the sequence. The accuracy of the identification was checked by means of the magnification on the right-hand screen.

The experimenter recorded the times and whether the target had been identified correctly, and reset the clocks. A maximum of 300 sec was allowed for locating the target (second clock), after which the response was scored as incorrect. The sequence was repeated for the remaining 29 targets and scenes. The slides were rearranged in a random sequence between each test series.

RESPONSE MEASUREMENTS

At the time of these human response experiments, there had been no decision as to what measurements would be used in formulating the prediction metric (section IV). To give a wide choice, the complete data were recorded as shown in table I. As it turned out, only the average recognition time for each slide was used. These medians are tabulated in the third column of table I, and plotted graphically in figure 3. Plate 21 is omitted from figure 3 because none of the subjects identified this target within the 300-sec time limit.

Because 30 plates and 30 subjects were used, the total correct and incorrect identifications would be expected to total 900. They total only 867 because plate 8 was found to be unsatisfactory after seven tests, and there were malfunctions in 26 other instances. One of the practice plates was substituted for the defective slide and designated plate 8b.

In figure 4, the plates are arranged in groups of five in the order in which they were viewed. The time required for recognition was about the same for plates 1 through 5, 11 through 15, and 21 through 25, and about the same for plates 6 through 10, 16 through 20, and 26 through 30. Thus, there was no indication that learning acquired during the tests affected the results.

TABLE I

ACTUAL TARGET-IDENTIFICATION TIMES, ORIGINAL RADAR PLATES

Plate	Identification time (sec)			Number correct	Percent correct	Number incorrect	Percent incorrect	Time to study target (sec)
	Mean	Median	Standard deviation					
19	4.8	5.0	1.4	28	93.3	2	6.7	6.9
3	5.1	4.5	1.8	30	100.0	0	0.0	8.6
16	6.6	5.0	3.6	28	93.3	2	6.7	9.7
10	7.2	6.0	3.9	30	100.0	0	0.0	9.3
18	7.7	6.0	6.0	29	96.7	1	3.3	8.7
4	8.1	6.0	5.7	28	96.6	1	3.4	8.7
23	8.8	6.0	6.7	30	100.0	0	0.0	8.9
14	9.8	5.0	8.5	30	100.0	0	0.0	7.3
7	10.1	6.0	9.0	29	96.7	1	3.3	10.7
17	10.8	6.5	9.2	30	100.0	0	0.0	7.3
25	12.3	12.0	7.7	21	84.0	4	16.0	9.9
30	14.7	10.0	13.4	27	90.0	3	10.0	12.2
15	16.8	11.0	14.2	23	92.0	2	8.0	9.2
20	18.4	11.5	17.3	20	66.7	10	33.3	10.7
24	19.3	7.5	20.4	22	75.9	7	24.1	11.5
27	19.7	17.0	15.3	18	60.0	12	40.0	6.2
5	20.7	9.0	29.5	28	93.3	2	6.7	7.2
9	20.8	15.5	19.7	26	86.7	4	13.3	9.2
28	24.4	14.0	33.8	27	90.0	3	10.0	9.5
26	26.2	21.0	26.7	25	83.3	5	16.7	8.9
13	30.4	23.0	30.7	27	96.4	1	3.6	10.5
11	34.3	26.0	31.8	21	72.4	8	27.6	9.2
12	37.9	36.0	20.9	14	60.9	9	39.1	10.6
8b	45.6	34.5	25.1	16	69.6	7	30.4	11.5
6	62.6	52.5	40.1	24	80.0	6	20.0	7.3
29	64.1	25.0	74.4	12	40.0	18	60.0	7.5
1	65.8	49.0	55.6	13	48.1	14	51.9	9.1
2	72.3	47.0	77.3	23	76.7	7	23.3	8.1
22	114	145.0	73.5	11	37.9	18	62.1	10.0
21	300	. . .	. . .	0	0.	30	100.0	11.3
All slides	36.64	21.46	23.55	690	78.35	117	21.65	9.2

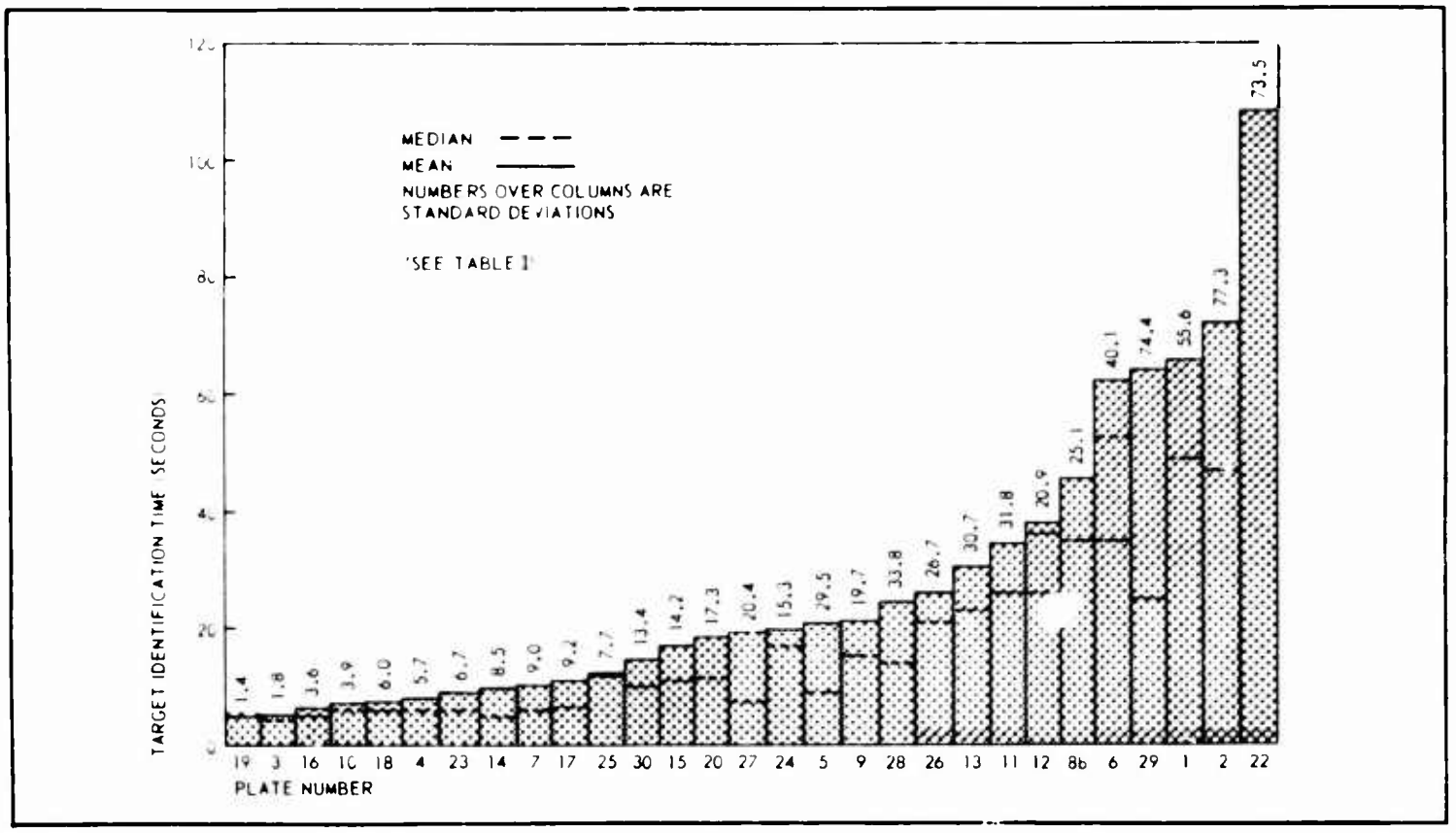

Figure 3 - Actual Target-Identification Times, Original Radar Plates

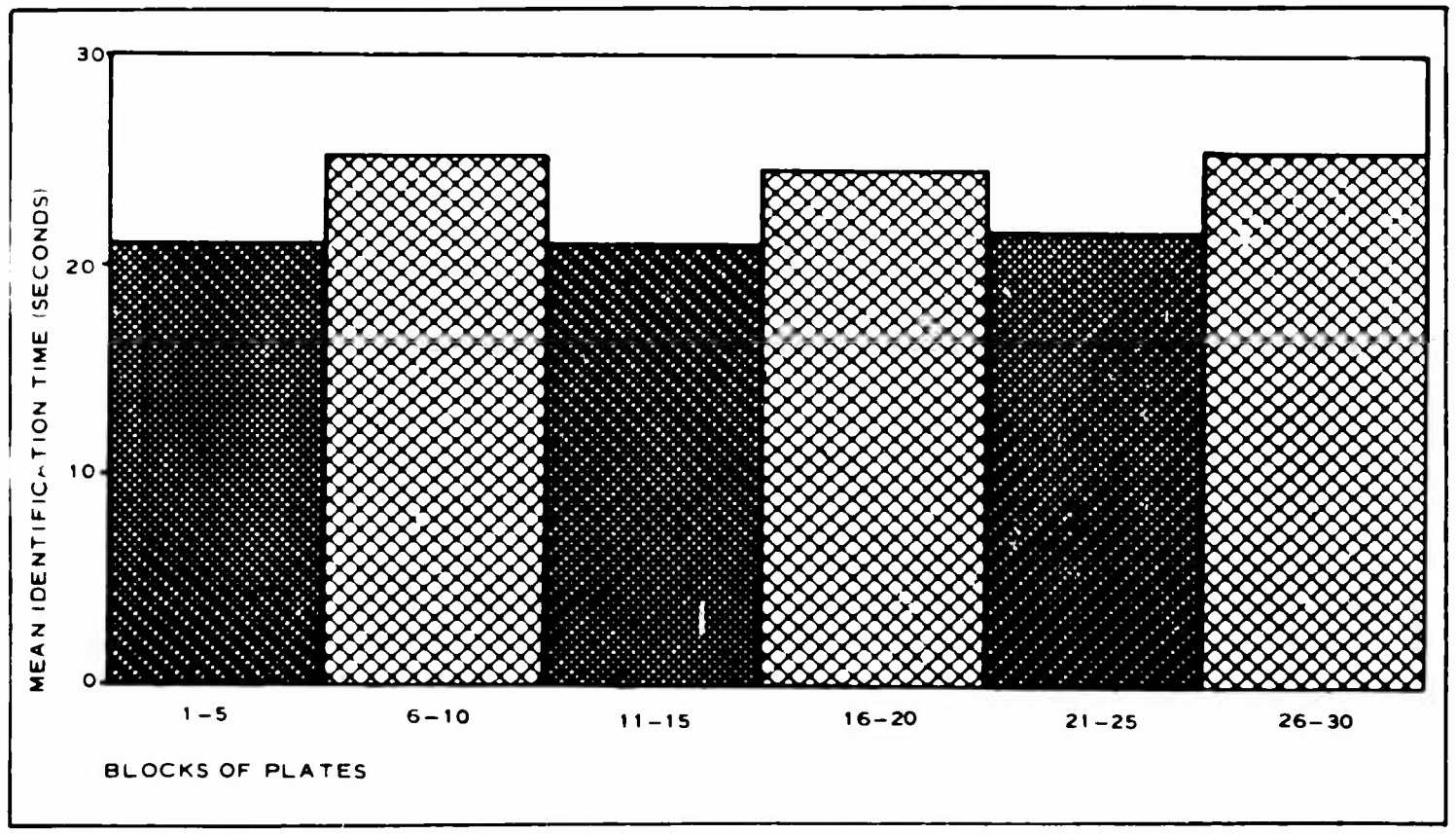

Figure 4 - Order of Presentation of Original Radar Plates versus Target-Identification Times

SECTION III

SELECTION AND MEASUREMENT OF PICTURE CHARACTERISTICS

INTRODUCTION

Duplicates of the positive plates of the high-resolution radar pictures used in the human response experiments were used to establish the other data required for the prediction metric - the measurements of the physical characteristics that were believed to influence the target-recognition times. The selection of these characteristics was based on many considerations. The number of possible indices of the characteristics was large, and it was reasonable to suppose that many would have low correlation with the human response data. The problem was to select characteristics that were believed to affect the target-finding performance and that could be measured automatically with instruments available under the contract. A further limitation required that such qualities as resolution, emulsion graininess, and acutance be ignored.

The detection of targets in high-resolution radar displays presents peculiar problems. Ground-range displays were used; because of the type of projection, these have more resemblance to topographic maps than to optical photographs. For example, objects the same distance apart on the ground appear at the same relevant distance apart on such radar displays, independent of how far away they are from the radar sensor; in optical photographs, of course, the farther the objects are from the camera, the closer together they appear on a picture. Also, the brightness of an object illuminated by radar is considerably different from that in ordinary photography. Furthermore, the appearance of an object changes, often radically, with even small changes in the direction from which it is viewed by the radar because the reflection angles of the surfaces of the objects differ with the direction of the illuminating beam.

However, certain geometric features of ground objects remain the same in radar pictures regardless of changes in viewing angle, weather, time of day, and, to a great extent, the season. Such features are valuable guideposts to which an observer may mentally attach local geographical coordinates. In general, they have strong contour sufficiently distinguishable by the sensor against a variety of backgrounds. They also possess connectivity in the psychological sense, which preserves their identity in spite of noise corruption and gives them spatial extent. Runways, land-water boundaries such as shore lines, rivers, and other drainage nets, and communication lines such as roads, railroads, and bridges belong in this category along with metal towers of power lines, whose truss work produces nonchanging radar reflections, towns and cities with their prominent street patterns, and industrial complexes and depots, military or otherwise.

In spite of their individuality, even these targets often are difficult to locate because of the complexity of the background in which they are embedded. Their visual detection and identification depends either on characteristic and outstanding individual invariants, or features such as texture that may be expressed in statistical terms. Even invariant features may not make a target immediately obvious when the background surrounding it contains similar features or when the picture scale is inappropriate. Picture interpretability under these circumstances may depend upon differences between pertinent statistical parameters of the target, on the one hand, and of the background on the other.

SELECTION OF CHARACTERISTICS

On basis of the above considerations, five physical characteristics of the pictures were selected for measurement. One was the size of each target. The other four were based on transmissivity; that is, the clearness or opaqueness of the positive glass plates that governed the passage of light through them. These characteristics were:

> The average transmissivity of each target, μ_t, in relation to the average transmissivity of the area immediately surrounding each target, μ_T (see Measurement of Characteristics, below)
>
> The variance (spread about the mean) of the transmissivity of each target, s_t, in relation to the variance (spread about the mean) of the transmissivity of the area immediately surrounding each target, s_T
>
> The average rate of change (detail) in the transmissivity of each target, μ_d, in relation to the average rate of change (detail) in the transmissivity of the area immediately surrounding each target, μ_D
>
> The variance (spread about the mean) of the rate of change (detail) in the transmissivity of each target, s_d, in relation to the variance (spread about the mean) of the rate of change in the transmissivity of the area immediately surrounding each target, s_D

These were dimensionless quantities expressed in ratios.

MEASUREMENT OF CHARACTERISTICS

The transmissivity of each radar picture was measured by scanning it with a flying spot scanner. The light that passed through the positive transparency was focused on a photomultiplier tube whose output was a voltage that varied in direct proportion to the intensity of the light. This voltage was fed to an analog computer programmed to process it mathematically into four respective signals representing measurements of the four selected transmissivity characteristics.

A flying spot scanner was built for the measurements. It is shown in figure 5. It had two identical channels, one to scan the picture and generate signals to the computer, and the other to display the scan to the scanner operator for monitoring and location of the targets. Generally, in these devices the point of light (flying spot) is generated in a cathode-ray tube and moved across the face of the tube in paths that give the desired scan pattern, or raster. Usually, this scan is in continuous single lines traversing horizontally, as in TV sets.

The high-resolution radar pictures required a sequential two-direction orthogonal scan because many of the gradients were oriented in a direction other than horizontal. This sweep voltage was programmed by the computer to scan each of 256 square cells of the picture individually 10 times and 10 times vertically in the sequence shown in figure 6. Figure 7 is an enlargement of the

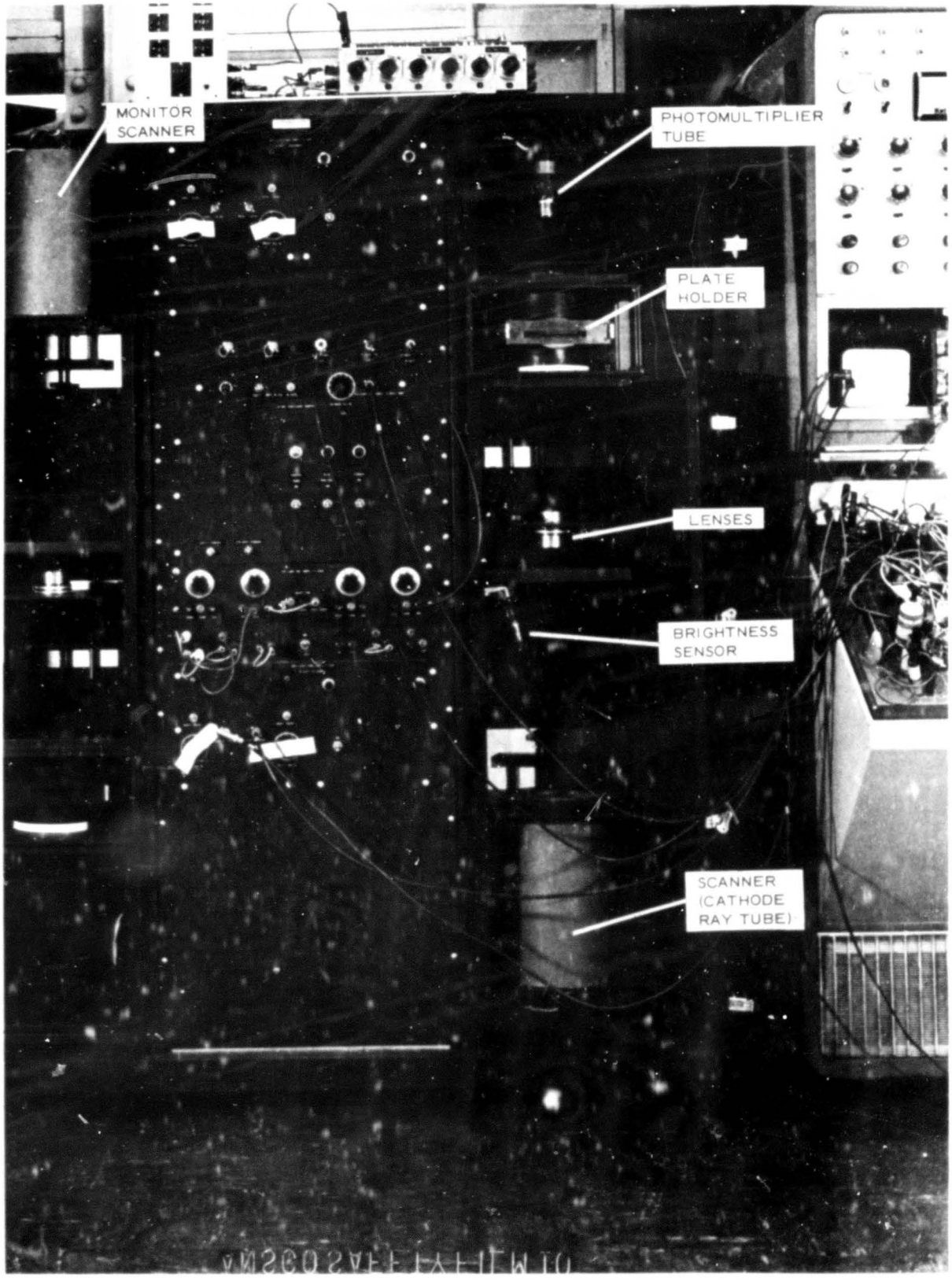

Figure 5 - Flying Spot Scanner and Portion of Analog Computer

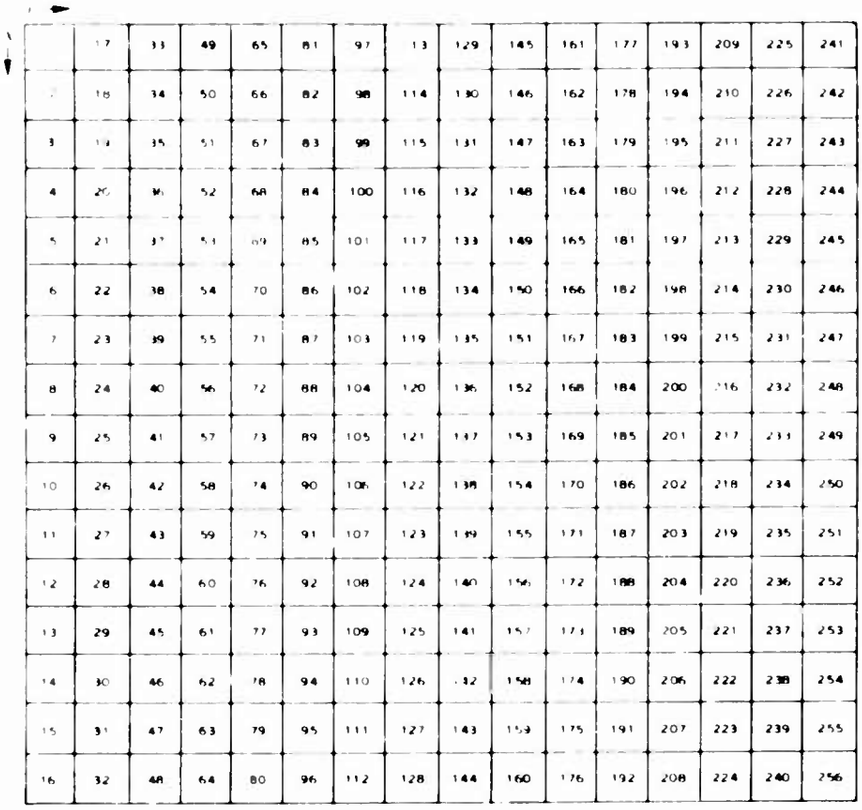

	17	33	49	65	81	97	13	129	145	161	177	193	209	225	241
2	18	34	50	66	82	98	114	130	146	162	178	194	210	226	242
3	19	35	51	67	83	99	115	131	147	163	179	195	211	227	243
4	20	36	52	68	84	100	116	132	148	164	180	196	212	228	244
5	21	37	53	69	85	101	117	133	149	165	181	197	213	229	245
6	22	38	54	70	86	102	118	134	150	166	182	198	214	230	246
7	23	39	55	71	87	103	119	135	151	167	183	199	215	231	247
8	24	40	56	72	88	104	120	136	152	168	184	200	216	232	248
9	25	41	57	73	89	105	121	137	153	169	185	201	217	233	249
10	26	42	58	74	90	106	122	138	154	170	186	202	218	234	250
11	27	43	59	75	91	107	123	139	155	171	187	203	219	235	251
12	28	44	60	76	92	108	124	140	156	172	188	204	220	236	252
13	29	45	61	77	93	109	125	141	157	173	189	205	221	237	253
14	30	46	62	78	94	110	126	142	158	174	190	206	222	238	254
15	31	47	63	79	95	111	127	143	159	175	191	207	223	239	255
16	32	48	64	80	96	112	128	144	160	176	192	208	224	240	256

Figure 6 - Scan Geometry

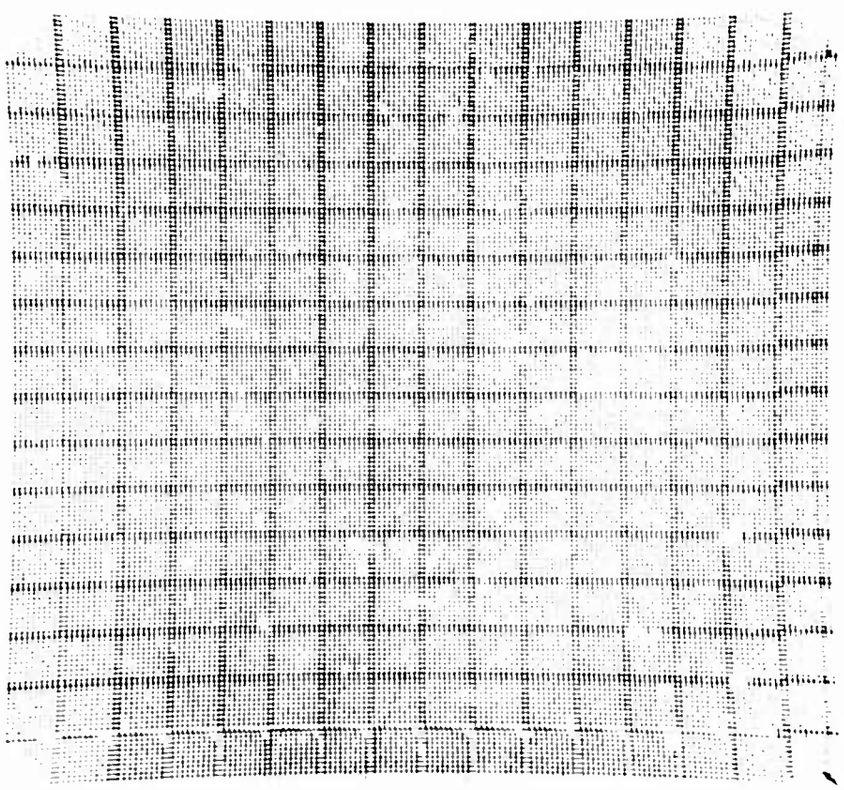

Figure 7 - Scan Pattern

scan pattern for an entire picture. The single dots were caused by crossings of the vertical and horizontal scan lines; the boundaries of the 256 cells are marked by dots caused by overlapping sweeps. The distortion was due to the large f-stop of the lens in the optical path. Figure 8 shows how the flying spot scanner translated an optical photograph with this scan. In this case, the light transmitted through the positive by the flying spot was recorded on an unexposed photographic film.

The computer generated four simultaneous outputs that were recorded as voltage variations as shown in figure 9. Each of the channels represented the average values of one of the transmissivity characteristics measured cell by cell. A fifth channel related these average values to the individual cells. The measurements were dimensionless, since only their ratios were of concern.

The scanner-computer system was connected and programmed to perform the following four operations for each of the 256 picture cells:

$$\mu_{ti} = \frac{1}{2m} \sum_{j=1}^{m} \left[\frac{1}{x_{i+1} - x_i} \int_{x_i}^{x_{i+1}} t(x, y_j)\, dx + \frac{1}{y_{i+1} - y_i} \int_{y_i}^{y_{i+1}} t(x_j y) dy \right], \quad (1)$$

which was a measure of the average (mean) transmissivity;

$$s_{ti} = \frac{1}{2m} \sum_{j=1}^{m} \left[\frac{1}{x_{i+1} - x_i} \int_{x_i}^{x_{i+1}} t^2(x, y_j) dx + \frac{1}{y_{i+1} - y_i} \int_{y_i}^{y_{i+1}} t^2(x_j y) dy \right] - \mu_{ti}^2, \quad (2)$$

which was a measure of the variance (spread about the mean) of the transmissivity;

$$\mu_{di} = \frac{1}{2m} \sum_{j=1}^{m} \left[\frac{1}{x_{i+1} - x_i} \int_{x_i}^{x_{i+1}} \left| \frac{\partial t}{\partial x} \right|_{y_i} dx + \frac{1}{y_{i+1} - y_i} \int_{y_i}^{y_{i+1}} \left| \frac{\partial t}{\partial y} \right|_{x_j} dy \right], \quad (3)$$

which was a measure of the detail (the average absolute value of the rate of change of the transmissivity); and

$$s_{di} = \frac{1}{2m} \sum_{j=1}^{m} \left[\frac{1}{x_{i+1} - x_i} \int_{x_i}^{x_{i+1}} \left| \frac{\partial t}{\partial x} \right|_{y_j}^2 dx + \frac{1}{y_{i+1} - y_i} \int_{y_i}^{y_{i+1}} \left| \frac{\partial t}{\partial y} \right|_{x_j}^2 dy \right], \quad (4)$$

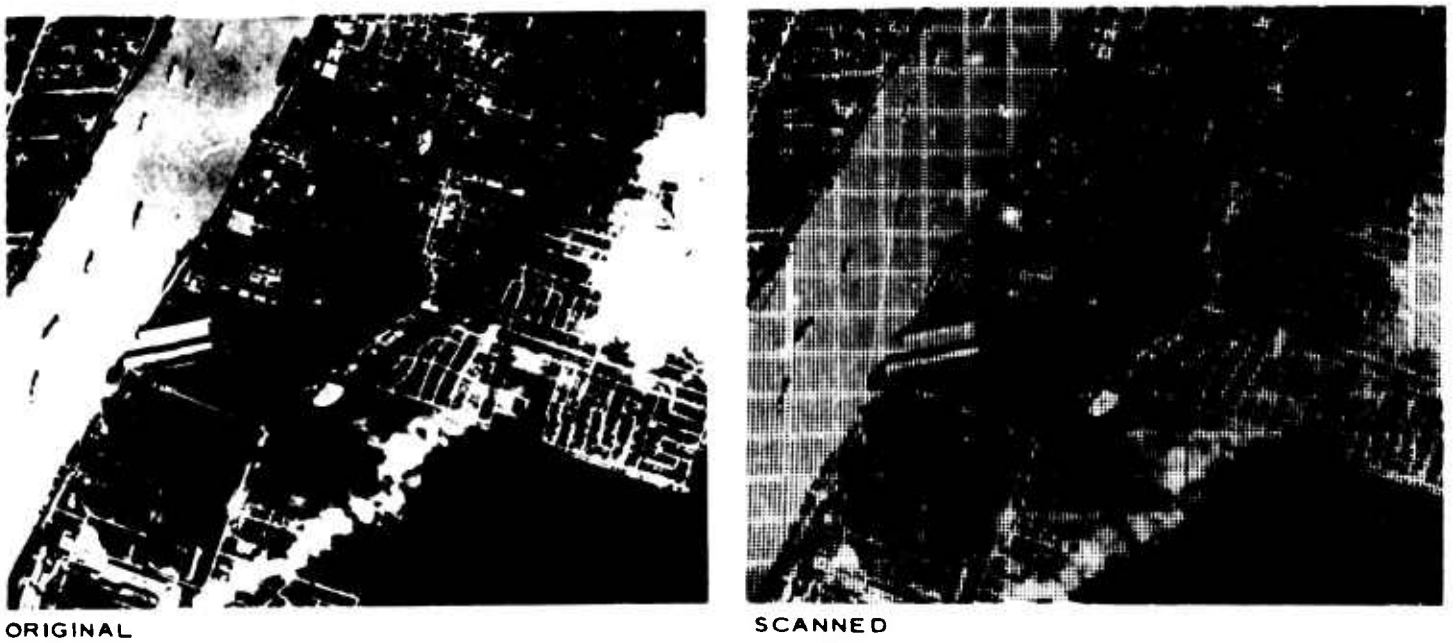

ORIGINAL SCANNED

Figure 8 - Example of Scan (Optical Photograph)

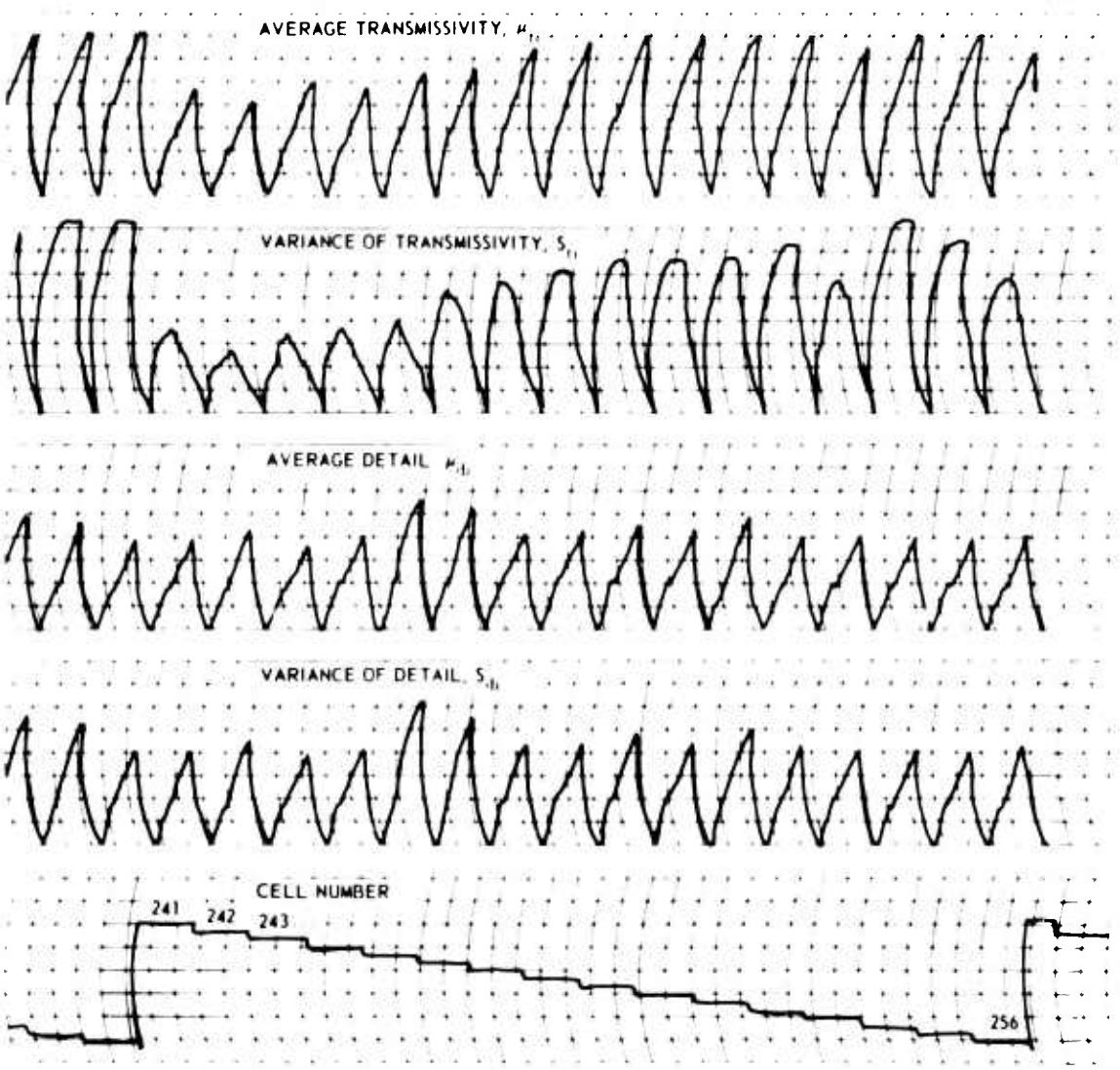

Figure 9 - Illustrative Analog Computer Outputs

which was a measure of the variance of detail. The area (α) of each cell occupied by a target was measured by

$$\alpha_i = (x_{i+1} - x_i)(y_{i+1} - y_i) , \tag{5}$$

for use as the unit of measurement for target size.

In the above equations,

i is the cell number in the cell matrix;

m is the total number of equidistant scans in the x or y direction within each cell (in this case, $m = 10$);

j is the order number of each individual scan;

$x_{i+1} - x_i$ is the size of each cell in the x-axis direction;

$y_{i+1} - y_i$ is the size of each cell in the direction of the y axis (the two sides were chosen to be equal, hence $\overline{x} = x_{i+1} - x_i = y_{i+1} - y_i = \overline{y}$);

t(x, y) is the transmissivity of the picture depending on the position x, y within the cell; and

$\frac{\partial t}{\partial x}$ and $\frac{\partial t}{\partial y}$ are the partial derivatives of t(x, y) with respect to x and y.

On the basis of these cell values, the five parameters were computed separately for the background and the target. For example, in the case of the average transmissivity, the value for the whole picture (the sum total of the $N = 256$ cells) was

$$\mu_T = \frac{1}{N} \sum_{i=1}^{N} \mu_{ti} , \tag{6}$$

and for the target alone the average transmissivity was

$$\mu_t = \frac{1}{n} \sum_{i=1}^{n} \mu_{ti} . \tag{7}$$

In the expression immediately above, only the n cells occupied by the target were considered. The other transmissivity parameters were determined in similar fashion:

$$s_T = \frac{1}{N} \sum_{i=1}^{N} s_{ti} , \tag{8}$$

$$s_t = \frac{1}{n} \sum_{i=1}^{n} s_{ti} , \tag{9}$$

$$\mu_D = \frac{1}{N} \sum_{i=1}^{N} \mu_{di} , \tag{10}$$

$$\mu_d = \frac{1}{n} \sum_{i=1}^{n} \mu_{di} , \tag{11}$$

$$s_D = \frac{1}{N} \sum_{i=1}^{N} s_{di} , \tag{12}$$

and

$$s_d = \frac{1}{n} \sum_{i=1}^{n} s_{di} . \tag{13}$$

The relative size of each target to the entire picture area (all 256 cells) was computed on the basis of

$$\alpha_T = N \bar{x}\bar{y}$$

and (14)

$$\alpha_t = n \bar{x}\bar{y} .$$

Where a cell was filled completely by a portion of a target, the computer gave the actual average of each of the four characteristics for that particular cell. However, the periphery of each target cut through many cells and in these cases the computer did not distinguish between the cell target area and the cell background area. This required manual analysis and computation for each such cell for each of the four characteristics.

Figure 10 is an illustrative case of the above. Here, λ_i is the portion of a cell belonging to a target, and $1 - \lambda_i$ is the portion of the same cell belonging to the background. The computer found the average transmissivity, μ, of the entire cell by means of

$$\lambda_i \mu_{ti} (1 - \lambda_i) \mu_T = r_i ,$$

with

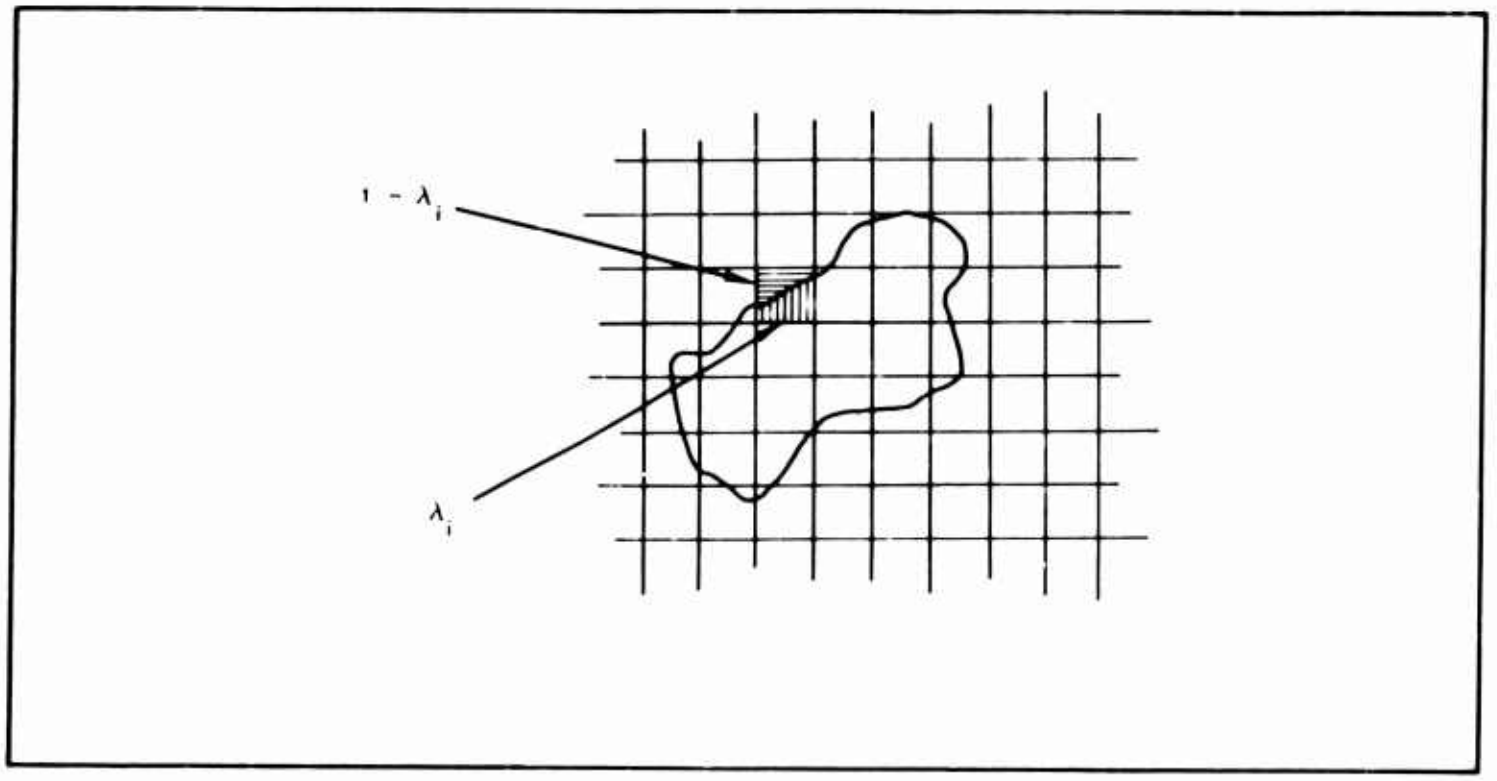

Figure 10 - Geometry of Target Cell-Size Measurement

μ_{ti} = transmissivity of the cell target area,

μ_T = transmissivity of the cell background area, and

r_i = the computer readout of the average for the entire cell.

To find the average transmissivity of a cell target area, λ_i was estimated by visual examination and the following was solved manually:

$$\mu_{ti} = \frac{r_i - (1 - \lambda_i)\mu_T}{\lambda_i}.$$

Then for all such cells (n),

$$\mu_t = \frac{1}{n} \sum \mu_{ti}$$

or

$$\frac{\mu_t}{\mu_T} = \frac{1}{n}\left(\frac{1}{\mu_T} \sum_{i=1}^{N} \frac{r_i}{\lambda_i} - \sum_{i=1}^{N} \frac{1 - \lambda_i}{\lambda_i}\right).$$

Similar manual computations were required for all such cells to determine the other desired ratios. In the first measurement attempts, positive plates representing 18- by 18-nautical-mile ground areas were used. Because of the distortion limitations of the flying spot scanner optical path, these pictures were limited to 2.25 by 2.25 in. Thus each of the 256 cells into which each picture was divided represented a ground area of 1.265 square nautical miles. At this scale, the cell target areas (λ_i) could not be estimated accurately. Also, targets of the airfield category had to be excluded because it was all but impossible to estimate their contributions (for this and other reasons, the original 30 plates were reduced to 20). Many of the other ratios had negative values, as shown in table II, that indicated unacceptable errors of measurement due to the small scale. In these measurements, the background transmissivity was taken as the average for all 256 cells. This average was computed manually from the recordings.

A new scale factor was adopted. This was done by enlarging each target and its immediate surrounding area six times, which incidentally was about the same scale as the projections in the human response experiments. The 20 new positive plates were scanned and measured as before by the flying spot scanner and the analog computer, and the required manual computations were repeated. At this new scale, each of the 256 cells covered a ground area of only 0.035 square nautical mile. This reduced the effect of target and background mixing, because now the targets were sufficiently large to allow better estimation of the contribution of the target area in each partially occupied cell, and the matrix was so placed that there were fewer cells so occupied. However, even at this scale, airfields had to be excluded because they could not be measured.

Two sets of data were prepared from the large-scale pictures. One expressed the ratios of the four transmissivity characteristics of the targets to the background transmissivity characteristics averaged over all 256 cells, as shown in table III. The other expressed these ratios to the background transmissivity averaged over the immediate background of each target; that is, those cells partially occupied by a portion of a target, and those touching the edge of a target. The second set of data are shown in table IV. Whether a limited or overall background was used had little effect on the transmissivity ratios, as shown by comparison of the first columns in the tables.

Unexpectedly, it was found that the four transmissivity characteristics varied in unison in almost direct proportion from cell to cell in many of the pictures. This is shown in figure 11, which is part of the computer recording for one of the large-scale pictures. The scatter diagram for μ_{ti} versus μ_{di} for all 256 cells of this picture (plate 17) is plotted in figure 12. It shows a high degree of curvilinear correlation of the type

$$\mu_{ti} = k\mu_{di}^{m} + c ,$$

where k, m, and c are constants. Similar correlations are indicated by figures 13 and 14, which are scatter diagrams for μ_t/μ_T versus μ_d/μ_D for limited and overall target backgrounds, respectively.

The unexpected correlation between these characteristics was undesirable because it weakened the descriptions of the pictures. When these characteristics

were selected, they had been expected to be independent of each other. Time prevented selection and measurement of new characteristics. Thus, the measurements discussed above were used in deriving the human-response prediction equation as discussed in section IV.

TABLE II

CHARACTERISTICS OF TARGET VERSUS OVERALL BACKGROUND, ORIGINAL RADAR PLATES AT SMALL SCALE

Cell location			Ratios of transmissivity characteristics[+]			
Plate	Column	Row	μ_t/μ_T	s_t/s_T	μ_d/μ_D	s_d/s_D
1	6	11 (0.35), 12 (0.10)	-0.5	-4.5	0.6	3.3
2	1	13 (0.45)	. . .	. . .	. . .	. . .
3	11	8 (0.80)	1.6	3.3	1.5	1.9
4	9	3 (0.10)	2.3	31.9	3.9	18.7
5	6	9 (0.65), 10 (0.05)	. . .	. . .	. . .	. . .
6	8	5 (0.25)	. . .	. . .	. . .	. . .
7	7	8 (1.00)	1.4	1.1	1.4	1.6
8	7	8 (0.25), 9 (0.35)	1.5	0.2	1.9	2.0
9	5	4 (0.50)	. . .	. . .	. . .	. . .
10	7	5 (0.40)	1.7	4.7	1.3	1.7
11	9	2 (0.10)	0.8	4.3	-0.4	-1.0
12	7	9 (0.90)	1.1	0.8	1.2	1.2
13	6	12 (0.03)	8.8	45.8	12.3	13.9
14	7	10 (0.15)	. . .	. . .	. . .	. . .
15	12	2 (0.50)	1.2	3.6	1.3	2.1
16	6	9 (0.50)	1.3	4.0	1.9	2.1
17	8 (0.05)[*]	9	. . .	. . .	. . .	. . .
	9 (0.70)	. . .	. . .	. . .	. . .	. . .
18	2	4 (0.15)	-0.1	4.1	-0.0	-0.2
19	4	4 (0.20), 5 (0.10)	. . .	. . .	. . .	. . .
20	5	4 (0.10)	. . .	. . .	. . .	. . .
	8	7 (0.10), 8 (0.50)	. . .	. . .	. . .	. . .
21	9	7 (0.10)	1.7	2.8	2.7	3.2
	12	10 (0.005)	. . .	. . .	. . .	. . .
22	11	5 (0.10)	1.8	18.9	2.3	3.3
23	1	15 (0.10)	-1.7	-7.7	-2.2	-2.0
24	6	8 (0.07)	. . .	. . .	. . .	. . .
	7	9 (0.10)	. . .	. . .	. . .	. . .
25	3	13 (0.20)	0.0	2.9	-0.5	-0.7
26	9	7 (0.08)	-3.1	8.5	-3.3	-2.7
27	5	5 (0.18)	1.5	13.3	2.2	2.4
28	7 (1.0)	7	1.6	1.4	1.6	1.7
	8	. . .	. . .	. . .	. . .	. . .
29	8	8 (0.05)	. . .	. . .	. . .	. . .
30	8	6 (0.50), 7 (0.10)	1.2	-3.2	-3.1	1.2

[*] Numbers in parentheses show percentage of cell occupied by target.

[+] μ_t/μ_T = target to background; s_t/s_T = target variance about mean to background variance about mean; μ_d/μ_T = target rate of change (detail) to background rate of change; s_d/s_D = target detail variance to background detail variance.

TABLE III

CHARACTERISTICS OF TARGET VERSUS OVERALL BACKGROUND, ORIGINAL RADAR PLATES AT LARGE SCALE

Plate	Ratios of transmissivity characteristics				Ratios of difference between target and background characteristics to background characteristics				Target size ($\alpha \times 256$)
	$\frac{\mu_t}{\mu_T}$	$\frac{s_t}{s_T}$	$\frac{\mu_d}{\mu_D}$	$\frac{s_d}{s_D}$	$\left\lvert\frac{\mu_t - \mu_T}{\mu_T}\right\rvert$	$\left\lvert\frac{s_t - s_T}{s_T}\right\rvert$	$\left\lvert\frac{\mu_d - \mu_D}{\mu_D}\right\rvert$	$\left\lvert\frac{s_d - s_D}{s_D}\right\rvert$	
1	1.53	1.42	1.65	1.30	0.53	0.42	0.65	0.30	3.7
2	. . .	. . .	. . .	. . .	. . .	. . .	. . .	. . .	. . .
3	1.99	2.30	1.41	1.44	0.99	1.30	0.41	0.44	5.1
4	3.00	3.02	1.71	1.94	2.00	2.02	0.71	0.94	1.9
5	. . .	. . .	. . .	. . .	. . .	. . .	. . .	. . .	. . .
6	. . .	. . .	. . .	. . .	. . .	. . .	. . .	. . .	. . .
7	0.68	4.63	0.96	1.22	0.32	3.63	0.04	0.22	7.7
8	1.01	1.10	1.47	1.45	0.01	0.10	0.47	0.45	8.0
9	. . .	. . .	. . .	. . .	. . .	. . .	. . .	. . .	. . .
10	1.15	0.80	0.94	1.01	0.15	0.20	0.06	0.01	3.3
11	1.41	1.39	1.45	2.05	0.41	0.39	0.45	1.05	2.0
12	1.35	1.52	1.31	1.33	0.35	0.52	0.31	0.33	13.5
13	1.77	3.00	1.07	1.29	0.77	2.00	0.07	0.29	0.8
14	. . .	. . .	. . .	. . .	. . .	. . .	. . .	. . .	. . .
15	2.22	2.50	1.54	1.63	1.22	1.50	0.54	0.63	3.6
16	2.10	9.6	1.44	2.51	1.10	8.6	0.44	1.51	5.0
17	. . .	. . .	. . .	. . .	. . .	. . .	. . .	. . .	. . .
18	1.41	2.85	0.79	1.22	0.41	1.85	0.21	0.22	1.5
19	. . .	. . .	. . .	. . .	. . .	. . .	. . .	. . .	. . .
20	1.08	1.99	0.95	1.14	0.08	0.99	0.05	0.14	15.7
21	. . .	. . .	. . .	. . .	. . .	. . .	. . .	. . .	. . .
22	0.87	0.58	0.73	0.54	0.13	0.42	0.27	0.46	0.6
23	3.64	7.72	2.22	2.94	2.64	6.72	1.22	1.94	1.0
24	. . .	. . .	. . .	. . .	. . .	. . .	. . .	. . .	. . .
25	3.07	2.83	5.54	8.22	2.07	1.83	4.54	7.22	1.6
26	1.50	2.82	1.09	1.60	0.50	1.82	0.09	0.60	0.9
27	1.43	6.38	1.86	2.15	0.43	5.38	0.86	1.15	2.5
28	1.46	1.6	1.22	1.22	0.46	0.68	0.22	0.22	24.4
29	. . .	. . .	. . .	. . .	. . .	. . .	. . .	. . .	. . .
30	1.16	4.00	1.49	1.64	0.16	3.00	0.49	0.64	12.8

TABLE IV

CHARACTERISTICS OF TARGET VERSUS IMMEDIATE BACKGROUND, ORIGINAL RADAR PLATES AT LARGE SCALE

Plate	Ratios of transmissivity characteristics				Ratios of difference between target and background characteristics to background characteristics				Target size ($a \times 256$)
	$\frac{\mu_t}{\mu_T}$	$\frac{s_t}{s_T}$	$\frac{\mu_d}{\mu_D}$	$\frac{s_d}{s_D}$	$\left\lvert\frac{\mu_t - \mu_T}{\mu_T}\right\rvert$	$\left\lvert\frac{s_t - s_T}{s_T}\right\rvert$	$\left\lvert\frac{\mu_d - \mu_D}{\mu_D}\right\rvert$	$\left\lvert\frac{s_d - s_D}{s_D}\right\rvert$	
1	1.34	1.15	1.57	1.11	0.34	0.15	0.57	0.11	3.7
2	. . .	. . .	. . .	. . .	. . .	. . .	. . .	. . .	. . .
3	2.04	2.50	1.44	1.50	1.04	1.60	0.44	0.50	5.1
4	2.98	2.82	1.66	1.85	1.98	1.82	0.66	0.85	1.9
5	. . .	. . .	. . .	. . .	. . .	. . .	. . .	. . .	. . .
6	. . .	. . .	. . .	. . .	. . .	. . .	. . .	. . .	. . .
7	0.68	4.56	0.98	1.23	0.32	3.56	0.02	0.23	7.7
8	1.01	1.11	1.25	1.19	0.01	0.11	0.25	0.19	8.0
9	. . .	. . .	. . .	. . .	. . .	. . .	. . .	. . .	. . .
10	1.22	0.84	0.85	0.91	0.22	0.16	0.15	0.09	3.3
11	1.48	1.48	1.43	2.01	0.48	0.48	0.43	1.01	2.0
12	1.15	1.54	1.13	0.89	0.15	0.54	0.13	0.11	13.5
13	1.57	2.47	0.89	1.04	0.57	1.47	0.11	0.04	0.8
14	. . .	. . .	. . .	. . .	. . .	. . .	. . .	. . .	. . .
15	2.32	2.13	1.57	1.63	1.32	1.13	0.57	0.63	3.6
16	1.89	6.22	2.06	2.32	0.89	5.22	1.06	1.32	5.0
17	. . .	. . .	. . .	. . .	. . .	. . .	. . .	. . .	. . .
18	1.45	2.75	0.83	1.24	0.45	1.75	0.17	0.24	1.5
19	. . .	. . .	. . .	. . .	. . .	. . .	. . .	. . .	. . .
20	1.08	2.15	0.94	1.14	0.08	1.15	0.06	0.14	15.7
21	. . .	. . .	. . .	. . .	. . .	. . .	. . .	. . .	. . .
22	0.86	0.50	0.77	0.56	0.14	0.50	0.23	0.44	0.6
23	4.57	11.23	2.57	0.98	3.57	10.23	1.57	0.02	1.0
24	. . .	. . .	. . .	. . .	. . .	. . .	. . .	. . .	. . .
25	3.05	12.19	5.29	6.66	2.05	11.19	4.29	5.66	1.6
26	1.93	3.33	1.32	1.88	0.93	2.33	0.32	0.88	0.9
27	1.24	3.15	1.55	1.73	0.24	2.15	0.55	0.73	2.5
28	1.38	1.68	1.13	1.13	0.38	0.68	0.13	0.13	24.4
29	. . .	. . .	. . .	. . .	. . .	. . .	. . .	. . .	. . .
30	1.17	3.94	1.47	1.53	0.17	2.94	0.47	0.53	12.8

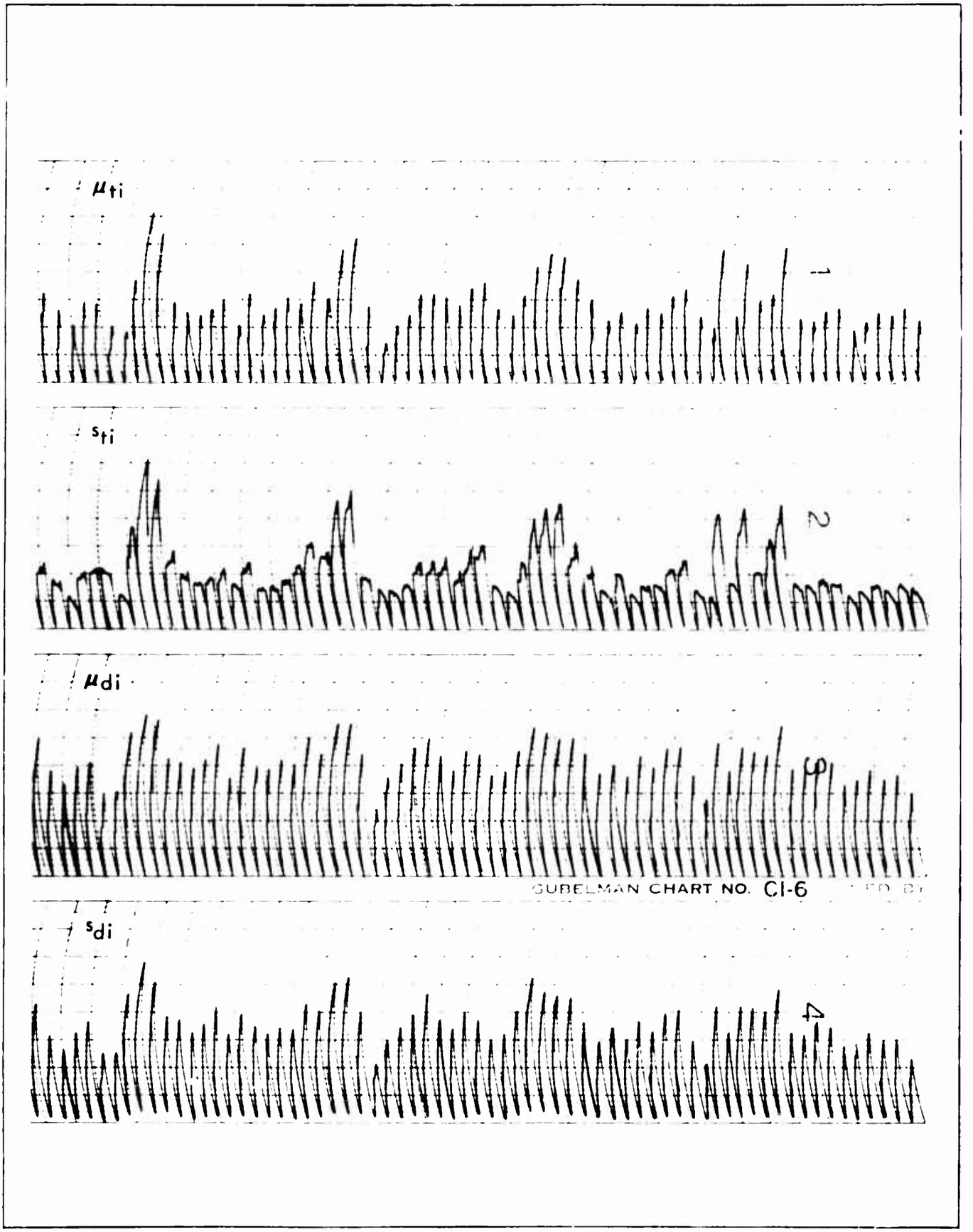

Figure 11 - Analog Computer Recordings Showing Correlation between Cell Parameters (Original Radar Plate 17)

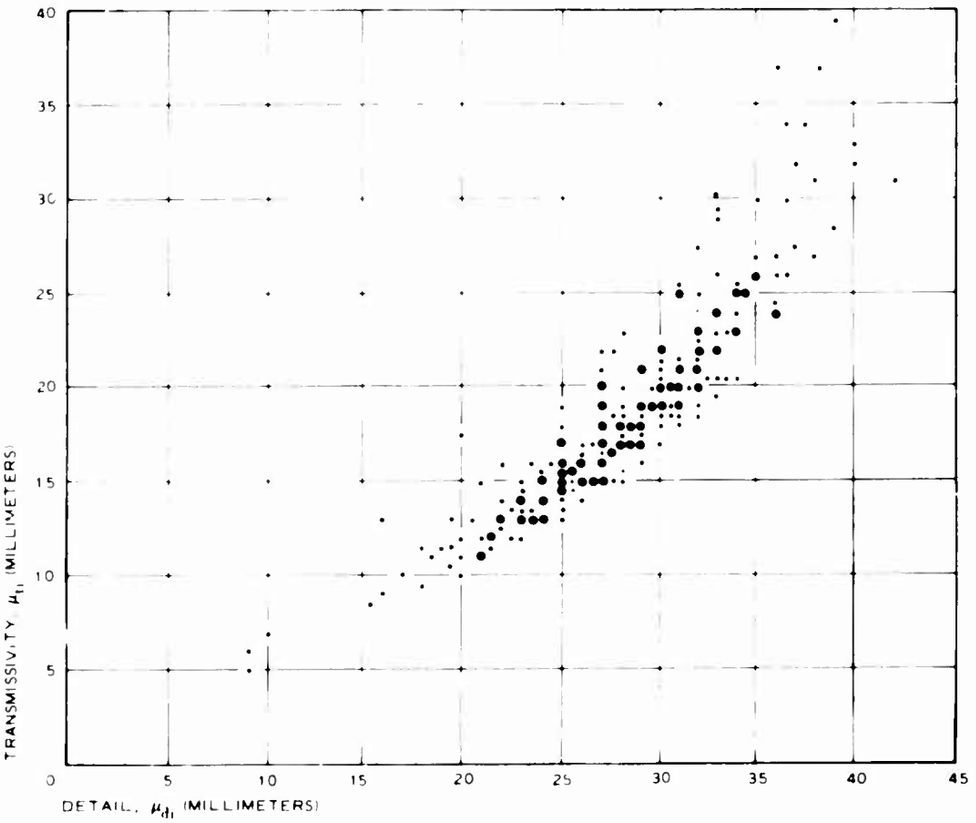

Figure 12 - Scatter Diagram of Cell-by-Cell Transmissivity versus Detail (Original Radar Plate 17)

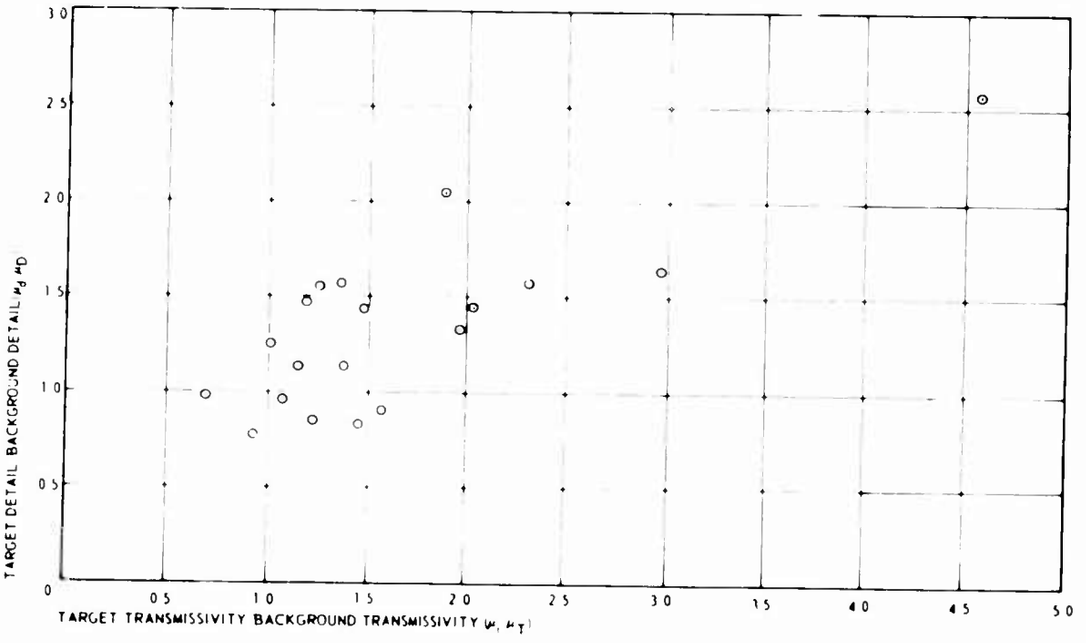

Figure 13 - Scatter Diagram of Transmissivity and Detail Ratios, Immediate Background, Original Radar Plates at Large Scale

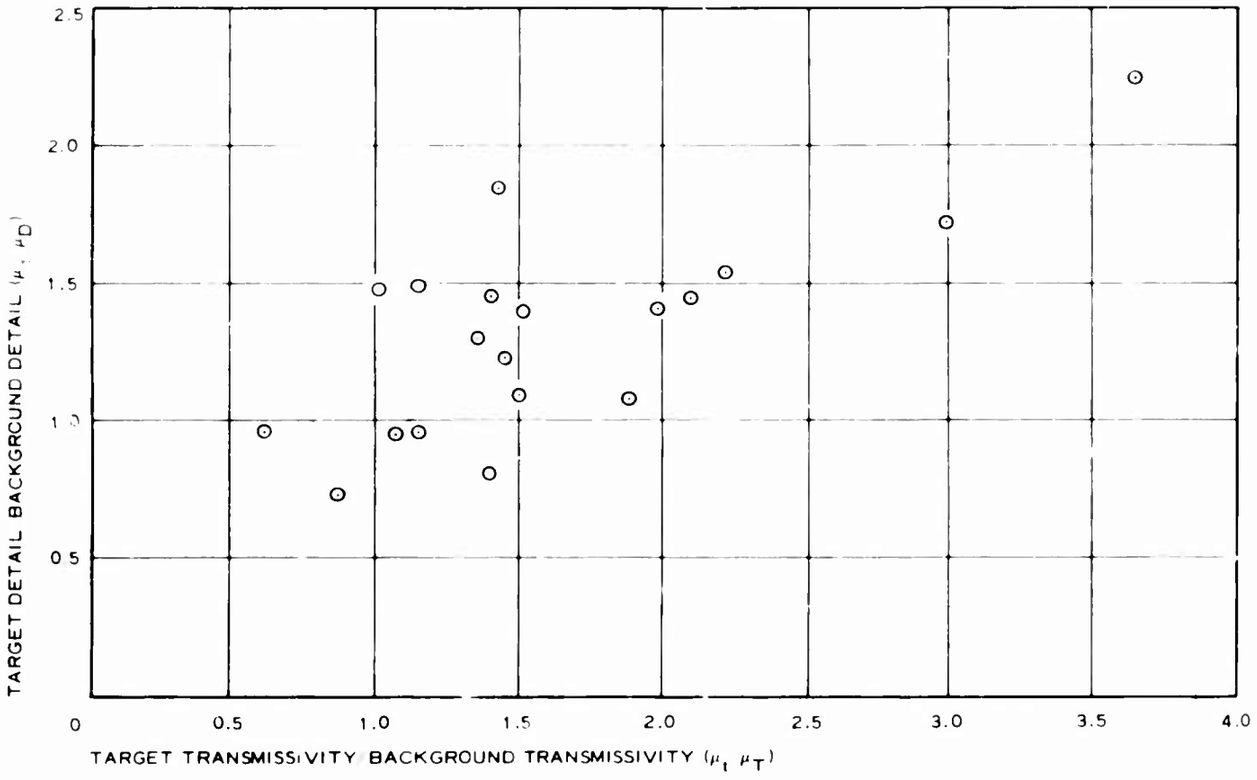

Figure 14 - Scatter Diagram of Transmissivity and Detail Ratios, Overall Background, Original Radar Plates at Large Scale

SECTION IV

SELECTION OF THE HUMAN PERFORMANCE PREDICTION EQUATION

INTRODUCTION

With the human response data established and the physical characteristics of the pictures measured, the problem was to define a metric that would relate these two sets of data in a prediction equation. Three metrics were defined by three teams working independently. Metric I related the two sets of data in a logarithmic equation as discussed below. Metrics II and III were predicated on the same general type of picture characteristics as used in Metric I but the relationships were utilized differently, as explained in appendixes I and II, respectively. Lack of time prevented attempts to validate Metrics II and III.

SYNTHESIS OF METRIC I

In synthesizing Metric I, the intention was to relate the four transmissivity characteristics of target and background, as well as target relative size, to the psychophysical scores of the human observers. The following corresponding characteristics for target and background in the form of ratios were chosen:

$$\frac{\mu_t}{\mu_T}, \frac{s_t}{s_T}, \frac{\mu_d}{\mu_D}, \frac{s_d}{s_D}, \text{ and } \frac{\alpha_t}{\alpha_T} .$$

The aim was to combine these ratios in a manner to bring out the differences between target and background in both brightness and detail. Two such ways, both attractive for their computational simplicity, were considered. The first one arranged each parameter pair (such as μ_t and μ_T) in the form of the sum of their ratio and the inverse of the ratio. With the general terms b and B denoting any one of the parameter pairs, then

$$\beta = \frac{b}{B} + \frac{B}{b} + c .$$

This arrangement was required because an observer attempting to distinguish the target from its background would benefit as much from b being greater than B as from the reverse.

For the cases of the four transmissivity characteristics, the value b for the target and the value B for the background could be such that

$$b \lesseqgtr B .$$

This, of course, would not be true about the target size, which would be subject to the condition

$$b < B .$$

The purpose of the constant c was to establish an appropriate scale origin for measuring β. On this basis, the following five dimensionless parameters were established:

$$\mu_\tau = \frac{\mu_t}{\mu_T} + \frac{\mu_T}{\mu_t} + c \ ,$$

$$s_\tau = \frac{s_t}{s_T} + \frac{s_T}{s_t} + c \ ,$$

$$\mu_\delta = \frac{\mu_d}{\mu_D} + \frac{\mu_D}{\mu_d} + c \ ,$$

$$s_\delta = \frac{s_d}{s_D} + \frac{s_D}{s_d} + c, \text{ and}$$

$$\alpha = \frac{\alpha_t}{\alpha_T} + c_o \ .$$

It was assumed that the contribution of each of the transmissivity parameters would become zero when target and background were the same as far as a particular parameter was concerned; thus

$$\beta = \frac{b}{B} + \frac{B}{b} + c = 0$$

when

$$\frac{b}{B} = 1 \ .$$

From these two equations,

$$c = -2 \ .$$

For the area ratio, however, α had to be zero when the size of the target α_t was zero. This made

$$c_o = 0 \ .$$

When these values of c and c_o were substituted in the above equations, then

$$\mu_\tau = \frac{(1 - \mu_t/\mu_T)^2}{\mu_t/\mu_T} \ ,$$

$$s_\tau = \frac{(1 - s_t/s_T)^2}{s_t/s_T} \ ,$$

$$\mu_\delta = \frac{(1 - \mu_d/\mu_D)^2}{\mu_d/\mu_D} \ ,$$

$$s_\delta = \frac{(1 - s_d/s_D)^2}{s_d/s_D} ,$$

and

$$\alpha = \frac{\alpha_t}{\alpha_T} ,$$

together with the condition that if

$$\alpha_t = 0 ,$$

then

$$\mu_t = \mu_T ,$$

$$s_t = s_T ,$$

$$\mu_d = \mu_D ,$$

and

$$s_d = s_D ,$$

because none of the dimensionless parameters would have any meaning when the target area was reduced to zero.

The other way of arriving at similar results was by defining

$$\beta = \left| 1 - \frac{b}{B} \right| ,$$

which was equivalent to

$$\beta = \frac{|B - b|}{B} ,$$

and, therefore, to saying that β was the ratio of the absolute value of the difference in transmissivity characteristics between target and background to the value of the same characteristic for the background. Thus,

$$\mu_\tau = \left| 1 - \frac{\mu_t}{\mu_T} \right| ,$$

$$s_\tau = \left| 1 - \frac{s_t}{s_T} \right| ,$$

$$\mu_\delta = \left| 1 - \frac{\mu_d}{\mu_D} \right|,$$

$$s_\delta = \left| 1 - \frac{s_d}{s_D} \right|,$$

and

$$\alpha = \frac{\alpha_t}{\alpha_T} .$$

Under the existing state of knowledge on perception and recognition, there was no psychophysical law that could dictate how the physical parameters discussed above affect human operator performance in target detection tasks. However, the values of the purely physical characteristics represented by the parameters had to be brought into some quantitative relationship with the scores obtained in the psychophysical experiments.

It was assumed that a group of observers, subjected to identical briefing and put into an identical experimental environment, when presented with the same picture containing a particular target would take different lengths of time to identify the target and that some of them would identify the wrong target sometimes. The two outcomes of primary interest in such experiments are the percent of correct decisions, p_c, and the time to reach a correct decision, s_c. Only the latter was retained for correlation with the physical picture characteristics already discussed. It was assumed that this correlation could be expressed mathematically in the form

$$\frac{1}{s_c} = f(\mu_\tau, s_\tau, \mu_\delta, s_\delta) .$$

Because available knowledge did not suggest a particular form of the function $f(\mu_\tau, s_\tau, \mu_\delta, s_\delta)$, a heuristic approach was employed. Forms of the equation tried were linear, vectorial, logarithmic, and exponential in the four transmissivity parameters, while the relative target size was either included or excluded in each case. Specifically, the following equations were tried:

(A)
$$\frac{1}{s_c} = k_1 \mu_\tau + k_2 s_\tau + k_3 \mu_\delta + k_4 s_\delta + k_5 , \tag{15}$$

(B)
$$\frac{1}{s_c} = \alpha(k_1 \mu_\tau + k_2 s_\tau + k_3 \mu_\delta + k_4 s_\delta) + k_5 , \tag{16}$$

(C)
$$\frac{1}{s_c} = \sqrt{k_1 \mu_\tau^2 + k_2 s_\tau^2 + k_3 \mu_\delta^2 + k_4 s_\delta^2 + k_5} , \tag{17}$$

(D)
$$\frac{1}{s_c} = \sqrt{\alpha^2 \left(k_1 \mu_\tau^2 + k_2 s_\tau^2 + k_3 \mu_\delta^2 + k_4 s_\delta^2\right) + k_5} , \tag{18}$$

(E) $$\frac{1}{s_c} = k_1 \ell n\, \mu_\tau + k_2 \ell n s_\tau + k_3 \ell n\, \mu_\delta + k_4 \ell n s_\delta + k_5 , \tag{19}$$

(F) $$\frac{1}{s_c} = \alpha(k_1 \ell n\, \mu_\tau + k_2 \ell n s_\tau + k_3 \ell n\, \mu_\delta + k_4 \ell n s_\delta) + k_5 , \tag{20}$$

(G) $$\frac{1}{s_c} = \exp\left(k_1 \mu_\tau + k_2 s_\tau + k_3 \mu_\delta + k_4 s_\delta + k_5\right) , \tag{21}$$

(H) $$\frac{1}{s_c} = \exp\left[\alpha\left(k_1 \mu_\tau + k_2 s_\tau + k_3 \mu_\delta + k_4 s_\delta\right) + k_5\right] , \tag{22}$$

where the ratios had the form of

(a) $$\beta = \frac{(1 - b/B)^2}{b/B} \tag{24}$$

or

(b) $$\beta = \left| 1 - \frac{b}{B} \right| . \tag{25}$$

Hence, the total of alternative expressions was 16: (A_a), (A_b), (B_a), (B_b), (C_a), (C_b), (D_a), (D_b), (E_a), (E_b), (F_a), (F_b), G(a), (G_b), (H_a), and (H_b). Two points should be explained at this juncture. First, $1/s_c$ was used in all these expressions and not s_c because the target recognition time, s_c, was expected to increase as the picture parameters β decreased. This suggested a type of inverse relationship between s_c and the β's.

Second, whenever the target size was included in the metric, it was used not as an additive term but as a multiplier. This was done because of the special role target size played here: if the target area diminished, recognition eventually would become impossible regardless of the values of the other parameters. Also, regardless of the value of the ratio α, no recognition would be possible if all the other parameters dealing with transmissivity characteristics were zero, because in this case, no structural feature would be present to distinguish the target from each background.

Consequently, α functioned as a multiplicative factor differing from μ_τ, s_τ, μ_δ, and s_δ, which could be taken additively. There was evidence (references 2 through 5) that recognition time, s_c, increases with display size, α_T, and decreases with target size, α_t. The reverse behavior had been noted for the probability, p_c, of correct decisions (reference 6).

A reasonable approach toward ascertaining the validity of the above postulated functional relationships between the picture physical parameters and the psychophysical scores was the use of multiple regression, a purely empirical procedure for deriving a mathematical relationship between the quantities of interest (β's and s_c). It is often useful because it yields estimates and predictions. It should be used, however, with the clear understanding that the

relationship is a purely mathematical device devoid of any specific cause-and-effect implications. The fact that a number of variables tend to vary together according to some mathematically desirable regularity does not in itself define the specifics of the mechanism involved. Multiple regression of the psychological variable s_c on the picture parameters , s , , s was the goal. It required the application of the least-squares method to the expression

$$\varepsilon^2 = \sum_{j=1}^{N} \varepsilon_j^2 = \sum_{j=1}^{N} \left[\frac{1}{s_{c_j}} - \left(k_1 \mu_{\tau_j} + k_2 s_{\tau_j} + k_3 \mu_{\delta_j} + k_4 s_{\delta_j} + k_5 \right) \right]^2$$

for the A_a case. Similar expressions were used for the rest of the cases, A_b through H_b.

Here, $\mu_{\tau j}$, $s_{\tau j}$, $\mu_{\delta j}$, and $s_{\delta j}$ were the values of the transmissivity characteristics for the j-th plate and s_{cj} was the average score of target recognition for all observers for the same j-th plate. N was the total number of plates. The regression computations were performed with the right-hand member of the tried metric equations A through H always in a linear form with respect to the constants k_1, k_2, k_3, k_4, and k_5. This meant that in the C case the metric was rearranged as

$$\frac{1}{s_c^2} = k_1 \mu_\tau^2 + k_2 s_\tau^2 + k_3 \mu_\delta^2 + k_4 s_\delta^2 + k_5$$

before being introduced in the expression for the total error squared, ε^2. Also, in the G case the metric was rearranged as

$$\log_e \frac{1}{s_c} = k_1 \mu_\tau + k_2 s_\tau + k_3 \mu_\delta + k_4 s_\delta + k_5 .$$

Similar rearrangements were applied to the D and H cases.

The least-squares technique yielded for ε^2 a system of five equations with five unknowns, k_1 through k_5. Solution of the system provided the numerical values of these unknowns. The system was obtained by equating to zero the derivatives of ε^2 with respect to each of the unknowns, k_1 through k_5; that is,

$$\frac{\partial}{\partial k_i} \varepsilon^2 = 0$$

with

$$i = 1, 2, 3, 4, 5 .$$

All operations involved in the multiple regression were performed by a digital computer. The criterion used to measure the goodness of fit in each case was the correlation coefficient, r, between target recognition times observed, s_{co}, and the corresponding times predicted, s_{ce}, by the equation. By definition, the correlation coefficient was

$$R = \frac{\sum_{j=1}^{N} (s_{co} - \bar{s}_{co})_j (s_{ce} - \bar{s}_{ce})_j}{n \sigma_{o_j} \sigma_{e_j}}, \tag{26}$$

where s_{co} and σ_o, and s_{ce} and σ_e were the average and standard deviations of s_{co} and s_{ce}, respectively, and N was the number of correlated scores. The values of R were computed as shown in table V.

The multiple-regression technique by the least-squares method showed that Alternative E_a (equations 19 and 24) most nearly fitted the target-finding times recorded in the original human response experiments. It had an R of 0.689. Thus, the human performance prediction equation, with the five k's replaced by their numerical values, became

$$\frac{1}{s_c} = 0.00480 \log_e \mu_\tau + 0.00411 \log_e s_\tau - 0.00476 \log_e \mu_\delta - 0.00954 \log_e s_\delta + 0.05993 \sec^{-1}. \tag{27}$$

Equation 27 was applied individually to the 20 original human-response pictures; the results are plotted in figure 15 and listed in table VI.

The hypothesis that in the population the multiple correlation was zero (that is, that the obtained R was not significantly different from 0) was tested by the F distribution with

$$F_{M,\ N-M-1} = \frac{R^2}{1 - R^2} \frac{N-M-1}{M},$$

where M was the number of predictor variables (M = 4). The value of $F_{M,\ N-M-1}$ computed with this formula was $F_{4,\ 15} = 3.37$. On the other hand, $F_{4,\ 15}$ at the 0.05 level of significance was 3.06; hence, the hypothesis that the population multiple correlation was zero was rejected at the 0.05 confidence level.

TABLE V

COMPUTER REGRESSION ANALYSIS OF

ALTERNATIVES AND CONSTANTS TO ESTABLISH METRIC I

Alternative	k_1	k_2	k_3	k_4	k_5	R
Overall background						
A_a	+0.03723	+0.00633	-0.00583	-0.00391	+0.05528	0.3896
B_a	+0.00856	+0.00015	-0.00063	-0.00018	+0.05078	0.4215
C_a	+0.00133	+0.00018	-0.00009	-0.00005	+0.00679	0.1510
D_a	+0.00020	$+0.00744 \times 10^{-5}$	-0.55555×10^{-5}	-0.00533	+0.00533	0.2446
E_a	+0.00480	+0.00411	-0.00476	-0.00954	+0.05993	0.6889
F_a	+0.00442	+0.00310	-0.00524	-0.00307	+0.07435	-0.0428
G_a	+0.54791	+0.12176	-0.02150	-0.04802	-3.24445	0.4784
H_a	+0.13099	+0.00251	-0.00255	-0.00156	-3.28359	0.4716
A_b	+0.02888	+0.00582	-0.01247	+0.00082	+0.04831	0.5421
B_b	+0.05873	+0.00023	-0.02243	+0.01233	+0.06788	0.3840
C_b	+0.00102	+0.00008	-0.00710	+0.00271	+0.00676	0.3959
D_b	$+0.00777 \times 10^{-2}$	$+0.00144 \times 10^{-3}$	-0.00067	+0.00025	+0.00840	0.0991
E_b	+0.00702	+0.02906	+0.02392	-0.03569	+0.07475	0.0629
F_b	+0.00023	+0.00680	-0.00452	-0.01223	+0.07371	0.2286
G_b	+0.39191	+0.11566	+0.22360	+0.08337	-3.35328	0.5301
H_b	+0.08067	+0.00742	-0.33230	+0.20830	-3.08208	0.4818
Immediate background						
A_a	-0.08211	+0.10242	-0.60466	+0.23663	+0.05689	-0.145
B_a	+0.00902	+0.00049	-0.03039	+0.01507	+0.04939	0.5418
C_a	-0.08829	+0.01376	-0.56107	+0.23613	+0.04214	-0.0832
D_a	$+0.00584 \times 10^{-2}$	$+0.00044 \times 10^{-3}$	-0.00990×10^{-2}	$+0.00252 \times 10^{-2}$	+0.00613	0.4396
E_a	+0.02511	-0.00577	-0.00191	-0.00011	+0.11756	0.0483
F_a	+0.00018	$+0.00173 \times 10^{-2}$	-0.00141	+0.00381	+0.07915	0.0728
G_a	+0.12104	+0.45311	-2.9451	+1.24569	-3.25104	0.4059
H_a	+0.15256	+0.01002	-0.61919	+0.31336	-3.33520	0.5922
A_b	+0.02811	+0.00868	-0.06374	+0.02720	+0.05110	0.5544
B_b	+0.02537	-0.00299	-0.02073	+0.02019	+0.06340	0.1116
C_b	+0.00107	+0.00012	-0.00700	+0.00341	+0.00683	0.4095
D_b	+0.00067	-0.00313×10^{-2}	+0.00068	-0.00037	+0.02370	-0.1164
E_b	+0.01516	+0.00803	-0.00472	+0.00085	+0.08159	-0.1729
F_b	+0.02329	-0.02354	-0.02139	+0.04355	+0.11253	0.1861
G_b	+0.44908	+0.20699	-1.37101	+0.61693	-3.33579	0.5301
H_b	+0.19977	+0.00286	-0.27337	+0.22434	-3.25509	0.5700

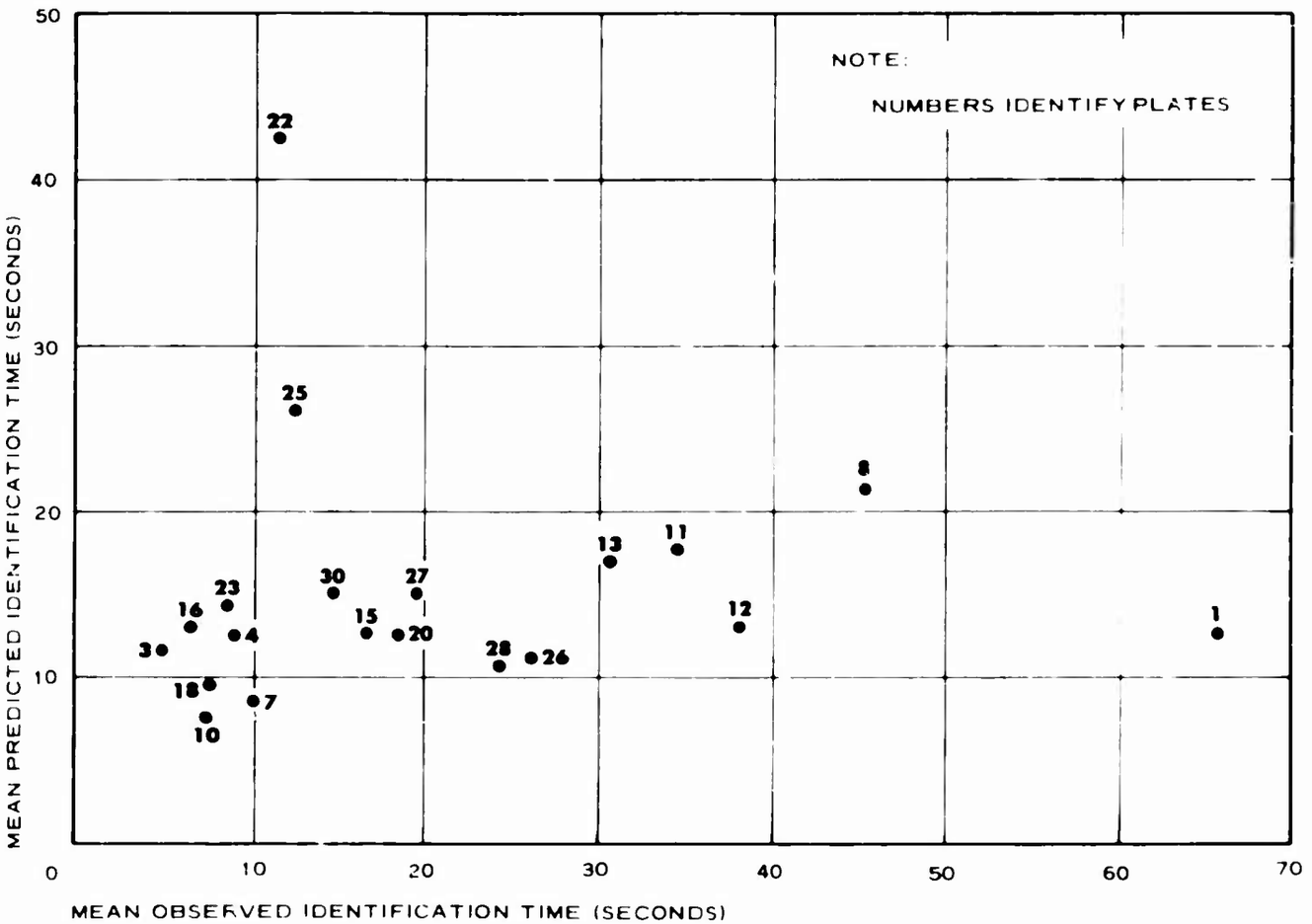

Figure 15 - Scatter Diagram of Metric I Predictions Applied to Original Radar Plates

TABLE VI

METRIC I APPLIED TO ORIGINAL RADAR PLATES TO VERIFY REGRESSION ANALYSIS

Plate	Time to identify target (sec)	
	Actual	Predicted
1	65.8	13.3
3	5.1	11.8
4	8.1	13.2
7	10.1	8.6
8	45.6	41.4
10	7.2	7.8
11	34.3	17.9
12	37.9	12.9
13	30.4	17.0
15	16.8	12.7
16	6.6	13.1
18	7.7	9.7
20	18.4	12.8
22	11.4	42.3
23	8.8	14.3
25	12.3	26.1
26	26.2	11.2
27	19.7	15.0
28	24.4	10.9
30	14.7	15.0

SECTION V

GENERALIZATION OF METRIC I

RADAR

Twenty radar photographs were selected to check the validity of equation 27. Thirteen were new ones selected from Quick Check flights; the other seven were carried over from the original human response experiments for direct comparison of the performance of two groups of subjects.

Positive glass plates were prepared of the 13 new pictures. The same characteristics, except for target relative size which was not a factor in the human-response prediction equation, were measured as before by the flying spot scanner-analog computer system and manual calculations.

The characteristics of three of the new radar plates (Nos. 3, 11, and 13) had negative values or could not be measured at all. These plates were discarded, reducing the number to 10, in addition to the seven held over from the original human-response experiments.

Table VII lists the numerical values of the characteristics and the predicted target-recognition times obtained by substituting these values into equation 27.

At the same time that the predicted target-identification times were being established for the new plates, actual recognition times were being recorded for duplicate plates in experiments with 22 SAC radar navigators at Lockbourne Air Force Base, Ohio. The equipment and procedures were the same as in the original experiments at Griffiss and Pease AFBs except that only five practice trials were run instead of seven. These five practice slides were selected from those used at Griffiss and Pease. At Lockbourne, all 13 of the new high-resolution pictures were used because it was not known at that time that the characteristics of three of them could not be measured. These experiments also included, of course, the seven plates held over from the original tests.

Table VIII shows the results of the Lockbourne experiments. These results are plotted in rank order in figure 16. As in the original experiments and for the same reasons, no data were collected in some tests.

Figure 17 shows the correlation of the identification times between the original and validation subjects for the seven slides common to both tests. The correlation was 0.97; it was significant at the 0.01 confidence level.

Table IX directly compares the predicted and actual target identifications for the 10 new high-resolution radar plates. The correlation coefficient, R, was 0.284, which was not significantly different from zero for this number of plates. When plate number two was omitted, the correlation between the obtained mean scores and the predicted scores for the remaining nine plates was only -0.034. When the median scores were used instead of mean scores, the correlation for the nine plates was -0.048.

The difficulty in measuring the target cells with adequate precision took such

TABLE VII

METRIC I APPLIED TO NEW RADAR PLATES TO PREDICT TARGET-IDENTIFICATION TIMES

Plate	Ratios of transmissivity characteristics				Ratios of differences between target and background characteristics to background characteristics				Predicted identification time (sec)
	$\frac{\mu_t}{\mu_T}$	$\frac{s_t}{s_T}$	$\frac{\mu_d}{\mu_D}$	$\frac{s_d}{s_D}$	μ_τ	s_τ	μ_δ	s_δ	
1	1.44	0.65	1.20	0.70	0.1399	0.1885	0.0333	0.1286	12.6
2	1.73	2.42	1.49	1.72	0.3109	0.8332	0.1611	0.3014	13.6
3	. . .	. . .	. . .	. . .	. . .	. . .	. . .	. . .	. . .
4	0.67	0.56	0.47	0.63	0.1625	0.3457	0.5977	0.2173	15.7
5	1.09	1.58	1.03	1.08	0.0074	0.2129	0.009	0.0059	8.9
6	0.28	2.98	0.50	0.57	1.8514	1.3156	0.5000	0.3244	12.8
7	1.31	0.73	0.75	0.79	0.0734	0.0999	0.0833	0.0558	12.7
8	2.26	1.49	1.51	1.45	0.7025	0.1611	0.1723	0.1397	12.8
9	2.71	2.30	2.05	2.25	1.0790	0.7348	0.5378	0.6944	15.4
10	1.23	1.76	1.01	1.13	0.0430	0.3228	0.0001	0.0150	9.8
11	. .	. . .	. . .	. .	. . .	.	. . .	. . .	. .
12	2.73	8.84	1.56	2.14	0.0963	6.953	0.2010	0.6073	12.4
13	. . .	. . .	. .	. .	. .	. .	. . .	. .	. . .

TABLE VIII

ACTUAL TARGET-IDENTIFICATION TIMES, NEW SET OF RADAR PLATES

Plate	Identification recognition time (sec)			Number correct	Percent correct	Number incorrect	Percent incorrect
	Mean	Median	Standard deviation				
8	7.8	5.5	5.8	22	100.0	0	0.0
12	8.5	4.0	11.5	22	100.0	0	0.0
19	9.4	9.0	4.9	21	100.0	0	0.0
14	10.0	6.0	8.3	22	100.0	0	0.0
10	10.2	5.5	9.7	22	100.0	0	0.0
5	12.1	8.0	10.0	21	95.5	1	4.5
17	14.9	9.0	16.5	22	100.0	0	0.0
6	16.0	11.0	12.9	21	95.5	1	4.5
11	16.3	4.0	31.5	22	100.0	0	0.0
16	29.5	29.0	22.9	15	68.2	7	31.8
7	31.7	15.0	32.6	19	86.4	3	13.6
9	33.9	21.0	87.2	20	90.9	2	9.1
4	39.8	19.5	42.4	18	81.8	4	18.2
15	42.9	20.0	42.5	16	72.7	6	27.3
18	51.6	43.0	30.3	14	63.6	8	36.4
3	54.5	33.0	43.9	13	59.1	9	40.9
1	80.6	49.0	72.7	13	59.1	9	40.9
20	92.1	57.0	74.0	11	50.0	11	50.0
13	115.0	115.0	75.0	2	9.1	20	90.9
2	216.3	255.0	80.7	3	13.6	19	86.4

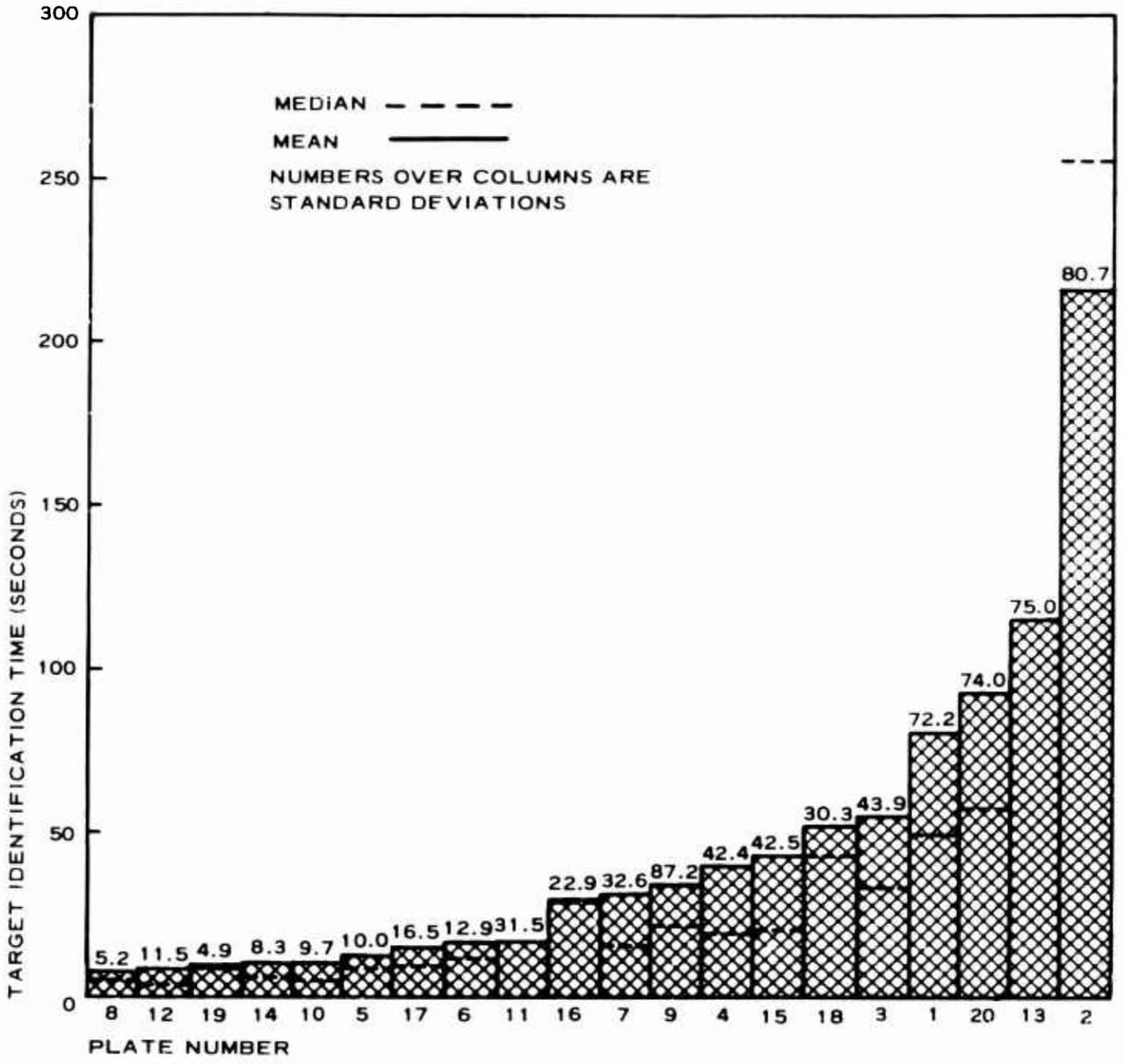

Figure 16 - Actual Target Identification Times, New Set of Radar Plates

a toll of time and resources that it was impossible to use sufficient plates in the validation experiments to assure a significant statistical result. The original R of 0.689 could be expected to shrink considerably with new pictures and subjects even though both groups of subjects had the same abilities and degree of learning. The original and validation groups did have these qualifications, as indicated by the R of 0.97 for the seven common slides; thus the obtained shrinkage is attributable to lack of validity of the prediction equation when utilized with new imagery. The minimum number of plates required to reject the null hypothesis for an R shrunk to 0.284 would have been about 110. This was determined by use of the following formula:

$$F_{4,\ (N-5)} = \frac{0.284^2}{1 - 0.284^2} \frac{N - 5}{4}$$

$$= 0.022(N - 5) .$$

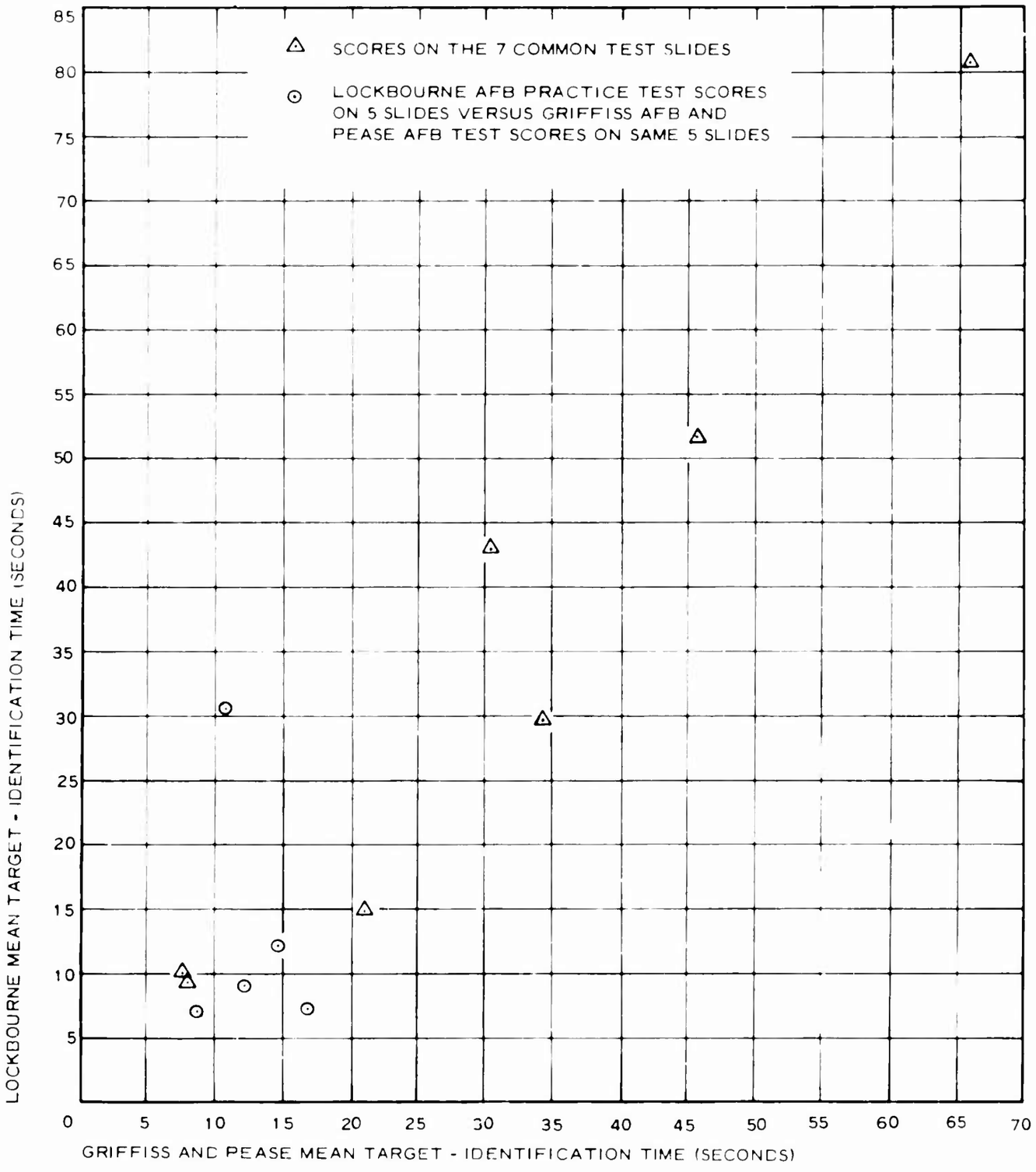

Figure 17 - Target-Identification Times for Seven Radar Slides Common to Two Groups of Subjects

TABLE IX

PREDICTED VERSUS ACTUAL

TARGET-IDENTIFICATION TIMES,

NEW SET OF RADAR PLATES

Plate	Mean identification time (sec)	
	Predicted	Actual
1	12.6	80.6
2	13.6	216.3
4	15.7	39.8
5	8.9	12.1
6	12.8	16.0
7	12.7	31.7
8	12.8	7.8
9	15.4	33.9
10	9.8	10.2
12	12.4	8.5

From an F-distribution table, an $F_{4,\ (N\ -\ 5)}$ was sought that would yield an F significant at the 0.05 level. For N = 130, $F_{4,\ 125}$ = 2.64 from the above equation and $F_{4,\ 125}$ = 2.44 from the table. For N = 105, the corresponding figures were 2.20 and 2.46; thus the total plates required would be about 110. However, there appears to be no tenable reason to suspect that with a large number of plates the correlation would have been as high as 0.284. It can only be concluded that no validity for the precision equation has been demonstrated.

INFRARED AND OPTICAL

Thirteen infrared and 15 optical pictures were selected to check the application of the human-response prediction equation to these two types of imagery. The infrared pictures were acquired during daylight at low altitude in Quick Check flights in equipment that utilized a cooled detector sensitive to near-infrared energy. The optical pictures were acquired at 10,000-ft altitude by a T-11 camera with a 6-in. lens at a scale of 1 to 20,000. The target categories were baseball diamonds, shopping centers, industrial complexes, drive-in theaters, and stadiums.

Positive glass plates were prepared and the same physical characteristics were measured in the same manner as for the high-resolution radar pictures. Table X lists these values and the predicted target-recognition times obtained by substituting them into equation 27. Plate 7 is shown in three parts because it contained three targets.

TABLE X

METRIC I APPLIED TO INFRARED AND OPTICAL PICTURES TO PREDICT TARGET-IDENTIFICATION TIMES

Picture	Ratios of transmissivity characteristics				Ratios of differences between target and background characteristics to background characteristics				Predicted identification time (sec)
	$\frac{\mu_t}{\mu_T}$	$\frac{s_t}{s_T}$	$\frac{\mu_d}{\mu_D}$	$\frac{s_d}{s_D}$	μ_τ	s_τ	μ_δ	s_δ	
Infrared									
1	0.54	1.61	1.04	1.03	0.3919	0.2311	0.0015	0.0009	13.1
4	0.90	0.91	1.31	1.32	0.0111	0.0089	0.0738	0.0755	16.9
5	0.73	1.35	1.16	1.13	0.0999	0.0907	0.0221	0.0150	14.9
6	0.34	1.03	0.78	0.90	1.281	0.0009	0.0625	0.0111	15.3
7a	0.86	1.85	1.13	1.14	0.228	0.3905	0.0150	0.0172	15.0
7b	0.68	1.02	0.84	0.81	0.1506	0.0005	0.0305	0.0445	16.4
7c	0.32	1.59	0.89	0.85	1.445	0.1057	0.0136	0.0265	14.3
10	0.34	1.05	0.78	0.73	1.281	0.0024	0.0621	0.0999	16.1
11	1.62	0.65	1.35	1.31	0.2346	0.1885	0.1885	0.0734	15.7
12	1.03	0.32	1.43	1.42	0.0009	1.445	0.2272	0.2369	17.3
13	0.69	0.62	1.03	0.98	0.1393	0.2329	0.0009	0.0004	12.9
14	0.22	2.47	0.88	0.82	2.765	0.8745	0.0164	0.0052	13.5
15	0.93	0.98	1.52	1.43	0.0053	0.0052	0.1779	0.1293	17.8
16	1.47	3.52	1.47	1.57	0.1503	1.804	0.1503	0.2069	15.8
19	1.03	3.47	1.29	1.36	0.0009	1.758	0.0652	0.953	16.5
Optical									
20	1.31	0.52	1.11	1.87	0.0734	0.4431	0.0109	0.4048	16.0
22	1.40	4.18	1.36	1.39	0.1143	2.419	0.0953	0.1094	15.4
23	1.17	1.49	1.09	1.08	0.0247	0.1611	0.0074	0.0059	14.5
24	1.48	3.05	1.53	1.58	0.1557	1.378	0.1836	0.2129	15.9
25	1.78	10.65	1.72	1.94	0.3418	8.734	0.3014	0.4555	15.8
26	1.86	1.84	1.44	1.64	0.3976	0.3835	0.1344	0.2498	15.6
27	1.18	1.82	1.25	1.24	0.0275	0.3695	0.0500	0.0465	15.6
28	1.51	2.50	1.37	1.45	0.1723	0.9000	0.0999	0.1397	15.7
29	1.09	0.02	0.99	1.05	0.0074	48.02	0.0001	0.0238	13.6
30	1.04	1.24	1.01	0.94	0.0015	0.0470	0.0001	0.0038	14.3
33	1.15	3.23	1.21	1.21	0.0196	1.540	0.3645	0.0365	15.2
34	1.55	3.19	1.52	1.61	0.1952	1.504	0.1779	0.2311	15.9
35	1.36	1.30	1.29	1.35	0.0953	0.0692	0.0333	0.0907	14.9
36	1.18	1.70	1.14	1.11	0.0275	0.2882	[illegible]	0.0109	14.8
37	0.93	2.63	1.01	1.01	0.0053	1.010	[illegible]	0.0001	13.9

The validation tests for the near-infrared and optical pictures were conducted with 21 interpreters at the Photo Intelligence School at Lowry Air Force Base, Colo. Glossy prints were used. The targets were cut from duplicate prints and fixed to cards with transparent tape. Except that the tape darkened them, the targets were exact duplicates of those that the subjects were to identify.

A standard set of instructions was read to each subject (see appendix V). Six practice trials were run and the tests proceeded in the same manner as the original tests in the radar experiments. The operator timed the responses with a decimal stop watch. These data are plotted in figure 18 and tabulated in table XI.

Table XII gives a direct comparison of the predicted and actual target identification times. The correlation coefficient was 0.040 for the near-infrared pictures and 0.068 for the optical. By F-test, neither was significantly different from zero. As in the case of the high-resolution radar pictures, the number of plates was insufficient to ensure significant statistical results, but it was obvious from the very low correlations that the human-response prediction expression (equation 27) was not applicable to infrared and optical pictures.

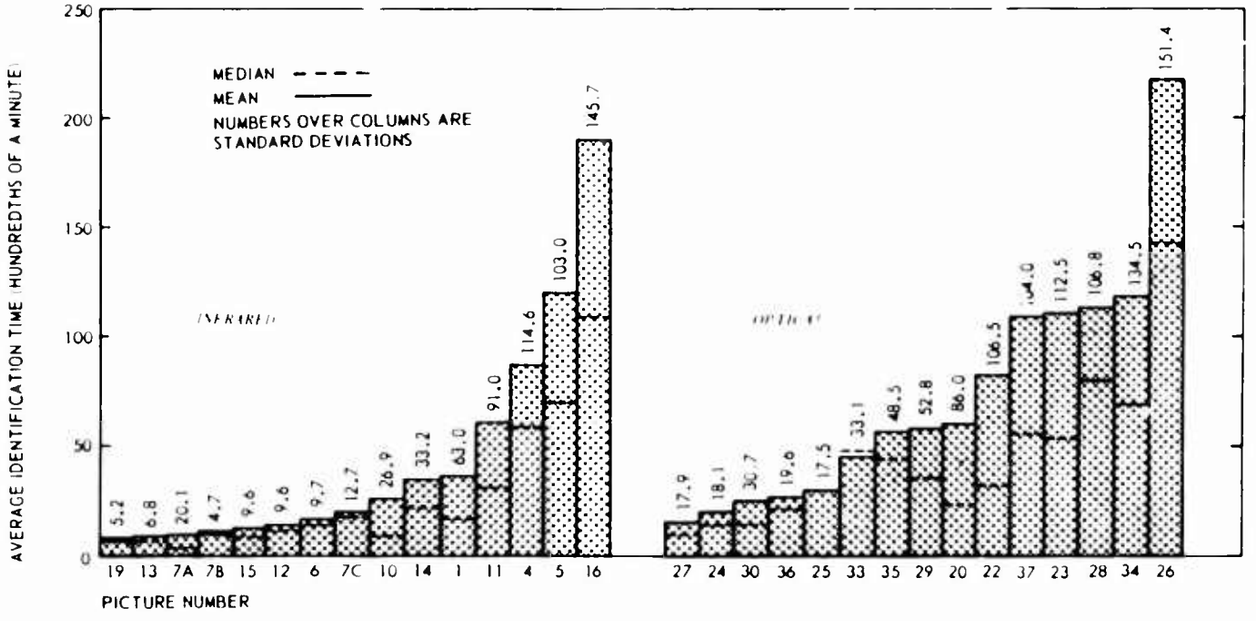

Figure 18 - Actual Target-Identification Times, Infrared and Optical Pictures

TABLE XI

ACTUAL TARGET-IDENTIFICATION TIMES, INFRARED AND OPTICAL PICTURES

Picture	Identification time (hundredths of a second)			Number correct	Percent correct	Number incorrect	Percent incorrect
	Mean	Median	Standard deviation				
Infrared							
19	7.2	6.0	5.2	21	100.0	0	0.0
13	8.4	6.0	6.8	21	100.0	0	0.0
15	12.4	8.0	9.6	21	100.0	0	0.0
12	13.8	11.0	9.6	20	100.0	0	0.0
6	16.3	14.0	9.7	21	100.0	0	0.0
10	26.1	8.5	26.9	20	95.2	1	4.8
14	34.9	21.0	33.2	21	100.0	0	0.0
1	36.3	16.0	63.0	21	100.0	0	0.0
11	61.0	31.0	91.0	21	100.0	0	0.0
4	87.1	59.0	114.6	16	76.2	5	23.8
5	119.2	70.5	103.0	20	95.2	1	4.8
16	189.2	109.5	145.7	10	47.6	11	52.4
7a	9.0	3.0	20.1	21	100.0	0	0.0
7b	11.7	10.0	4.7	21	100.0	0	0.0
7c	20.1	17.0	12.7	21	100.0	0	0.0
Optical							
27	14.9	9.5	17.9	20	100.0	0	0.0
24	19.7	13.0	18.1	20	100.0	0	0.0
30	24.2	13.0	30.7	20	100.0	0	0.0
36	26.4	20.5	19.6	20	100.0	0	0.0
25	29.3	29.5	17.5	20	100.0	0	0.0
33	44.5	47.0	33.1	20	100.0	0	0.0
35	56.5	44.0	48.5	20	100.0	0	0.0
29	57.3	35.0	52.8	20	100.0	0	0.0
20	59.7	23.0	86.0	19	95.0	1	5.0
22	81.9	32.0	106.5	17	85.0	3	15.0
37	108.5	55.0	104.0	20	100.0	0	0.0
23	110.1	54.0	112.5	15	75.0	5	25.0
28	113.4	79.5	106.8	20	100.0	0	0.0
34	118.6	69.0	134.4	14	70.0	6	30.0
26	217.1	143.5	151.4	18	90.0	2	10.0

TABLE XII

PREDICTED VERSUS ACTUAL TARGET-IDENTIFICATION TIMES, INFRARED AND OPTICAL PICTURES

Picture	Mean identification time (sec)	
	Predicted	Actual
Infrared		
1	13.1	21.8
4	16.9	52.3
5	14.9	71.5
6	15.3	9.8
7a	15.0	5.4
7b	16.4	7.0
7c	14.3	12.1
10	16.1	15.7
11	15.7	36.6
12	17.3	8.3
13	12.9	5.0
14	13.5	20.9
15	17.8	7.4
16	15.8	113.5
19	16.5	4.3
Optical		
20	16.0	35.8
22	15.4	49.1
23	14.5	66.1
24	15.9	11.8
25	15.8	17.6
26	15.6	130.3
27	15.6	8.9
28	15.7	68.0
29	34.4	13.6
30	14.3	19.5
13	15.2	26.7
34	15.9	71.2
35	14.9	33.9
36	14.8	15.8
37	13.9	65.1

SECTION VI

CONCLUSIONS AND RECOMMENDATIONS

CONCLUSIONS

Any correlation coefficient obtained as a measure of the goodness of fit of a prediction equation to the target-recognition times used to establish the constants for the equation can be expected to shrink when applied to new pictures. Metric I, which was developed and tested in this study, had an original coefficient of 0.689 which shrank to 0.284 when applied to new pictures. This was too small to be of practical value. While disappointing, this was not entirely unexpected. It was due partly to the unexpected correlation between the four variables chosen for measurement. A contributing factor was the difficulty in calculating the area of each cell occupied by a target. These calculations had to be carried out manually and in general were based on approximations.

Had time permitted, only two of the four selected picture characteristics would have been retained: the average transmissivity and detail. The latter would have been redefined as the number of crossings of the average transmissivity level by the signal instead of as the absolute derivative of the signal. This would make the two independent of each other.

In addition, at least one more characteristic would have been introduced by making use of the crosscorrelation of the target with the whole picture including the target as described in Metric II. The outcome of such crosscorrelation is a surface having a maximum at the location of the target and many secondary peaks at locations where picture elements appear more or less similar to those of the target. The number and relative strength of these peaks could be combined into one additional characteristic. Also, other promising data from Metrics II and III could be combined with the foregoing quantities to quantify image complexity by automatic devices in a more effective manner.

RECOMMENDATIONS

The development of a new metric is recommended. Most, if not all, of the parameters have been identified and the techniques for measuring them have been developed. The slide projector-viewer has been modified for airborne use and currently is being used to obtain operator performance data on another program. These data could be used for both metric derivation and validation studies.

Some minor modifications to the flying spot scanner-analog computer system and procedures would increase the accuracy of the parameter measurements and reduce the time required per measurement. This would require adding an analog-to-digital converter and card-punch unit to the equipment readout and using larger-scale pictures for the target area measurements.

The new prediction equation should be developed with Metric I as the basis. The average transmissivity variable should be retained along with the revised detail variable, and combined with the most promising Metric II and III data to form an equation that would be more effective in quantifying image complexity by automatic devices.

APPENDIX I

METRIC II, STATISTICAL DESCRIPTION OF TARGET-IDENTIFICATION TIME AND PROBABILITY OF CORRECT IDENTIFICATION

INTRODUCTION

One of the objectives of the image-quantification program was to provide a quantitative analytical description or model of the photo-interpretation task. The photo-interpreter was required to examine the photograph and to detect the targets of interest within it. The prediction of target-identification time and the probability that the targets would be correctly detected are considered under the appropriate headings below.

In the photo-interpretation task that was to be used for experimental verification of Metric II, the photo-interpreter was to be given, with each photograph, a graphic representation of the target and associated cues. The graphic representation primarily would show relative locations rather than shapes. The examination time and the correctness of the target identification would be recorded for each photograph.

It was assumed for the analytical description of this task that the photo-interpreter first would select a major reliable cue, and then coarsely (in accordance with the size of the cue) scan the photograph for the presence of this cue. At each scan point that appeared to contain the cue, the photograph would be examined in greater detail with a fine scan for the detection of the actual target or other cues that would reinforce the reliability of the target location. The probabilistic determination of the coarse and fine scanning times for a given photograph would provide an estimate of the time required for proper examination of the photographs. These times were taken to be functions of (1) target complexity, (2) the similarity between the targets and their immediate environments, (3) the number of false match points, and (4) the number of cues required to identify the target and their cue-to-environment similarity. The target parameters were to be evaluated in terms of statistical data obtained through television raster scans of the photographs restricted to targets having the same brightness as the cues. The video signal output of the scanner was to be fed through a low-pass filter to limit the effective resolution of the signal to approximately one-fifth of the cue length. Analytical relationships between these experimentally obtained distribution functions and the scanning times would determine the desired prediction model of the photo-interpretation time.

A photo-interpreter recognizes a target primarily by its shape or pattern, as in airfield runways, railroad yards, and petroleum tank farms, or by its texture and intensity, as in cities and bodies of water. These target characteristics, in addition to the relative locations of targets, may be presented to the photo-interpreter as part of his briefing; more usually they are acquired by him during previous photo-interpretation training and experience. Therefore, the probability that a photo-interpreter will correctly identify the targets of a given picture is essentially the probability that these unique target characteristics are indeed associated with the targets of the picture and are absent from the background.

The evaluation of this probability of the presence of target recognition characteristics requires that these characteristics be converted to a set of target-defining parameters that can be experimentally obtained from the picture. In practice, the picture is subdivided into a matrix of equal target-size areas, and a set of parameters is obtained for each target-size area. Each target class that is of interest to the photo-interpreter can be described in terms of a unique set of experimentally acquired statistical density functions for the distributions of these parameters. Insertion of the parameter values, measured for a given target-size area, into the target-class statistical density functions permits evaluation of the probability that this set of parameters, and therefore the given area that the set represents, is associated with a certain target-class.

TARGET-IDENTIFICATION TIME

Qualitative Description of Photo-Interpretation Task

The photo-interpreter would be given a graphic representation (primarily with respect to location rather than shape) of each target and its associated cues. With this representation he would be required to examine the photograph and correctly detect the target.

Many targets, such as airfields, industrial sites, military installations, and railroad marshalling yards, could not be used as primary cues because they were too small for the photographic scale (20 by 20 nautical miles). Therefore, large neighboring cues, such as culture and rivers, and smaller reinforcing cues, such as roads, railroads, and drainage patterns, were to be used by the photo-interpreter to pinpoint the locations of the targets. In the photo-interpretation procedure, a large and reliable cue would be selected and a coarse scan (the coarseness of which would be set by the size of the cue) would be used to locate and identify the selected cue. To obtain maximum simplicity and reliability in locating the target, the photo-interpreter would select his primary cue to be the brightest (such as cities or culture) or the darkest (such as rivers or lakes) pattern in the photograph. The photo-interpreter then would be concerned only with those patterns having the same intensity level as the given cue.

Once the cue had been located, a more detailed search in the neighborhood of the cue would be necessary to verify, through the remaining auxiliary cues given in the reference graphic, that the located cue was indeed the true one. The complete interpretation process therefore would be one of (1) scanning for patterns of the same brightness level as the cue, (2) locating patterns that matched the shape of the cue, and (3) determining that the cue was either true or false. Statistical estimates of the times required for each of the three subprocesses are given in the following paragraphs. The terminology used to obtain the statistical time estimates is given in table XIII.

Location of Targets

The initial coarse scan to locate the targets of proper brightness (referred to herein as cue-level or i-level patterns) will become more difficult and time-consuming as the similarity between the intensity levels of the target and its immediate environment increases. A measure of pattern-to-environment dissimilarity may be obtained from the statistical distribution of the values for the gradients that exist at the ends of the i-level patterns.

TABLE XIII

TERMINOLOGY FOR TIME FOR

CORRECT TARGET IDENTIFICATION, METRIC II

Symbol	Identification
C_p	Photo-interpreter capacity (bits per second) associated with his recognition of the cue
C_h	Capacity of photo-interpreter (bits per second) to scan a sequence of nonuniform targets
C_x	Number of different i-level target lengths in a given picture
g	Absolute-value intensity gradient before and after each i-level target
I_j	Cue complexity (bits) represented by information transmitted by cue
j_t	Number of cues associated with the desired target
N_f	Number of false match points obtained upon the use of a given cue
N_m	Total number of subareas examined in a given picture
$N(x_i)$	Number of i-level targets with a length of x_i cells
P_i	Probability of encountering an i-level cell
P_m	Probability that the matched cue is not associated with the desired target (probability of a false match point)
P_o	Probability that a cue is matched
T_e	Expected total time required by photo-interpreter to locate the desired target within the photograph
T_ℓ	Total time used by photo-interpreter to locate a target
T_m	Total time required to distinguish between true and false target areas when all the pattern cues are used
$t_s(g)$	Average time delay associated with extraction by the photo-interpreter of a target with edge-gradient g
T_s	Average photo-interpreter time delay resulting from the target-to-environment similarity
x_i	Lengths of i-level targets
Δt_m	Time required to distinguish between the true and false target areas when a single cue is used

Experimentally, the instantaneous absolute-value gradient, g, will be available before and after each i-level pattern; however, the average gradient at each edge will be a better measure of target-to-environment similarity and should be used when possible. A probability density function of the gradient, g, can be derived from its experimentally obtained first two mo nents (reference 7). It will be a truncated Gaussian (reference 8):

$$P(g) = \exp - (a_i + b_i g + c_i g^2) , \tag{28}$$

where $g > 0$.

The term $t_s(g)$ represents the time delay associated with the locating of a target with edge-gradient g. The average (over the entire scene) time-delay per target, T_s, because of target-to-environmental similarity, will become

$$T_s = \int_{g_{min}}^{\infty} \left[t_s(g) \right] \left[\exp - (a_i + b_i g + c_i g^2) \right] dg . \tag{29}$$

A secondary time delay in scanning a sequence of i-level targets (those having the same brightness as the major cue) will be incurred because of nonuniformity of target lengths. Such nonuniformity can be measured from the informational entropy of the distribution, $p(x_i)$, of i-level target lengths:

$$\sum_{x_i = 1}^{x_i = \infty} P(x_i) \log_2 P(x_i) .$$

in bits per target. If C_h represents the capacity of the photo-interpreter in bits per second to scan a sequence of nonuniform targets, the average time delay per target because of target nonuniformity will be

$$\frac{1}{C_h} \sum_{x_i = 1}^{x_i(max)} P(x_i) \log_2 P(x_i) . \tag{30}$$

The total number of i-level targets in the photograph will be

$$\frac{nP_i}{\langle x_i \rangle} ,$$

where

n = the number of cells in the photograph (cell length is assumed to be one-fifth the length of cue),

P_i = probability of encountering an i-level cell, and

$\langle x_i \rangle$ = average length of i-level targets.

The total target location time, T_ℓ, will be

$$T_\ell = \left(\frac{nP_i}{\langle x_i \rangle}\right) \int_{g_{min}}^{\infty} \left[t_s(g)\right]\left[\exp - (a + bg + cg^2)\right] dg +$$

$$\frac{1}{C_h} \sum_{x_i = 1}^{x_{i(max)}} P(x_i) \log_2 P(x_i) \; . \tag{31}$$

Scanning of True and False Match Points

Once a possible match is found for the primary cue of the reference graphic, the photo-interpreter will initiate a finer and more detailed scan to locate and identify the remaining cues of the graphs and thus verify that the possible match point is either true or false. The number of false match points that probably will be encountered in a given scan will be obtained by assuming that the cue is composed of a group of one-dimensional patterns having C_x different lengths and that there are $N(x_i)$ targets within a given x_i length class. The probability, P_o, then will be

$$P_o = \prod_{i = 1}^{i = C_x} P(x_i)^{N(x_i)} \; . \tag{32}$$

$P(x_i)$, the distribution in the photograph of the i-level target lengths, is presented in connection with equation 31.

The deviation from perfect match will be assumed to have taken place independently at any of the cells of the cue so that, for targets that are almost matched, the probability of cue match, P_m, can be expressed as a binomial distribution in terms of P_a, the probability that an individual cell of the cue is matched. The cells will be assumed to have lengths equal to one-fifth that of the cue. If there are N_c cells in the cue, the value for P_a will be obtained from

$$P_o = P_a^{N_c} \; ,$$

$$= \prod_{i = 1}^{i = C_x} P(x_i)^{N(x_i)} \; . \tag{33}$$

Since the briefing knowledge concerning the primary cue will not necessarily be complete, the actual matching of the primary cue with its counterpart in the scene will not be perfect. The degree of mismatch will depend upon the cue. Bodies of water, since they are usually adequately surveyed and therefore accurately located, will exhibit a high degree of match; culture, conversely, cannot be accurately predicted and will in general show a low degree of match. If there are N_c cells in the cue and if m/N_c represents the degree of match between the primary cue and its counterpart in the scene, the probability of match, P_m, at other points in the scene (which in fact is the probability that a false match point has been encountered) will be

$$P_m = \sum_{k=m}^{k=N_c} \frac{N_c!}{(N_c - K)!\, K!} P_a^{\,k} (1 - P_a)^{N_c - k} \tag{34}$$

The problem of establishing a correspondence or match between each cue may be thought of as matching a square area just large enough to include the cue. The quantitized possible match positions are referred to as a correlation matrix.

If N_m is the number of points in this correlation matrix and L (in cells) is the average length of the cue, the probable number of false match-point loops encountered in the scan will be approximately

$$N_f = \frac{N_m P_m P_i}{L} . \tag{35}$$

The time, Δt_m, spent in the investigation of a false or true match point will be a function of the number and complexity of the reference cues that must be identified before the decision is made that the match point is true or false. A cue-identification time, t_j, may be assigned to a given class of cues so that the total match-point time (Δt_m) becomes

$$\Delta t_m = \sum_{j=1}^{j_m} t_j . \tag{36}$$

The value for j_m will, of course, depend upon the number of cues required to render the true or false match-point decision. In general, all the cues present, $j_m = j_t$, in the reference graphic will be used in the true match-point decision, while some lesser j_f (probably 2 or 3) will provide a reliable false match-point decision. With equation 34 used to evaluate P_m, the total scan time, T_m, for the analysis of the true and false match points will become

$$T_m = \left(\frac{N_m P_m P_i}{L}\right)\left(\sum_{j=1}^{j_f} t_j\right) + \sum_{j=1}^{j_t} t_j . \tag{37}$$

Cue Examination Time

The time required to examine a cue depends upon the complexity of its pattern.

Cue patterns vary from the very simple straight roads, railroads, or circular blobs that represent small cultural areas to the more complex drainage patterns, meandering rivers, and large cultural areas.

The complexity of a cue may be quantitatively determined by calculating the amount of information, I, transmitted by the cue (reference 9). For example, the amount of information transmitted by an auxiliary "straight-road" cue due to its orientation and location may be calculated as follows. The probability of a certain orientation of the road is 1/36. This assumes that the photo-interpreter can discern the orientation of the road within a 10-deg azimuthal interval. The probability that the cue is in a certain location will be the ratio of the auxiliary cue length (for the road this is approximately 200 ft) to the length of the primary cue (assumed to be 10,000 ft), and for the road will be equal to 1/50. The information transmitted by the road will be

$$I(\text{road}) = -\log_2 \frac{1}{36} - \log_2 \frac{1}{50} ,$$

$$= 9.07 \text{ bits} . \qquad (38)$$

In this manner, one can obtain a quantitative estimate, in bits, of the complexity associated with the various cues of a given graphic. The actual measured times required by the photo-interpreter to recognize the various cues will provide, in conjunction with the above "informational" values of cue complexity, an estimate of the photo-interpreter capacity, C_p, in bits per second to recognize cues. The average human information rate is approximately 25 bits per second (references 10 and 11) and thus it appears that a cue examination time of less than a second will be sufficient. However, the actual recognition time per cue probably will be much longer because the photo-interpreter will usually refer back and forth from the photograph to the reference graphic during the fine scanning process for reinforcement of his stored description of the cue. Furthermore, a discriminating task, wherein high accuracy rather than speed is the goal, is almost always more difficult (reference 10, pp 130 and 131).

The above calculations of cue-recognition time assume that the contrast between the brightness of the cue and its immediately adjacent background (the edge gradient) will be sufficiently high so that no time delay will be incurred in the reading of the cue pattern. If the contrast is low, an additional time-delay term will be required. This term is of the order of $t_s(g)$. Thus, the cue-examination time, t_j, for a given j-cue will be a function of the complexity of the j-cue, I_j; the photo-interpreter capacity, C_p; and if applicable, the time delay, $t_s(g_j)$, associated with the contrast, g_j, of the given cue, or

$$t_j = \left(\frac{I_j}{C_p} \right) + t_s(g_j) . \qquad (39)$$

Total Photo Examination Time

The total time, T_e, for examination of the photograph will be the sum of the expected pattern-location and match-point analysis times (equations 31 and 37):

$$T_e = \frac{nP_i}{\langle x_i \rangle} \left\{ \int_{g_{min}}^{\infty} \left[t_s(g) \right] \left[\exp - (a + bg + cg^2) \right] dg + \frac{1}{C_h} \sum_{x_i = 1}^{x_{i(max)}} P(x_i) \log_2 P(x_i) \right\} +$$

$$\left\{ \sum_{k=0}^{k=m} \left[\frac{N_c!}{(N_c - K)!\, K!} \right] P_a{}^k (1 - P_a)^{N_c - k} \right\} \times$$

$$\left(\frac{P_i N_m}{L} \right) \left(\sum_{j=1}^{j_f} t_j \right) + \sum_{j=1}^{j=j_t} t_j \,. \qquad (40)$$

Equation 40 will give an average value. Since the total time will be made up of several independent contributions, the variance will be the sum of the individual variances of the several contributions. The various terms of the expression will be either picture-derived and require statistical readout of the photograph and reference graphic or will depend upon the photo-interpreter and be obtained from actual photo-interpretation tests.

Measurement of Picture Parameters

Experimental Acquisition of Picture-Derived Terms

The picture-derived terms will apply to those patterns that have the same brightness as the primary cue and will include the two distribution functions, $P(g)$ and $P(x_i)$, the pattern probability, and average length, P_i and x_i. The average cue length, L, the number of cells in the picture, n, the number in the cue, N_c, and the number in the equivalent correlation matrix, N_m, will be obtained from the picture. Also required will be an automatic or visual observation of the number and complexity of the reference cues, and a restricted scan of the target area on the problem scene to obtain the average cue-to-background contrasts. These measurements will permit calculation of the cue-recognition times, t_j.

The majority of the photographic data will be derived from two quadrature raster scans of the photograph. For the initial coarse scan, the photo-interpreter will adjust the coarseness of the scan and therefore the cellular resolution of his field of vision to accommodate the size of the cue. The cellular size of the two quadrature data-acquiring scans should be made equal to that used by the photo-interpreter in his coarse scan of the photograph (approximately one-fifth the average cue length). In most cases, this will require that the video from the flying spot scanner pass through a low-pass filter with the

filter time constant being determined by the cue size. In addition, a power-relationship with an exponent typically equal to one-half will exist between the physical brightness of a given image and psychophysical judgments of that brightness (reference 12). The video from the flying spot scanner should be further modified to provide this same one-half power relationship. All data measurements are to be made with this modified video.

To simplify the target extraction process and make it more reliable, the photo-interpreter will select for his primary clue a prominent target that is either the brightest or the darkest in the picture. If eight distinguishable brightness bands characterize a given photograph, the picture patterns of interest will lie in either the top or the bottom brightness band. However, a photo-interpreter can distinguish a much finer brightness difference than that accorded by eight bands. This will occur when two narrowly separated levels of brightness associated with a fine brightness-difference characterize adjacent patterns. Accordingly, a pattern length x_i will be of interest when the pattern brightness lies in the same brightness band as the cue and the change in brightness between the target and its neighbor at either edge of the length exceeds an empirically obtained minimum distinguishable value, g_{min}.

The measurement and recording of the above pattern lengths will permit derivation of an analytical distribution function, $P(x_i)$, of these lengths. Integration of all the measured lengths, x_i, will permit the evaluation of P_i (the probability that an x_i pattern exists). The distribution function, $P(g)$, may be derived in a similar manner through the measurement and recording of the gradients that occur at the edges of the pattern lengths, x_i. The remaining parameters n, N_c, and N_m will be a function of the cell size, which is assumed to be one-fifth of L, the average length of the cue.

Empirical Photo-Interpretation Terms

The remaining terms such as the pattern location time, $t_s(g)$, the capacity of the photo-interpreter to discern nonuniform patterns, C_h, and, in a partial sense, the cue identification times, t_j, will be obtained from actual photo-interpretation tests.

Summary

The above photo-interpretation model will be a quantitative estimate of the times required for the photo-interpreter to complete his several subtasks, which begin with a reference graphic that contains a complex of target cues and culminate in the recognition of the target of interest. The photo-interpretation procedure is assumed to be that of first scanning the photograph in a coarse manner for the location of the most prominent and reliable graphic cue. Then those areas that are thought most likely to contain the target will be examined in detail through the use of the other graphic cues for verification of this target area and recognition of the desired target.

It is presumed that the photo-interpreter can largely ignore all targets except those that are at the same brightness level as the target cue. Accordingly, the model will use such experimentally obtained functions of the cue-level targets as the distributions of their pattern lengths and of their pattern-to-environment contrasts along with the percent of the photographic area that these patterns occupy.

These will be combined to form an estimate of the coarse scan time and of the number of false cue-location points that are to be examined further. The complexity of the environment in which the cue is located as well as the complexity of the cue itself will be incorporated into the estimate of the fine-scan time required to examine the smaller areas within which the cues and targets are assumed to lie.

PROBABILITY OF CORRECT TARGET IDENTIFICATION BY THE PHOTO-INTERPRETER

Target Signatures

Table XIV gives the terminology used in the derivation of the probability that the photo-interpreter will correctly identify the target area. A target usually is recognized by a two-dimensional uniqueness of either its pattern, texture, or intensity, or all three. The two-dimensional uniqueness of the target that is observed by the photo-interpreter is converted via a TV raster-like scan into a set of characteristic one-dimensional target signatures. For example, a TV scan, when applied to suitable differentiation (to mark the pattern edges) and interval-measuring (to obtain the pattern widths) circuitry, will generate a sequence of edge-to-edge spacings that is, in effect, a characteristic signature of the geometrical uniqueness of the target pattern. In addition, the sequential readout of the lengths of the edges forms a useful pattern-uniqueness signature. Restrictive storage of only those edges that follow another by a certain allowable distance permits generation of other signatures that would further enhance the targets' pattern uniqueness. This latter edge restriction would permit the preferential examination of targets of a certain width.

The above signatures are representative of the target only for a certain prescribed target orientation and, therefore, would be valid only if the target orientation is known a priori. In the general case, target orientation is not known, so that some preferred orientation must be used with each signature. Such an orientation for the edge-length signature is that in which the average edge length is maximum; the preferred edge-spacing signature has a minimum average spacing. In addition, the complete ensemble of signatures that are obtained at the many different possible pattern orientations forms an orientation-sensitive sequence of measurements that provides useful target-classification information.

Many targets, such as cities and bodies of water, are recognized primarily by their texture and intensity rather than their over-all shape. Signatures that characterize target intensity and texture are available through the readout of the amplitude and derivatives of the original flying spot scanner video before it is processed to form the target edges.

Target Signature Parameters

To facilitate the experimental processing of the data and to simplify the computation of the required probabilities, the many measurements of a target signature sequence will be reduced to a much smaller, but equivalent, set of parameters. Each generated target signature may be likened to a sampled electrical signal and, as such, can be described in terms of its energy and power, its d-c and a-c contents, and its spectral density. If the attribute to be measured at a given point, x_i, in a scan is $M(x_i)$ and if during the course

TABLE XIV

TERMINOLOGY FOR PROBABILITY OF CORRECT TARGET IDENTIFICATION, METRIC II

Symbol	Definition
A_{hi}, $A_{\ell o}$	D-c content or average amplitude of the high- and low-frequency signatures, f_{hi} and $f_{\ell o}$
A_{ij}, B_{ij}, C_{ij}	Experimentally obtained coefficients that determine the Gaussian probability density function, $P(U_i \mid A_j)$
A_j	Target class j
C	Average deviation between the recognition vector difference, a_{ij}, obtained by the photo-interpreter and the model-acquired difference, $R_{tj} - R_{ij}$
E	Total energy of $f(x_i)$
E_{hi}, $E_{\ell o}$	Energy of the high- and low-frequency signatures, f_{hi} and $f_{\ell o}$
f_{dc}	D-c content of $f(x_i)$
$f_{hi}(x_i)$, $f_{\ell o}(x_i)$	High- and low-frequency target signatures derived from $f(x_i)$
$f(x_i)$	The target signature or sequence of N parameter measurements
$G_i(x)$, $G_i(y)^*$	Absolute-value gradient at i-level target edges (both first and second moments)
$M(x_i)$	Parameter measurement obtained at the given scanning point
N	Number of scanning points within a given-size target area
$N_g(x)$, $N_g(y)^*$	The number of i-level-intensity target edges
P_{cj}	Probability that the photo-interpreter has made the correct "no-target" decision at each of the "no-target" subareas; that is, he has correctly located the target
$P(A_j)$, $P(U_i)$	Experimentally obtained prior probabilities of obtaining target class A_j and cumulative parameter value U_i, respectively
$P(A_j \mid U_1 U_2 \cdots U_n)$	Conditional probability that a given subarea represents target class A_j given the set of n cumulative parameter values U_1 through U_n
$P(U_i \mid A_j)$	Gaussian probability density function of the distribution of cumulative parameters, U_i, in target class A_j
R_{ij}	Target class A_j recognition vector obtained from a no-target subarea i
R_j	Target recognition vector for class A_j, obtained by evaluating $\log_e\left[P(A_j \mid U_1 \cdots U_n)\right]$
R_{tj}	The value of the target class A_j recognition vector associated with a subarea known to contain the target class
$\langle t_x \rangle \langle t_y \rangle^*$	Average transmissivity of X and Y scans of a given subarea
$\langle t_x^2 \rangle, \langle t_y^2 \rangle^*$	Transmissivity second moments
U_i	Experimentally obtained value for a given cumulative measurement as f_{dc}, E, A_{hi}, $A_{\ell o}$, E_{hi} or $E_{\ell o}$ of a given parameter signature, $f(x_i)$
x_i	Location of a given scanning point
x_i, y_i^*	Lengths associated with i-intensity-level targets
x_{ij}	Equivalent difference between the target and no-target subarea recognition vectors as obtained by the photo-interpreter
σ^2	Variance of the deviations between the photo-interpreter-obtained recognition vector differences and the model-acquired recognition differences (both C and σ^2 reflect the abilities of the photo-interpreter and are obtained from the results of many photo-interpretation experiments)
$\left\langle \left\lvert \frac{\partial t}{\partial x} \right\rvert \right\rangle, \left\langle \left\lvert \frac{\partial t}{\partial y} \right\rvert \right\rangle^*$	Average of absolute-value gradients
$\left\langle \left\lvert \frac{\partial t}{\partial x} \right\rvert^2 \right\rangle, \left\langle \left\lvert \frac{\partial y}{\partial y} \right\rvert^2 \right\rangle^*$	Gradient second moments

*Cumulative parameters suggested for measurement.

of a single scan there are N- such measurements, the resulting signature of the measured target will be a sampled signal:

$$f(x) = \sum_{i=1}^{i=N} M(x_i)\,\delta(x - x_i)\,, \tag{41}$$

wherein the sampling interval depends upon the attribute to be measured and may or may not be independent of time. The d-c content, f_{dc}, and energy, E, of the complete signature will be obtained by

$$f_{dc} = \sum_{i=1}^{i=N} M(x_i) \tag{42}$$

and

$$E = \sum_{i=1}^{i=N} \left[M(x_i)\right]^2 . \tag{43}$$

A third parameter, N, the number of sample points in the signature, can be obtained readily.

An analysis of the information provided by a parameter in a recognition decision indicates that a computed parameter adds no more information to the decision than is already available from the individual component parameters that entered into its computation (see appendix IV).

The parameters f_{dc}, E, and N describe the signature. Additional energy parameters that may be used to describe an electrical signal, such as power, and d-c and a-c energies and amplitudes, will be computed from the original three parameters. Other parameters will be necessary to describe the signature spectrally. Such information is a function of the interdependence of adjacent signature measurements.

Since the sampling interval is arbitrary and completely independent of time, conventional high- and low-pass filters for temporal analysis of the spectral content of electrical signals are useless. However, high- and low-pass filters are, in effect, differentiating and integrating circuits, and the operations of differentiation and integration can certainly be applied to the pattern signatures.

Accordingly, the output of an equivalent high-pass filter will become

$$f_{hi} = \sum_{i=1}^{i=N} \left[M(x_i) - M(x_i + 1)\right]\left[\delta(x - x_i)\right] , \tag{44}$$

and that of a low-pass signal will become

$$f_{\ell o} = \sum_{i=1}^{i=N} \left[M(x_i) + M(x_i + 1)\right]\left[\delta(x - x_i)\right] . \qquad (45)$$

The d-c content, or amplitude, A, and energy, E, of these spectral components (the number of sample points N has already been explained) will be

$$A_{hi} = \sum_{i=1}^{i=N-1} \left[M(x_i) - M(x_i + 1)\right] , \qquad (46)$$

$$E_{hi} = \sum_{i=1}^{i=N-1} \left[M(x_i) - M(x_i + 1)\right]^2 , \qquad (47)$$

$$A_{\ell o} = \sum_{i=1}^{i=N-1} \left[M(x_i) + M(x_i + 1)\right] , \qquad (48)$$

$$E_{\ell o} = \sum_{i=1}^{i=N-1} \left[M(x_i) + M(x_i + 1)\right]^2 . \qquad (49)$$

Further differentiation and integration of the high- and low-pass spectral components (equations 44 and 45) will provide more detailed spectral descriptions of the signature. Greater spectral detail will be required as the interdependence among adjacent measurements extends beyond one or two intervals.

Statistical Distributions of Target Parameters in Reference Target Classes

The previously described parameters, generated from the target signatures, will form from each signature a set of numbers, U_1, U_2 . . . U_n, for calculation of the desired target detection probability. However, before this can be done, conditional probability distributions, $P(U_i|A_j)$, of the various parameters U_1 through U_n must be determined for each target class A_j. These will be obtained experimentally as follows. The prior readout of many sample patterns of a given target class will provide a set of values for each parameter. From each set of values, an experimental probability-density function of the following form for a single parameter will be derived:

$$P(U_i|A_j) = e^{-(A_{ij} + B_{ij}U_i + C_{ij}U_i^2)} . \qquad (50)$$

Such a function, a truncated Gaussian, can be obtained (see appendix IV) for any set of values that are clustered in a single group, whether the group be tight or loose. However, value sets that contain two or more distinct clusters cannot be adequately represented by the above probability density function. Such data are to be divided into as many portions as there are clusters, with

a probability density function of the above form assigned to each cluster. Details of the conversion of both single and multicluster data sets to the above exponential probability density functions appear in appendix IV.

Target Detection Probability

Target Recognition Vector

In the evaluation of the target recognition vector from which the target detection probability will be obtained, use will be made of the conditional probability, $P(A_j|U_1 \ldots U_n)$, that a given target-size area that is characterized by a parameter set $U_1 \ldots U_n$ belongs to a target class A_j. In accordance with Bayes' rule (reference 13, p 318), and since the parameters will be independent of one another, the probability of target class A_j can be placed in terms of the experimentally obtained parameter density function $P(U_i|A_j)$, or

$$P(A_j|U_1 \ldots U_n) = \frac{P(A_j)P(U_1|A_j)P(U_2|A_j) \ldots P(U_n|A_j)}{P(U_1)P(U_2) \ldots P(U_n)} . \qquad (51)$$

The terms $P(A_j)$ and $P(U_1)$ through $P(U_n)$ refer respectively to the prior probabilities of the target class and of the areas parameter set $U_1 \ldots U_n$. Similar probabilities for the presence of the other target classes within a given area will be formed from the set of parameters associated with a given area. Comparison of the values for the several target probabilities thus obtained will indicate to which target class the area belongs. When the probabilities are converted to logs to facilitate the computations and the prior parameter probabilities, $P(U_1)$ through $P(U_n)$, are omitted (since they are common to all the target class probabilities), a target recognition vector, R_j, for each target class, A_j, can be formed from equations 50 and 51;

$$R_j = \log P(A_j) - \sum_{i=1}^{i=n} A_{ij} + B_{ij}U_i + C_{ij}U_i^2 . \qquad (52)$$

A similar recognition vector will be formed for the nontarget background. The largest recognition vector, among the several that are formed from a given area, will identify the target or nontarget class to which the area most probably belongs. The difference between the two largest target class vectors (since they are logs) will be equivalent to the ratio of the corresponding two target class probabilities (equation 51) and therefore will be proportional to the odds that the given area belongs to a given target class rather than to its nearest competitor.

Recognition Vector Profile

The photo-interpreter for this program is required to locate and identify one or more targets in a given picture, so that in effect he will examine each target-s. subarea for the probability that it contains one of the targets he knows is present. Therefore, a model that is to predict the probability that the photo-interpreter has correctly identified the targets that are known to be present must evaluate at each subarea the recognition vectors for the above known-to-be-present target classes. The sequence of recognition vectors evaluated at each subarea for a given target class form a recognition vector

profile of the given target class. The recognition vectors of a given target class profile are compared with one another so that the area having the larges recognition vector most probably contains the target. Even though the parameter values differ from one area to the next, the prior parameter probabilities may still be neglected, since these probabilities, $P(U_i)$, are assumed to be constant and independent of the value of U_i obtained.

The difference between the two largest recognition vectors of the recognition profile is proportional to the odds that the target is contained in a given subarea rather than in its nearest competitor. A difference can also be found for the recognition vector, (R_t), that corresponds to the area known to contain the target, and for the largest vector among all the other subarea vectors. This latter difference represents the odds that the target is indeed at the target area rather than at its nearest competitor, and is therefore related to the probability that the photo-interpreter has correctly identified the given target. Other useful information may be extracted from the recognition profile. For example, the difference between the target area vector and the average value of the other vectors is a measure of the difficulty the photo-interpreter has in locating and identifying the given target.

Evaluation of the Target Detection Probability

The actual evaluation of the target detection probability (the probability that the photo-interpreter is correct) must relate the varying abilities of the photo-interpreter to detect the targets with the recognition vector results obtained by the model.

One approach is to assume that the model-acquired, target-class, recognition-vector differences $(R_{tj} - R_{ij})$ differ by a constant (C) from the equivalent results obtained by an "average" photo-interpreter. It is further assumed that a Gaussian distribution function describes the variations in the target detection abilities of the various photo-interpreters. Assume (1) that α_{ij} represents the difference in the recognition vectors for target class j obtained by a photo-interpreter at the target subarea and at a given no-target subarea, i (a correct decision will be made by a photo-interpreter at subarea i if the previously determined target vector is greater than the area i recognition vector or $\alpha_{ij} > 0$), and (2) that $R_{tj} - R_{ij}$ is the model-acquired difference between the recognition vectors for target class j evaluated (equation 52) at target area (R_{tj}) and subarea i (R_{ij}). The probability that a correct photo-interpreter decision is made with respect to subarea i will be

$$P(\alpha_{ij} > 0) = \int_0^{\infty} \frac{1}{\sqrt{2\pi}\sigma} \exp\left\{ \frac{\left[- \alpha_{ij} - (R_{tj} - R_{ij}) + C \right]^2}{2\sigma^2} \right\} d\alpha_{ij} . \qquad (53)$$

This probability may be converted into the simpler error function form if

$$x = \frac{\alpha_{ij} - (R_{tj} - R_{ij}) + C}{\sqrt{2}\,\sigma} .$$

Then

$$P(\alpha_{ij} > 0) = \frac{1}{2} \int_{\frac{C - (R_{tj} - R_{ij})}{\sqrt{2}\sigma}}^{\infty} \frac{2}{\sqrt{\pi}} e^{-x^2} dx .$$

This in turn reduces to

$$P(\alpha_{ij} > 0) = \frac{1}{2} \left[1 + \text{Erf} \left(\frac{R_{tj} - R_{ij} - C}{\sqrt{2}\sigma} \right) \right] \tag{54}$$

where

$$\text{Erf} \frac{R_{tj} - R_{ij} - C}{\sqrt{2}\sigma} = \frac{2}{\sqrt{\pi}} \int_0^{\frac{R_{tj} - R_{ij} - C}{\sqrt{2}\sigma}} e^{-x^2} dx , \tag{55}$$

and the values of the Erf function may be found from tables (for example, reference 14, p 116).

Finally the target detection probability, P_{cj}, for target class j is the probability that the photo-interpreter has made the correct no-target decision at each of the N no-target subareas:

$$\left.\begin{aligned} P_{cj} &= \prod_{i=1}^{i=N} P(\alpha_{ij} > 0) \\ \text{or} \\ -\log P_{cj} &= -\sum_{L=1}^{L=N} \log P(\alpha_{ij} > 0) . \end{aligned}\right\} \tag{56}$$

The constants C and σ associated with the Erf function (equation 55) reflect the different abilities of the photo-interpreters who are to participate in the actual psychophysical experiments and are to be obtained from the results of the experiments.

Parameter Measurements

To ensure that the parameter set effectively represents the photographic information that is available to the photo-interpreter, as many parameters as possible should be measured. The parameters that can be extracted from a given readout signature are listed under c above; signatures are suggested under b to describe the two-dimensional photographic characteristics of pattern, texture,

and intensity, which will be used by the photo-interpreter to achieve target recognition. Circuitry must be developed to obtain the suggested parameters and signatures.

Metric I required two signatures, each of which was obtained in the x and y readout directions: the photographic transmissivity, t_x and t_y, and the absolute gradient (the absolute value of the first derivative of the transmissivity).

The following parameters can be made available from the Metric I signature set for Metric II (reference 15, pp 3-25):

1. The average transmissivities, $\langle t_x \rangle$ and $\langle t_y \rangle$,

2. The transmissivity second moments, $\langle t_x^2 \rangle$ and $\langle t_y^2 \rangle$,

3. The average gradients, $\left\langle \left| \frac{\partial t}{\partial x} \right| \right\rangle$ and $\left\langle \left| \frac{\partial t}{\partial y} \right| \right\rangle$, and

4. The gradient second moments, $\left\langle \left| \frac{\partial t}{\partial x} \right|^2 \right\rangle$ and $\left\langle \left| \frac{\partial t}{\partial y} \right|^2 \right\rangle$.

The first and second moments, since the sampling interval and therefore the number of sample points, N, are constant, are equivalent to the signal d-c content and energy.

Two signatures involving the detection of target edges must be obtained for Metric II. These, obtained in both the X and Y directions, are the absolute gradients, $|G|$, that exist in the vicinity of the target edges, and the widths, x, between the successive edges. The readout video will be restricted so that edges are obtained only at the very high or very low transmissivity regions of the photograph; these restrictions are applied because the targets to be considered will have either a very high or very low transmissivity. These two signatures provide the following parameters:

1. Total number of pattern edges, $N_g(x)$ and $N_g(y)$,

2. D-c content of gradient, $\sum_{i=1}^{i=N_g(x)} |G_i(x)|$ and $\sum_{i=1}^{i=N_g(y)} |G_i(y)|$,

3. Energy of gradient, $\sum_{i=1}^{i=N_g(x)} |G_i(x)|^2$ and $\sum_{i=1}^{i=N_g(y)} |G_i(y)|^2$,

4. D-c content of pattern widths, $\sum_{i=1}^{i=N_x} (X_i)$ and $\sum_{i=1}^{i=N_y} (Y_i)$, and

5. Energy of pattern widths, $\sum_{i=1}^{i=N_x} (X_i)^2$ and $\sum_{i=1}^{i=N_y} (Y_i)^2$

These parameters for Metrics I and II are far from being a complete representation of the photographic information that is available to the photo-interpreter because they contain no information of the target orientation (only data from two orientation directions are obtained) or of the phase or interdependence of adjacent signature measurements. Other signatures have been suggested, such as edge length and spacing signatures obtained from edges that have a restricted separation.

Application of Recognition Vector Technique to Automatic Target Recognition

In accordance with the described model, the probability that the photo-interpreter correctly identifies the target within a given picture will be a function (equations 54 through 56) of the recognition vectors evaluated at the various subareas of the picture. An experimental program involving actual performance of the photo-interpretation task would test the validity of this concept.

Once the concept of the recognition vector is proved to be valid, the application of the vector can very readily be extended to actual automatic target-recognition decisions that will alleviate the target identification tasks of the photo-interpreter. The actual computation of the recognition vector (equation 52) from a set of signature parameters can be accomplished easily since only linear operations are involved. The three constants (A_{ij}, B_{ij}, and C_{ij}) of the distribution function for each target class and for the nontarget background class as well as for each parameter can be stored in the recognition equipment as three resistors. Summation of the parameter signal currents, U_i^2, applied to the proper resistors will provide an indication of the target-class recognition vector for a given subarea. Electronic comparison of the various target-class vectors for a given area, to determine the largest vector, will permit automatic identification of the area. The simplicity of the parameter measurement and decisioning process to form a recognition decision allows the entire recognition process to become airborne.

Summary

A model has been described that utilizes various raster readout signatures of the individual subareas of a given picture matrix to evaluate a target detection probability; that is, the probability that the photo-interpreter will correctly identify the target subarea.

The experimentally acquired signatures measure those characteristics as pattern texture and intensity that a photo-interpreter ordinarily uses to identify a target. Each signature of a given subarea, since it is in effect a sampled electrical signal, is described by a set of parameters that reflect the signal's electrical characteristics as signal length, energy, d-c content, and spectral energy distribution

Statistical distribution functions of these parameters are obtained from previously acquired experimental data for each target class that is of interest to

the photo-interpreter. Insertion of the parameters obtained from a given unknown subarea into the corresponding parameter-distribution functions of a given target class results in the formation of a target-class recognition vector for the subarea. This vector actually is the log of the probability that the subarea contains the target class. Comparison of the several target-class and nontarget recognition vectors that are formed at the given subarea from its set of signature parameters permits an identification of the area. Because of the equivalence between this identification decision and that rendered by the photo-interpreter at each subarea, the recognition vectors obtained at all the subareas may be combined (equations 54 through 56) to provide the desired target detection probability.

APPENDIX II

METRIC III, TARGET-IDENTIFICATION TIME

UTILIZING STATIC ANALYZER MEASUREMENTS

INTRODUCTION

Target recognition in Metric III was treated as the process of forming a sufficient correlation between the received data and some stored or a priori data possessed by the observer. A description of the recognition process must therefore be a function of the stored data as well as the received data. A description of data stored within a human observer is virtually impossible to obtain. The next best thing is to use the physical entity that gives rise to the stored data. This will be referred to as the reference graphic. This essentially is a pictorial prediction of selected portions of the area under consideration. At some point in the reference graphic, a target is located and the observer is to find the corresponding point in the complete picture -- the problem scene. Presumably, if the reference and the problem scene are identical, then the observer should experience the minimum difficulty in locating the target. However, the reference may differ considerably from the problem scene both in completeness and accuracy. Therefore, the difficulty of the recognition task appears to be a function of (1) content of reference, (2) difference between reference and scene, and (3) quality and complexity of problem scene. Items 1 and 2 are not independent, since the quality of the reference could, for example, be enhanced at the expense of creating a large difference between it and the problem scene. This model attempts to relate these ideas to the time an observer requires to locate a target. The measurements to be made utilize the correlation functions of the reference scene and the problem scene.

DEFINITION OF MODEL EQUATIONS

Figure 19 represents the reference wherein the origin of the coordinate system x', y' is placed for convenience at the target that is to be found by the observer. Various features or cues are indicated in the reference, and the target may or may not be represented by a feature. The problem then is to locate the corresponding point in the scene (B in figure 19); that is, the observer is to find the coordinates x, y of the target relative to an arbitrary coordinate system in the problem scene. If the problem scene and the reference did not differ in content, then the relationship between them could be expressed by

$$s(x, y) = r(x', y') = r(x - u, y - v), \quad (57)$$

where $x = u$, $y = v$ are the coordinates of the target in the problem scene. Equation 57 states that the scene and the reference look alike except for a shift u, v between their respective coordinate systems. In general, the scene and the reference will not have the same content, so that in addition to a coordinate shift there will be a difference, $n(x, y)$, that must be added to the reference before the two would be equal:

$$s(x, y) = r(x - u, y - v) + n(x, y). \quad (58)$$

The function $n(x, y)$ contains all the differences in content between the problem

scene and the references and is actually defined by equation 58; thus,

$$n(x, y) \equiv s(x, y) - r(x - u, y - v) . \tag{59}$$

The problem of finding the target may now be stated in terms of solving equation 56 for u and v. Thus, the observer, having been briefed with r(x', y'), now inspects s(x, y), seeking satisfactory values for u and v. Since the term n(x, y) is not known, the only recourse is to give it a probabilistic interpretation. This is equivalent to the statement that, although n(x, y) is unknown, certain constraints upon it are assumed. Solutions for u and v therefore will be probabilistic. The target coordinates x = u, y = v can never be known with certainty. It is only possible to maximize the probability that the correct values have been selected.

Dependent upon the assumptions, a probability distribution for the coordinates of the target is obtained. Associated with this final distribution is a gain of information due to the process. It is proposed that the model relate the recognition time, $\bar{t}$, to the gain of information, I_g; thus,

$$\bar{t} \propto \frac{1}{\bar{I}_g} . \tag{60}$$

In addition to the information gain, a term, C(s), expressing the complexity of the scene, is included. This is a measurement of the detail in the scene. The expression for t therefore becomes

$$\bar{t} = \frac{1}{k\bar{I}_g} + C(s) . \tag{61}$$

Two cases are considered, depending upon the form of the reference material. These are continuous-level and three-level (black, gray, and white). Equation 61 is developed as follows for each of these cases.

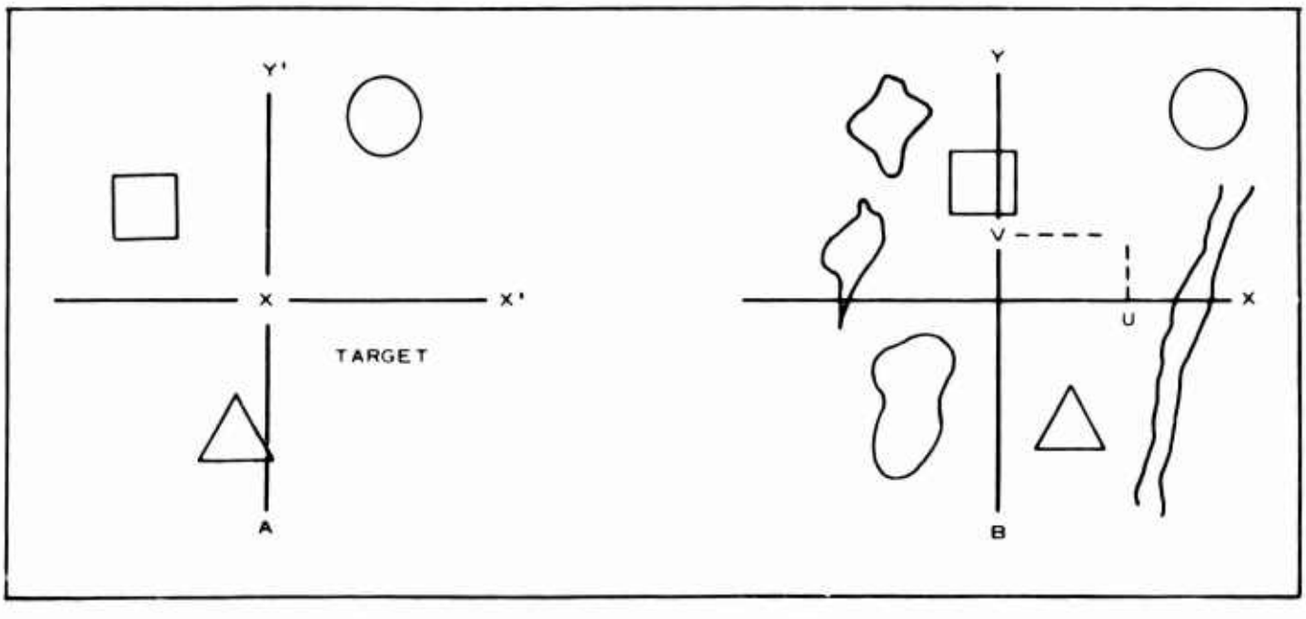

Figure 19 - Representation of Metric III Target Reference

CONTINUOUS-LEVEL REFERENCE

The variance of u is given by

$$\sigma u^2 = \frac{K\phi_o^2}{A_r R_i \left[\phi_u''(0,\,0)\right]^{3/2} \left[\phi_v''(0,\,0)\right]^{1/2}}, \tag{62}$$

and for v by

$$\sigma v^2 = \frac{K\phi_o^2}{\left[A_r R_i \phi_u''(0,\,0)\right]^{1/2} \left[\phi_v''(0,\,0)\right]^{3/2}}, \tag{63}$$

where

$\phi_o = \phi(0,\,0)$ = the amplitude of the peak of the autocorrelated reference,

$\phi_u''(0,\,0)$ = the second derivative of the autocorrelated reference with respect to the u direction evaluated at the peak,

$\phi_v''(0,\,0)$ = the second derivative of the autocorrelated reference with respect to the v direction evaluated at the peak,

A_r = the area of the reference,

R_i = the reference to noise power in the scene, and

K = a constant.

The information gain represented by equations 62 and 63 is given by

$$I_g = \log \frac{A_r R_i \phi_u''(0,\,0)\phi_v''(0,\,0)}{\left[K\,\phi(0,\,0)\right]^2}. \tag{64}$$

The complexity of the problem scene, C(s), is measured by the logarithm of its normalized derivative energy,

$$C(s) = k_2 \log \frac{1}{\phi(0,\,0)} \left[\phi_u''(0,\,0) + \phi_v''(0,\,0)\right], \tag{65}$$

where ϕ denotes the problem scene autocorrelation function. The model for this case, equation 61, therefore becomes

$$\bar{t} = k_1 \log \frac{K\left[\phi(0,\,0)\right]^2}{A_r R_i \phi_u''(0,\,0)\phi_v''(0,\,0)} + k_2 \log \frac{1}{\phi(0,\,0)} \left[\phi_u''(0,\,0) + \phi_v''(0,\,0)\right]. \tag{66}$$

THREE-LEVEL REFERENCE

The standard deviation of u is given by

$$\sigma u = K \frac{W_x W_y}{A_r R_i \left[\frac{\phi_u''(0,\ 0)}{\phi(0,\ 0)}\right]}, \tag{67}$$

where

$\phi_u''(0,\ 0)$ = the magnitude of the slope of the autocorrelated reference taken in the u direction evaluated at u = 0+,

W_x = the minimum width of cues in the x direction,

W_y = the minimum width of cues in the y direction, and

K = a constant.

For the v direction, the standard deviation is given by

$$\sigma v = K \frac{W_x W_y}{A_r R_i \left[\frac{\phi_v'(0,\ 0)}{\phi(0,\ 0)}\right]}, \tag{68}$$

where $\phi_v'(0,\ 0)$ is the magnitude of the slope of the autocorrelated reference taken in the v direction evaluated at v = 0+.

The information gain represented by equations 67 and 68 is given by

$$I_g = \log \left\{ \left(\frac{A_r R_i}{W_x W_y}\right)^2 \frac{\phi_u'(0,\ 0)\phi_v'(0,\ 0)}{K\left[\phi(0,\ 0)\right]^2} \right\}. \tag{69}$$

Again, by use of equation 65 for the complexity of the scene, the average time, from equation 62, becomes

$$t = k_1 \log \left\{ K \left(\frac{W_x W_y}{A_r R_i}\right)^2 \frac{\left[\phi(0,\ 0)\right]^2}{\phi_u'(0,\ 0)\phi_v'(0,\ 0)} \right\} + k_2 \log \left\{ \frac{1}{\phi(0,\ 0)} \left[\phi_u''(0,\ 0) + \phi_v''(0,\ 0)\right] \right\}. \tag{70}$$

The undetermined constants in equations 66 and 70 would be obtained by a least-squares fitting process similar to that discussed for Metric I.

APPENDIX III

ANALOG COMPUTER CIRCUITRY

INTRODUCTION

The four transmissivity characteristics of the pictures selected for Metric I were measured by a flying spot scanner-analog computer setup. The computer programmed the scan of the flying spot and read out the measurements of each characteristic on an individual channel. Each picture was divided into 256 equal areas, 16 vertical and 16 horizontal. Each area, or cell, was scanned 10 times horizontally and 10 times vertically (fast scan). The cells were scanned column by column and row by row (slow scan).

SCAN CONTROL CIRCUITRY

The fast scan is the basic clock pulse train that times and synchronizes the scan control. It is generated by means of a group of computer amplifiers (18, 19, and 20) in figure 20. Because of the limiter branches in its feedback, the output of amplifier 20 will be either +20 or -20 v. This output is compared to the ramp output of amplifier 19 at the input of amplifier 18. Each time the ramp reaches the 20-v level, the output of amplifier 18 changes polarity. This flips the output of amplifier 20 to the opposite state. The gains of the two input branches into amplifier 19 are adjusted to give a slowly rising ramp of one polarity and a fast-climbing ramp of the other polarity, the last corresponding to the fly-back time between scan lines. The upper trace of figure 21 shows the wave shape involved.

The short pulse, as reflected at the output of amplifier 20, is used to generate the slow-scan by means of integrator 24 and comparator 22. When the staircase output of 24 reaches the voltage set by potentiometer 13, relay R1 is energized and momentarily discharges the integrator back to zero. This happens every 11 steps, as shown by the middle tracing of figure 21. Two parallel blanking circuits energized by the fast and slow scans generate a short and a long blanking pulse which, after being shaped and properly biased in amplifiers 10 and 11, are applied either to the cathode of the scanner by amplifier 11 or to electronic switches at the computer operating on the video signal (amplifiers 4 and 4a). The short pulse exists at the beginning and at the end of each fast scan. The long pulse covers the transient time between one slow scan and the next, obliterating one of the 11 steps. Thus, each elemental square of the picture is covered by 10 scan lines in each direction. Blanking is applied at the scanner if the end product is to be a picture or at the electronic switch if the end product is to be a voltage. The blanking pulses are shown at the lower graph of figure 21.

The blanking circuits (figure 22) combine a level detector and a timed-pulse generator. They were built as separate units and added to the computer. The front part of the circuit is a Schmitt trigger, the level of which can be adjusted by means of a potentiometer. This establishes the timing of the leading edge of the blanking pulse. The output of the level detector (trigger) is applied to the adjustable-delay multivibrator shown at the right-hand side of the diagram. There, the duration of the generated pulse is controlled by capacitor C_d. The durations of intraline and interelement blankings are established by properly selecting the values of these capacitors.

The same pulse from relay R1 that discharges slow-scan integrator 24 also

triggers a bistable multivibrator circuit, called the alternator, whose alternating output pulses energize relays R2 and R3. These relays operate indicator lights, R and Y, and a counter C, and also switch the fast and slow scans alternately between the X and Y deflection coils of the scanner via amplifiers 11 and 12. Through the same amplifiers, constant bias voltages are added (potentiometers 4 and 5) to position the spot properly at one of the corners of the picture; also, either the horizontal or the vertical steps are introduced here. These steps originate at the alternator, which has two plate voltages. One voltage is differentiated to produce two pulses of opposite polarities per switching. One pulse is isolated through a biased diode and fed into the X-step generator, amplifiers 7 and 15. These amplifiers are arranged in the same manner as amplifiers 22 and 24; hence a staircase output is produced by amplifier 11.

The comparator amplifier, 15, is set through potentiometer 14 to operate when the alternator has completed 16 periods (when the 16 square elements of one row on the picture have been scanned). At the end of this interval, relay R4 discharges integrator 7 and at the same time increases the output of integrator 21 by one step, thus moving the scan one column over. As shown in figure 20, this output is added to the input of the other deflection amplifier, 12. Comparator amplifier 24B, in series with relay R4, is adjusted to energize relay R5 at the end of 16 steps out of integrator 21. This throws the computer to the "hold" position, freezing all voltages and terminating the process.

Figure 23 shows in succession the slow scan produced by amplifier 24; the pulse from relay R1 into the alternator; one of the alternator outputs; the pulse that is part of the derivative of this output and feeds integrator 7; the output of this integrator (horizontal steps); and the output of integrator 21 (vertical steps).

Figure 24 shows the alternator circuitry. The upper part is a monostable multivibrator actuated by the pulse from relay R1. Its purpose is to generate a reliable pulse of constant length undisturbed by the noise peaks of the input pulse arising from contact noise. The output of this part triggers the bistable multivibrator shown in the lower part of the figure, which turns on and off alternately a red and a yellow lamp indicating to the equipment monitor the direction of the fast scan (X or Y); it also steps counter C, which indicates the position of the elemental square last scanned.

The outcome of the scan control circuitry described above is the coverage of a square picture area with a length, L, on each side of

$$L = 2.25 \text{ in.} \tag{71}$$

by a matrix of N^2 square elements, where

$$N = 16, \tag{72}$$

each having side length of

$$\ell = 0.140 \text{ in.} \tag{73}$$

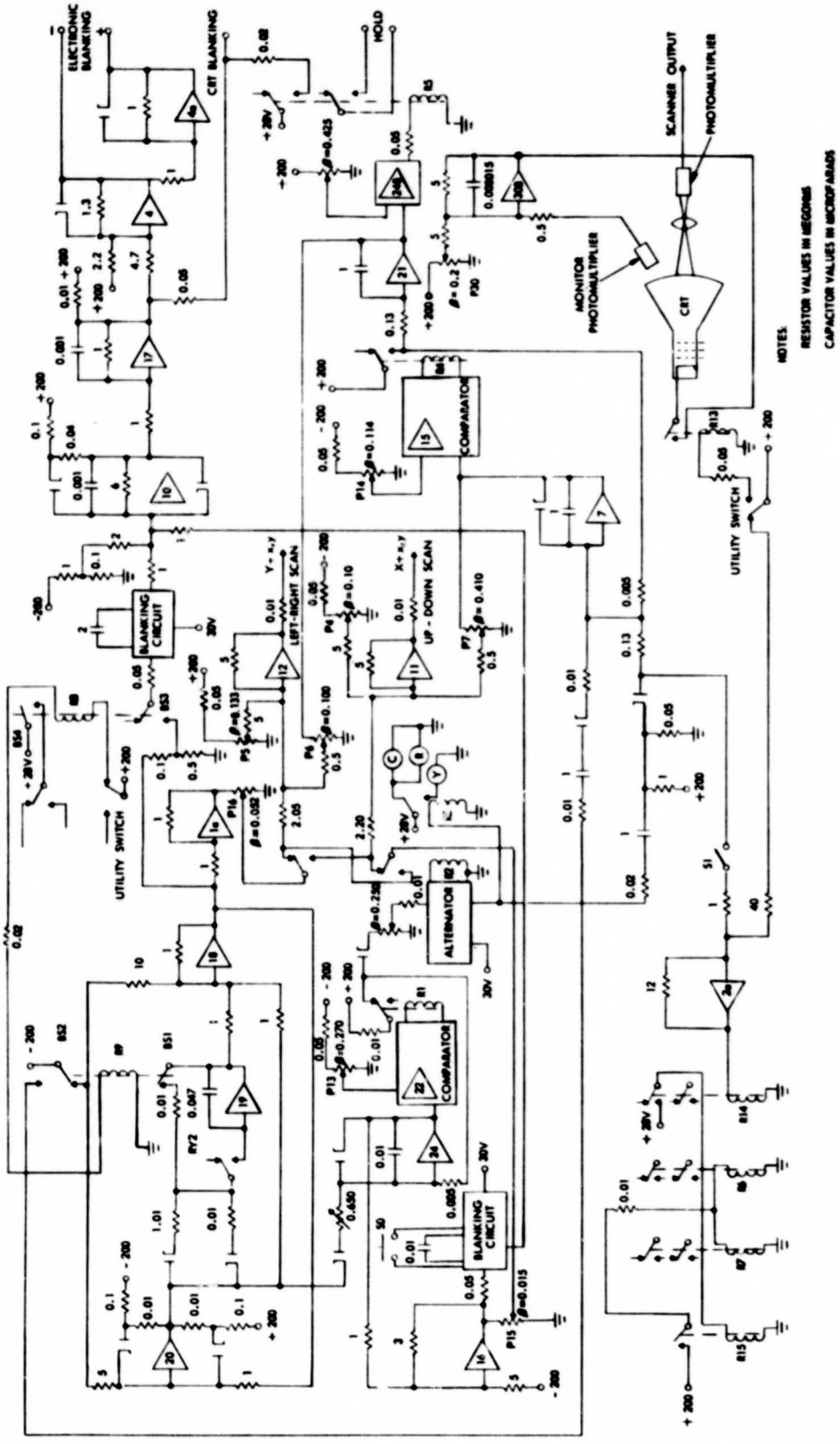

Figure 20 - Analog Computer Scan-Control Circuit

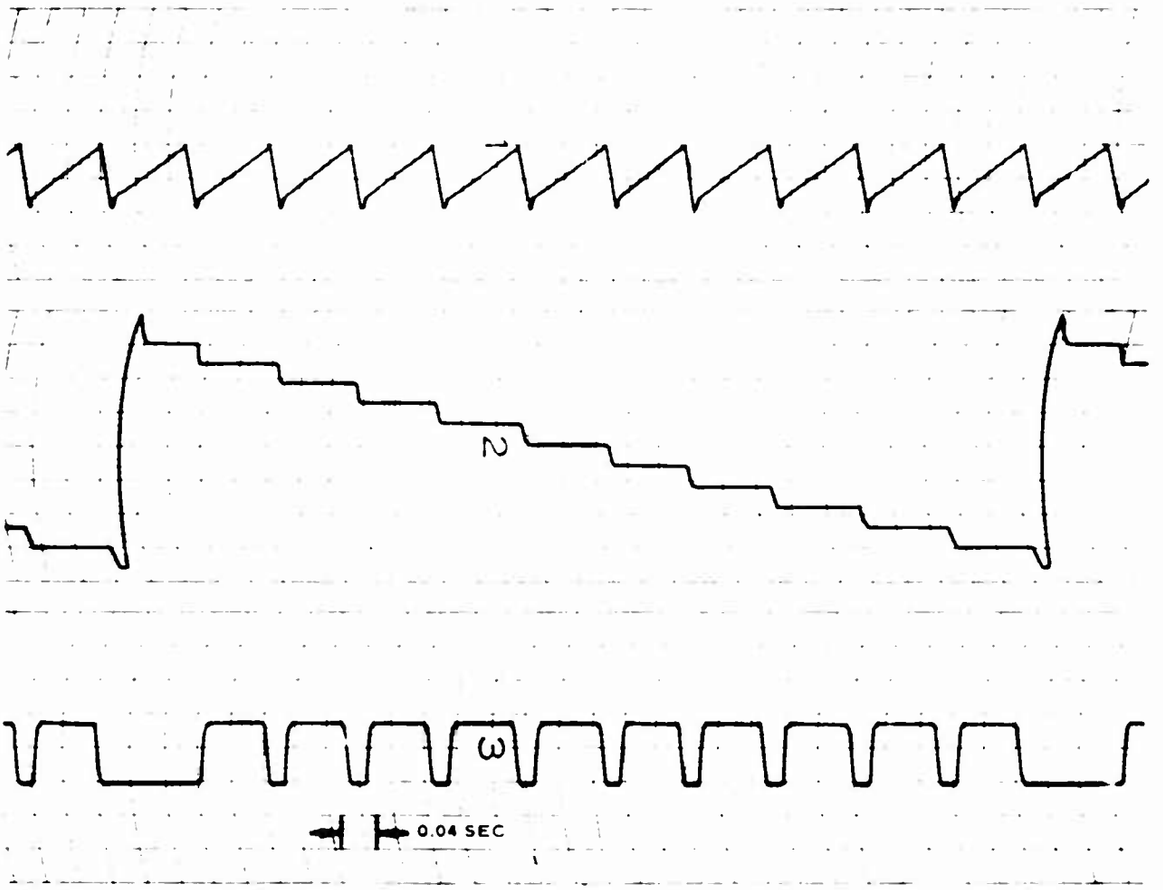

Figure 21 - Fast Scan Patterns

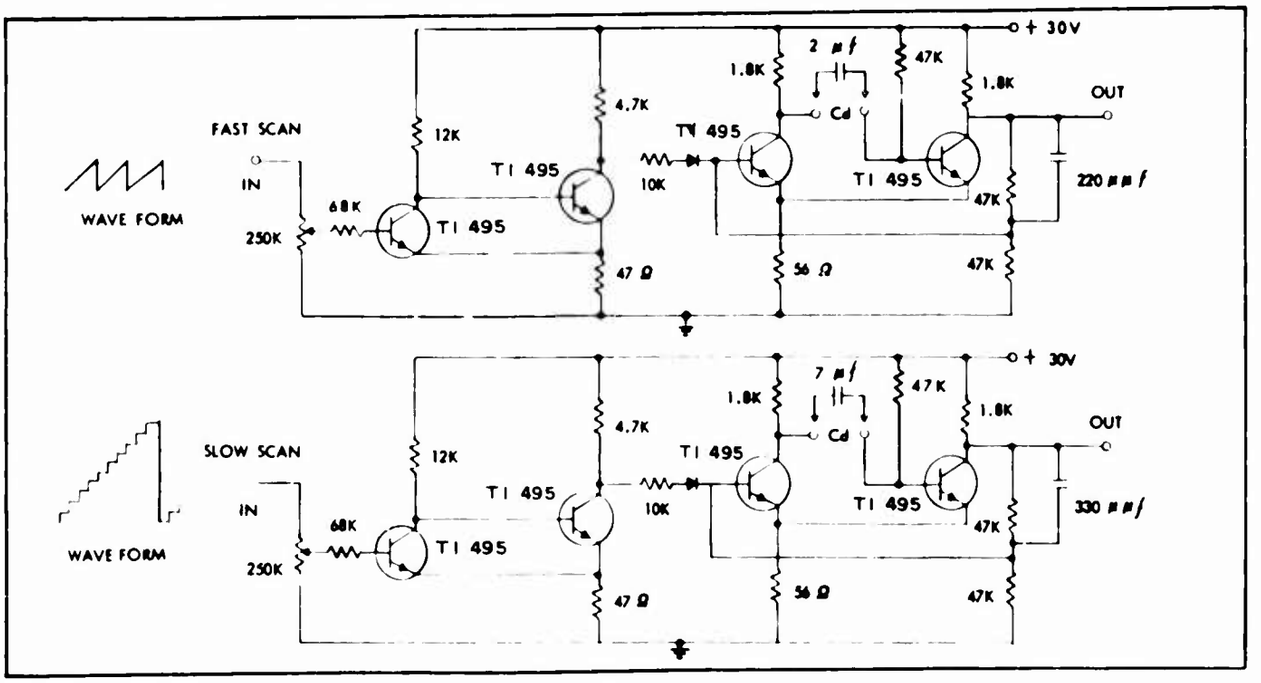

Figure 22 - Blanking Circuit

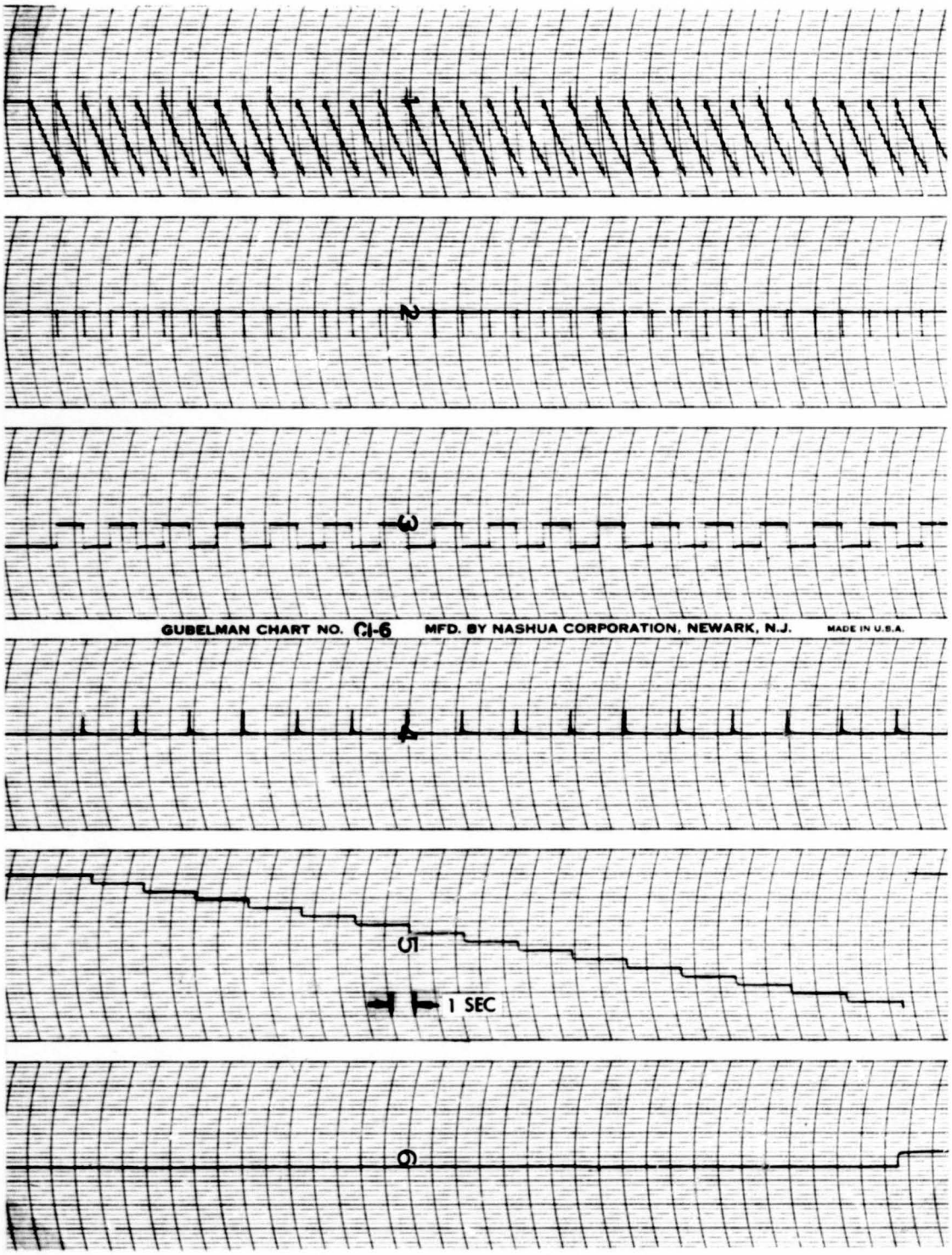

Figure 23 - Fast and Slow Scan Patterns

Each element in turn is scanned by a number of

$$n = 10 \tag{74}$$

equidistant parallel lines in the X direction and by as many in the Y direction. The duration of each scan line is

$$t_1 = 0.072 \text{ sec}, \tag{75}$$

and therefore the writing speed at the picture plane is very nearly

$$u = \frac{\ell}{t_1}$$

$$= 2 \text{ in. per second}. \tag{76}$$

A blanking interval of 0.024 sec is provided between adjacent lines and 0.120 sec between elements and between rows.

An additional feature of the scan control circuitry is the brightness control loop shown at the lower right-hand part of figure 20. In this loop, the output of a monitor photocell facing the cathode ray tube is continuously compared to a reference voltage (potentiometer P_{30}) at the input of amplifier 30B. The output of this amplifier, connected to the control grid of the crt, keeps the light flux emanating from the flying spot at a constant level.

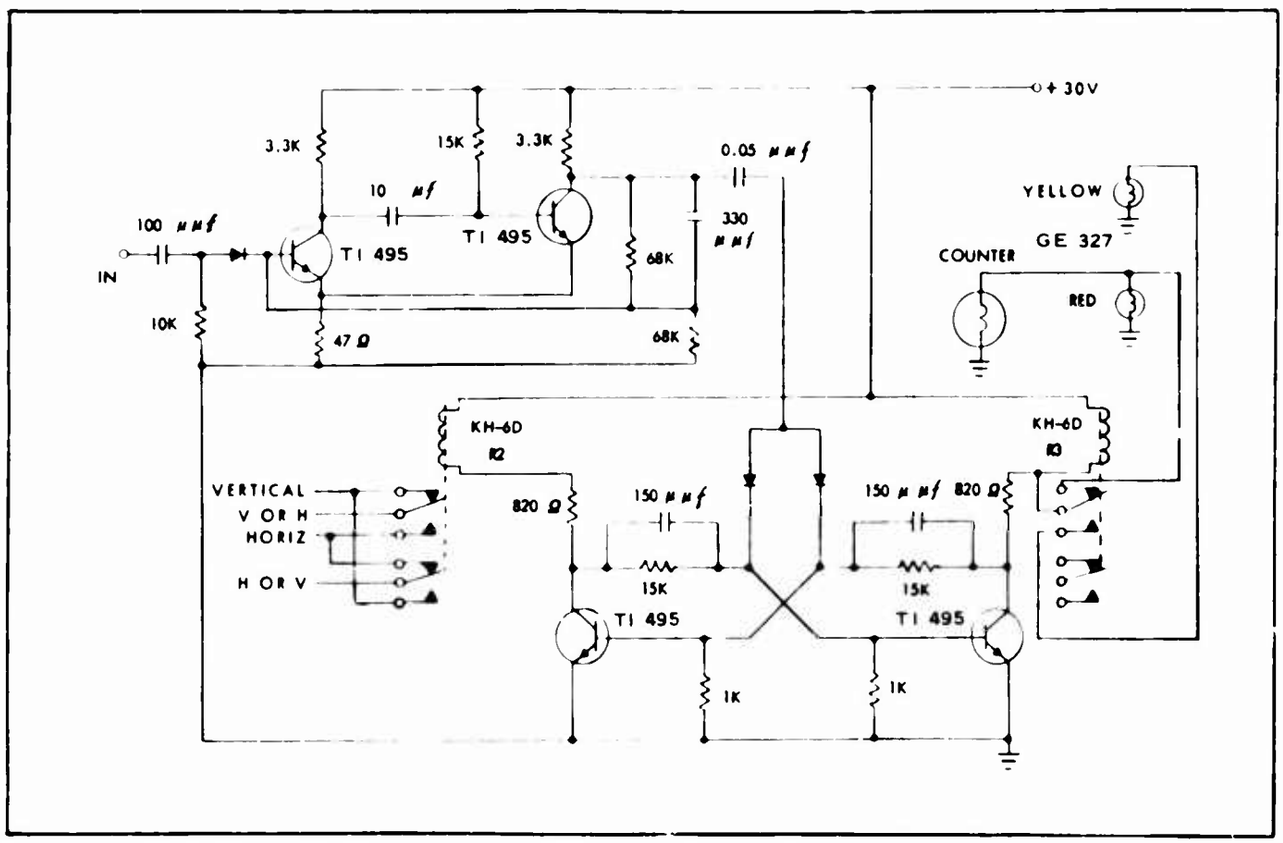

Figure 24 - Alternator Circuit

SIGNAL MEASURING CIRCUITRY

The electrical output of a photomultiplier tube (the video signal, v) is channeled to the computer via amplifier 1b, which is contained in the scanner, and a gain-control potentiometer, P, inserted between the amplifier output and ground. The signal is presented to the computation circuit (figure 25) by two buffer amplifiers, 14 and 17A, which have the transfer function

$$\frac{V_1}{v} = \frac{-k_1}{\tau_1^2 s^2 + 2\zeta\tau_1 s + 1}, \tag{77}$$

with

$$k_1 = 5,$$

$$\tau_1 = 3.35 \times 10^{-5} \text{ sec, and} \tag{78}$$

$$\zeta = 0.5.$$

The amplifier therefore behaves very much like a simple low-pass filter with a 3-db cut-off point at

$$f_1 = 4750 \text{ cps}, \tag{79}$$

corresponding to spatial cut-off frequency at the picture plane of

$$f_{1*} = \frac{f}{ru}$$

$$= 3165 \text{ cps per inch}, \tag{80}$$

where u is given by equation 76 and r is the magnification factor of the optical path between picture plane and crt face; that is,

$$r = \frac{L}{L_o} = 0.75. \tag{81}$$

The above frequencies provide a margin for additional filtering, rendering the circuit less sensitive to noise and stray pickups. This is so because, assuming a practical spot size of $z_o = 2.5$ mils at the crt face, or

$$z = rz_o = 1.87 \text{ mils} \tag{82}$$

at the picture plane, the cut-off point because of spot size will be

$$f_{2*} = \frac{1}{z} = 530 \text{ cps per inch} \tag{83}$$

or

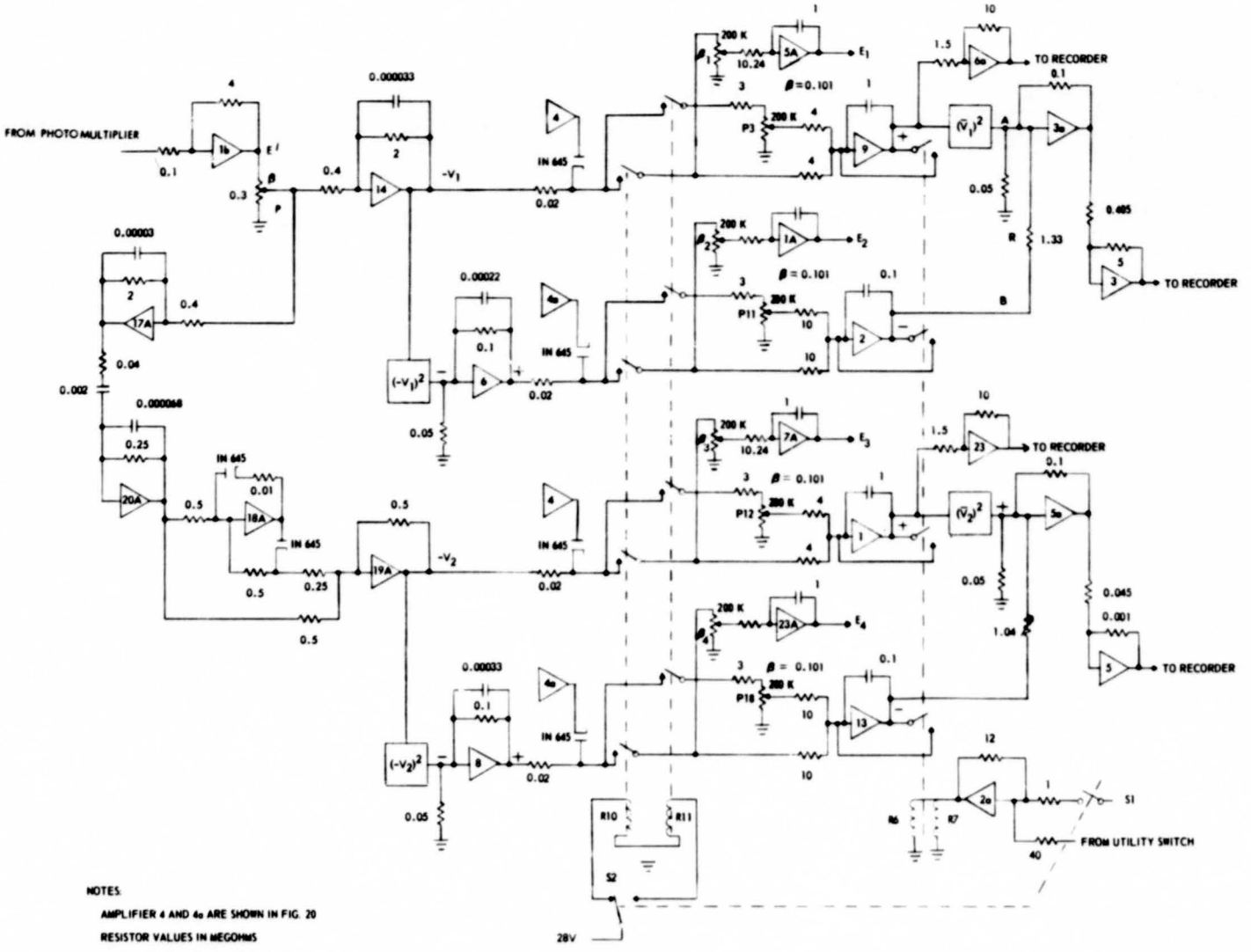

Figure 25 - Signal Processing and Measuring Circuit

$$f_2 = uf_{2*} = 1,060 \text{ cps} . \tag{84}$$

Thus, the crt spot contribution may be described by the approximate transfer function of

$$G_{crt}(s) = \frac{1}{1 + \tau_2 s} , \tag{85}$$

with

$$\tau_2 = \frac{1}{2\pi f_2} = 15 \times 10^{-5} \text{ sec} . \tag{86}$$

The additional filtering was implemented by means of a 33-$\mu\mu$f capacitor across the 2-meg feedback of amplifier 14 or 17A, corresponding to a time constant of $\tau_3 = 6.6 \times 10^{-5}$ sec and a cut-off frequency of 2410 cps, or about 1200 cycles per inch. Hence, equation 77 has to be changed to

$$\frac{V_1}{v} = \frac{-k_1}{(\tau_1^2 s^2 + 2\zeta s + 1)(\tau_3 s + 1)} , \tag{87}$$

with

$$\left.\begin{aligned} k_1 &= 5 , \\ \tau_1 &= 3.35 \times 10^{-5} \text{ sec} , \\ \zeta &= 0.5, \text{ and} \\ \tau_3 &= 6.6 \times 10^{-5} \text{ sec} . \end{aligned}\right\} \tag{88}$$

The measured response characteristics are shown in figure 26.

V_1 serves to derive the four parameters of interest for the present effort, namely the mean and variance of transmissivity and of detail, all of which have already been discussed.

In terms of voltages over each elemental square, these quantities will be

$$\mu_{ti} = \frac{1}{2mt_1} \sum_{i=1}^{m} \int_o^{t_1} \left[V_1(x, y_i) + V_1(x_i, y) \right] dt , \tag{89}$$

$$s_{ti} = \frac{1}{2mt_1} \sum_{i=1}^{m} \int_o^{t_1} \left[V_1^2(x, y_i) + V_1^2(x_i, y) \right] dt - \mu_{ti}^2 , \tag{90}$$

$$\mu_{di} = \frac{1}{2mt_1 u} \sum_{i=1}^{m} \int_o^{t_1} \left[\left| \frac{\partial}{\partial t} V_1(x, y_i) \right| + \left| \frac{\partial}{\partial t} V_1(x_i, y) \right| \right] dt \,, \tag{91}$$

$$s_{di} = \left\{ \frac{1}{2mt_1 u} \sum_{i=1}^{m} \int_o^{t_1} \left[\left| \frac{\partial}{\partial t} V_1(x, y_i) \right|^2 + \left| \frac{\partial}{\partial t} V_1(x_i, y) \right|^2 \right] dt - \mu_{di}^2 \right\} \,, \tag{92}$$

and also

$$\left.\begin{aligned} \alpha &= \ell^2 = 0.0196 \text{ in.}^2 \\ \text{or} \\ \alpha' &= 2mt_1 = 1.40 \text{ sec} \,, \end{aligned}\right\} \tag{93}$$

where α is the area of the elemental square, and α' its equivalent in time units. Accordingly, four parallel branches are needed to compute μ_{ti}, s_{ti}, μ_{di}, and s_{di} concurrently.

To measure μ_{ti}, integrator 9 of figure 25 is used after provisions are made to

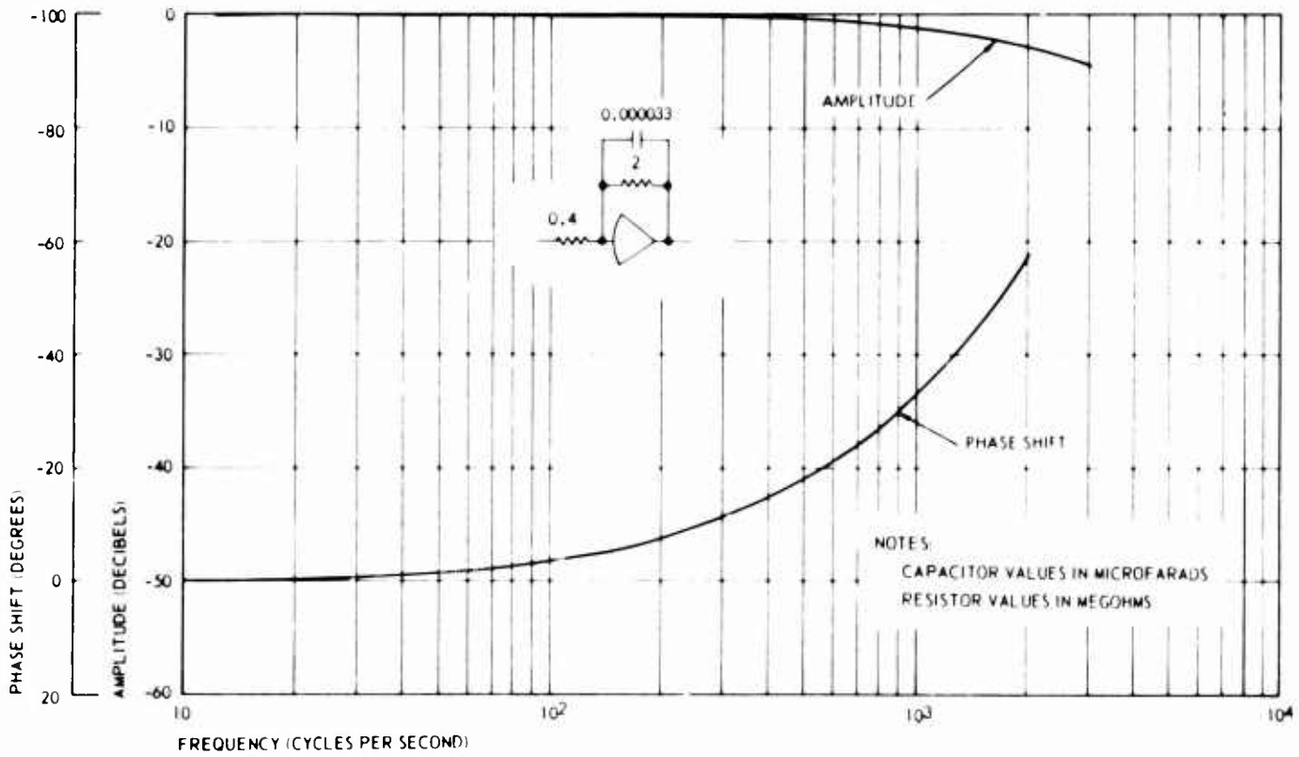

Figure 26 - Amplifier Characteristics

blank V_1 electronically between the ending of one line and the beginning of the next, as well as between square elements. To this end, the positive blanking pulse supplied by amplifier 4, figure 20, is used to annihilate the always negative V_1 at the input of the integrator amplifier 9 by driving to ground the diode shown in series with this amplifier output. A 0.2-v bias voltage would have been necessary at the same output to compensate for the diode dead-space characteristic. However, a similar diode across the feedback path of the amplifier causes its output to assume either a +0.2-v or -125-v value.

The same technique is employed (via amplifier 4a) in measuring s_{ti}, for which V_1 is squared in an electronic multiplier prior to being integrated in amplifier 2. At the same time, the output of integrator 9 is being squared and subtracted from that of integrator 2, thus yielding s_{ti} directly. The frequency and phase characteristics of the particular multiplier used as actually measured are shown in figure 27. The amplitude and phase response of the four-quadrant unit to the product of a 100-v d-c and a sinusoid voltage of 25 v peak-to-peak is given by the broken lines. The solid line shows the response of one quadrant to a half-wave rectified sinusoid of 50-v maximum amplitude. The latter arrangement is the manner in which squaring is obtained in the present setup. The d-c characteristic of a quadrant is

$$y = \frac{x^2}{100}$$

with a maximum error of 2 percent of the measured value, y.

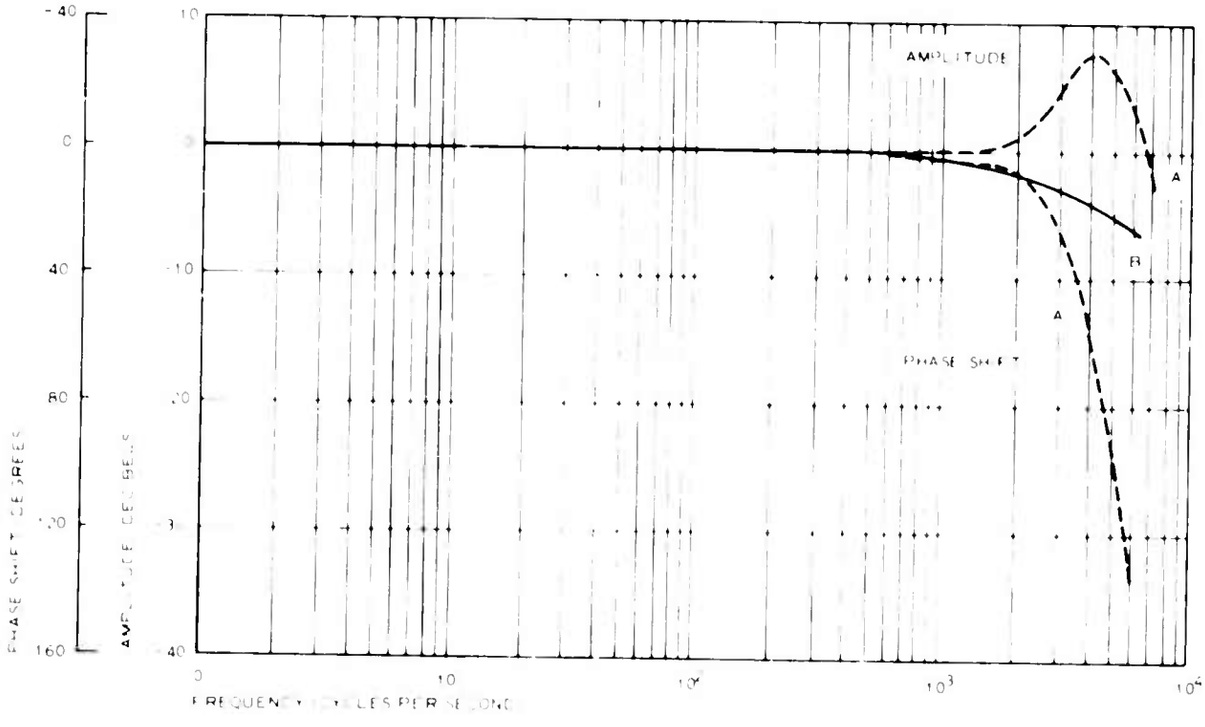

Figure 27 - Multiplier Frequency and Phase Characteristics

The third picture parameter μ_{di}, requires the differentiation of V_1 before averaging over each elemental square. This operation is performed in amplifier 20A which, besides the unavoidable input time delay needed in all electronic differentiators, was supplied with an additional delay term at its feedback to attenuate frequencies higher than 2400 cps. The resulting transfer function is

$$\frac{\dot{V}_1}{V_1} = \frac{-k_2 s}{(1 + \tau_4 s)(1 + \tau_5 s)} , \tag{94}$$

where

$$\begin{aligned} k_2 &= 0.0005 , \\ \tau_4 &= 0.00008 \text{ sec, and} \\ \tau_5 &= 0.000017 \text{ sec} . \end{aligned} \tag{95}$$

The measured gain and phase characteristics of amplifiers 17A and 20A combined are given in figure 28. On the other hand, as shown in figure 29, the 3-db cutoff point of amplifier 1b, which follows the photomultiplier in the scanner, occurs at a very high frequency for this amplifier to have any effect on the computations.

By contrast to μ_{ti} and s_{ti}, the derivatives $\partial V_1/\partial x$ and $\partial V_1/\partial y$ may be either positive or negative. Hence, after differentiation, the derivative is full-wave rectified in amplifiers 18A and 19A before being fed into integrator 1, where electric blanking is also applied.

The second moment s_{di} of detail is obtained in a manner similar to s_t. All four integrators, 9, 2, 1, and 13, are momentarily discharged to zero at the end of the complete scan of each elemental square. This is done by means of relays R6 and R7 actuated by the same pulse that steps up the vertical-step amplifier 7 through amplifier 2a. The insertion of relays R14 and R15 allows for some time delay, which is desirable. In addition, the same relays keep the integrator outputs to zero by means of an additional input to amplifier 2a, effected by the computer's utility switch when in "hold" position.

As shown in figure 25, signals A and B, which represent V_1^2 and V_1^2, are fed into amplifier 3 for subtraction. The output is

$$\left.\begin{aligned} e_1 &= \left[\frac{1}{100}\,\frac{1}{4.8}\int_o^T V_1 dt\right]^2 - \theta\left[\frac{1}{100}\,\frac{1}{1.2}\int_o^T V_1^2\, dt\right] \\ \text{or} \\ e_1 &= \frac{1}{100}\left[\frac{1}{23.04}\left(\int_o^T V_1 dt\right)^2 - \theta\,\frac{1}{1.2}\int_o^T V_1^2\, dt\right] , \end{aligned}\right\} \tag{96}$$

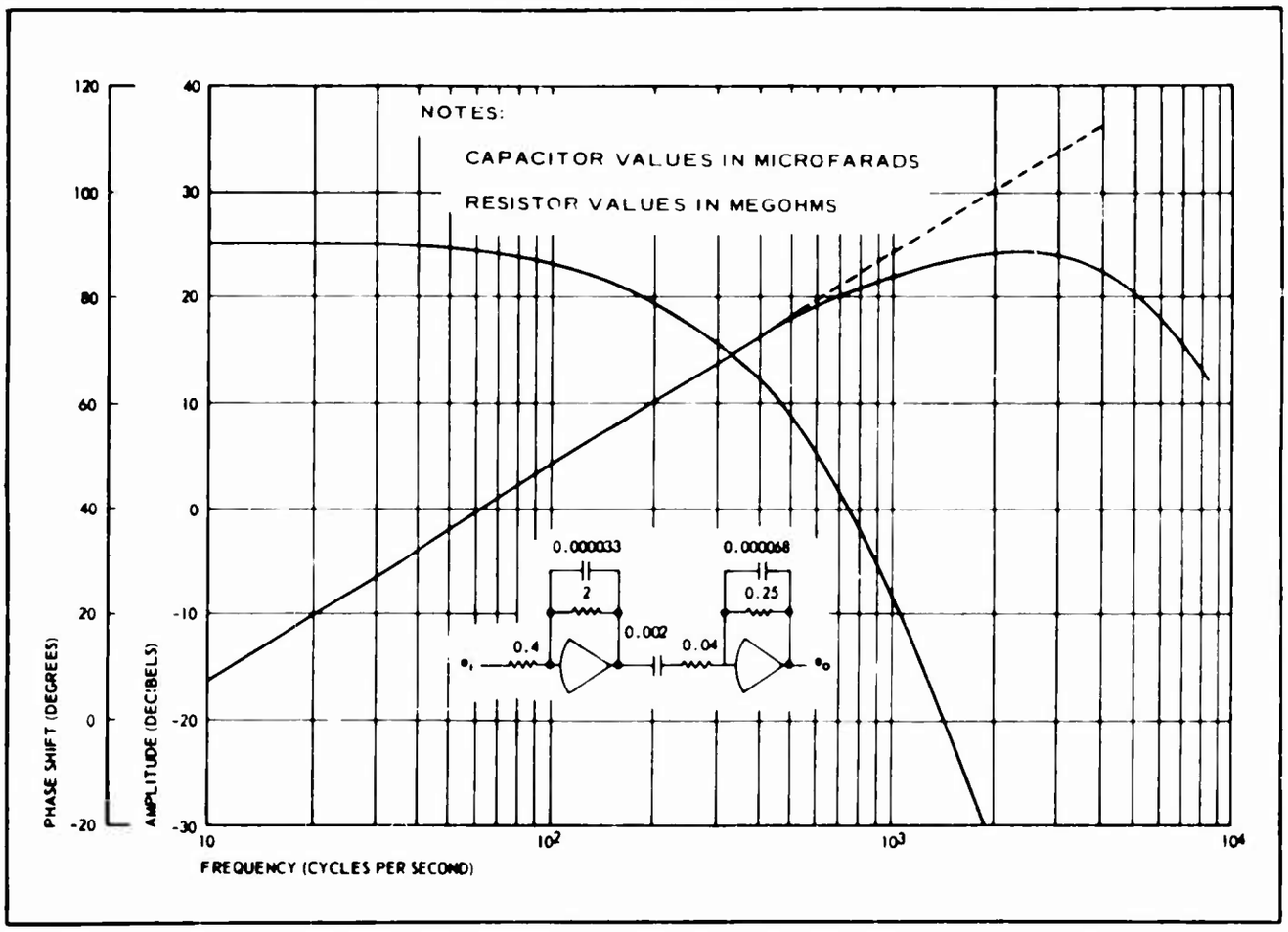

Figure 28 - Differentiator Characteristics

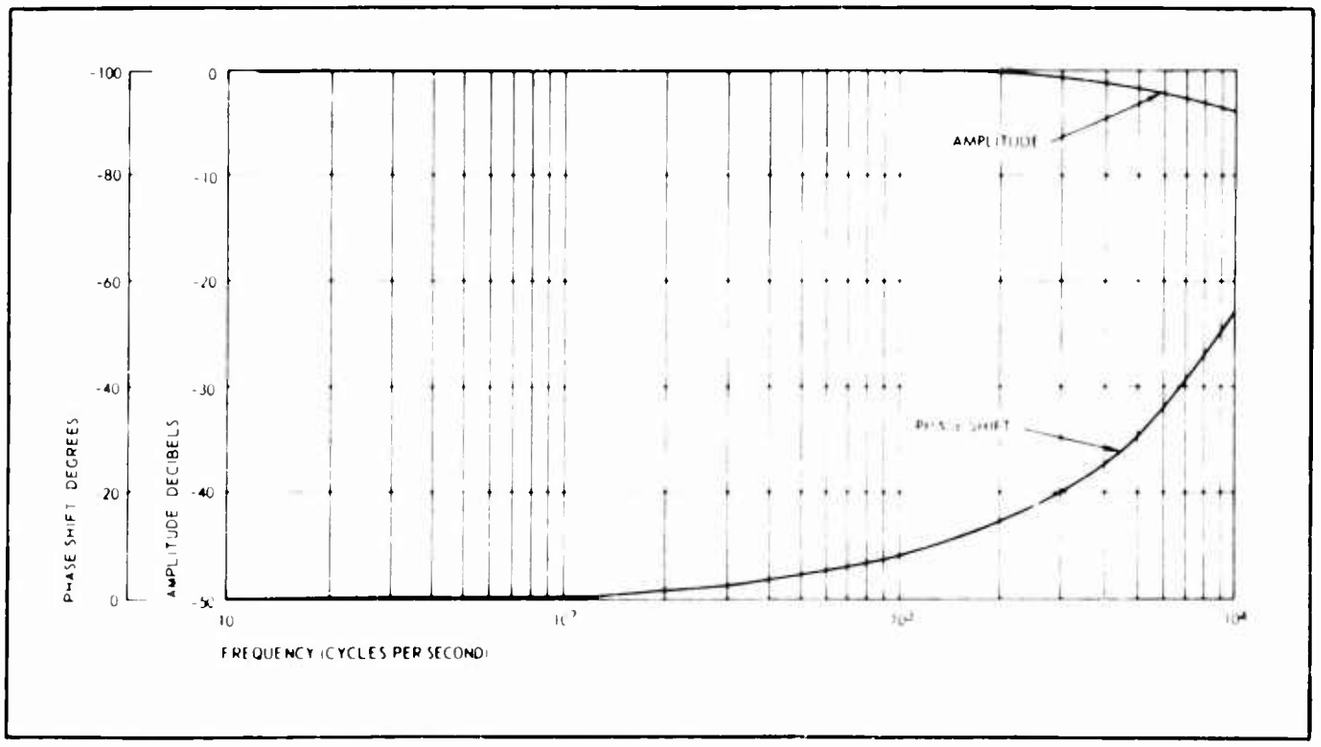

Figure 29 - Photomultiplier Amplifier Characteristics

where T is the effective integration time per elemental square when blanking is taken into account. The setting of the gain $\theta = 0.1/R$, where R is the input resistor associated with input B, is done on the basis of the condition

$$e_1 = 0 \text{ when } V_1 = K = \text{constant} . \tag{97}$$

Hence,

$$\frac{1}{23.04}\left(\int_o^T K dt\right)^2 = \frac{1}{12.0R}\int_o^T K^2 dt ,$$

from which

$$R = \frac{1.920}{T} . \tag{98}$$

Since from equations 74 and 84

$$T = 2mt_1 = 1.44 \text{ sec} , \tag{99}$$

it follows that R should have the value

$$R = 1.333 . \tag{100}$$

Of course, in view of the tolerances in all the condensers and resistors, the exact setting of R should be done experimentally on the basis of equation 97.

Similar reasoning is used in the case of amplifier 5a, where the subtraction of

$$\bar{V}_2^2 \text{ and } \overline{V_2^2}$$

is done. Figure 30 gives a sample of the recorded outputs of the four branches of the measuring circuit.

The computations shown below establish the values of the mean and variance of transmissivity and detail over a cell, and of the mean and second moment of transmissivity and detail over the whole picture. With reference to figure 25, it will be convenient to establish a factor that represents the input voltage level to the computing circuitry and that is carried through all computations. Thus the voltage E' out of the control potentiometer P is

$$E' = \frac{E}{\frac{1}{\beta} + 1.5(1 - \beta)} , \tag{101}$$

where E is the photomultiplier output and β the potentiometer setting. On the other hand, the output E is

$$E = \theta t , \tag{102}$$

where t is the transmissivity of the plate at the location of the flying spot and

$$\theta = \text{volts per 100 percent transmissivity} \tag{103}$$

is the photoelectric gain for a fixed setting of the crt brightness and of the brightness control feedback loop.

Hence,

$$E' = \frac{\theta}{\frac{1}{\beta} + 1.5(1 - \beta)}\, t \,. \tag{104}$$

Throughout the measurement period, frequent checks of θ were made by inserting a neutral density filter with a transmissivity of 39.81 percent at the face of the plate and measuring $E' = (E')_m$.

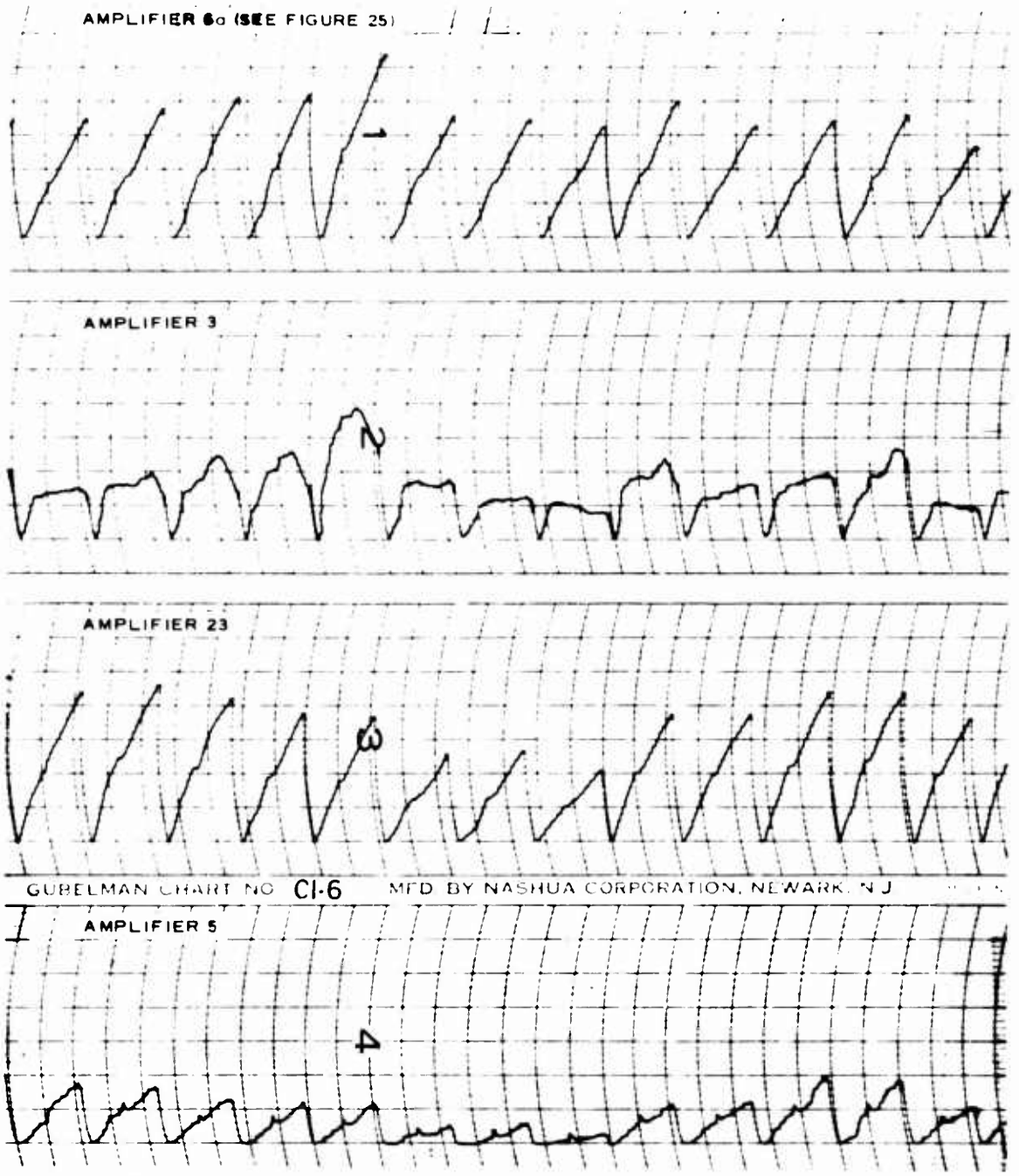

Figure 30 - Sample Recording of Picture Parameters

Therefore,

$$\frac{\frac{1}{\beta} + 1.5(1 - \beta)}{\theta} = \frac{1}{(E')_m} \frac{39.81}{100} . \tag{105}$$

This quantity is

$$K = \frac{\frac{1}{\beta} + 1.5(1 - \beta)}{\theta} , \tag{106}$$

and is measured in terms of E' as

$$K = \frac{0.398}{(E')_m} . \tag{107}$$

With this in mind, the following relationships are found (the amplifier numbers are used as subscripts to their output voltages).

1. Average Transmissivity over a Cell:

$$e_{6a} = \frac{10}{1.5} e_9 ,$$

$$= \frac{10}{1.5} \frac{1}{1.2} \frac{1}{4} \int_o^T V_1 dt ,$$

$$= \frac{10}{1.5} \frac{5}{4.8} \frac{1}{\frac{1}{\beta} + 1.5(1 - \beta)} T \left(T \int_o^T E \, dt \right) ,$$

$$= \frac{50 \times 1.44}{7.2} \frac{1}{\frac{1}{\beta} + 1.5(1 - \beta)} \mu_E .$$

Since $\mu_E = \theta \mu_t$,

$$e_{6a} = 10 \frac{\theta}{\frac{1}{\beta} + 1.5(1 - \beta)} \mu_{ti} = \frac{10}{K} \mu_{ti} = aw_1 ,$$

or

$$\mu_{ti} = 0.10 \, K(aw_1) \text{ transmissivity} . \tag{108}$$

2. Standard Deviation of Transmissivity over a Cell:

From equations 96 and 100,

$$e_{3a} = \frac{1}{(100)(11.111)}\left[\left(\frac{1}{T}\int_o^T V_1 dt\right)^2 - \frac{1}{T}\int_o^T V_1^2\, dt\right],$$

$$= \frac{1}{(100)(11.111)}\left[\left(\mu V_1\right)^2 - m_2 V_1\right],$$

$$= \frac{9}{10,000}\, s_{V_1};$$

$$e_3 = \frac{5}{0.405}\,\frac{9}{10,000}\, s_{V_1},$$

$$= \frac{1}{90}\, s_{V_1} = bw_2,$$

or

$$s_{V_1} = 90\ bw_2;$$

since

$$V_1 = 5E' = \frac{5}{\frac{1}{\beta} + 1.5(1-\beta)}\, E,$$

$$= \frac{5\theta}{\frac{1}{\beta} + 1.5(1-\beta)}\, t = \frac{5}{K}t,$$

$$s_{ti} = \left(\frac{K}{5}\right)^2 s_{V_1} = 3.6K^2(bw_2)\ \text{transmissivity}. \qquad (109)$$

3. Average Detail over a Cell:

$$e_{23} = \frac{10}{1.5}\, e_1$$

$$= \frac{10}{1.5}\,\frac{1}{1.2}\,\frac{1}{4}\int_o^T V_2\, dt$$

$$= \frac{10}{7.2}\,1.44\,\frac{1}{T}\int_o^T V_2\, dt,$$

$$e_{23} = 2\mu_{V_2};$$

$$V_2 = |e_{20A}| = 0.0005 \left|\frac{d}{dt} e_{17A}\right| = 0.0025 \left|\frac{d}{dt} E'\right| ,$$

$$= 0.0025 \frac{1}{\frac{1}{\beta} + 1.5(1 - \beta)} \left|\frac{d}{dt} E\right| ,$$

$$= 0.0025 \frac{\theta}{\frac{1}{\beta} + 1.5(1 - \beta)} \left|\frac{d}{dt} t\right| ,$$

$$= \frac{0.0025}{K} \left|\frac{d}{dt} t\right| .$$

But

$$\left|\frac{d}{dt} t\right| = \left|\frac{d}{dx} t \frac{dx}{dt}\right| = u \left|\frac{d}{dx} t\right| ,$$

where u is the speed of the flying spot, and by equation 76

$$\left|\frac{d}{dt} t\right| = 2 \left|\frac{d}{dx} t\right| = 2d .$$

$$V_2 = \frac{0.005}{K} d ,$$

$$\mu_{V_2} = \frac{0.005}{K} \mu_{di} ,$$

$$e_{23} = \frac{0.010}{K} \mu_{di} = cw_3 ,$$

$$\mu_{di} = 100\ K(cw_s)\ \text{transmissivity change per inch} . \qquad (110)$$

4. Standard Deviation of Detail over a Cell:

By analogy with e_{3a} in 2 above,

$$e_{5a} = \frac{9}{10,000} s_{V_2} .$$

Hence,

$$e_5 = \frac{5}{0.045} \frac{9}{10,000} s_{V_2} = \frac{1}{10} s_{V_2} = fw_4 ,$$

$$s_{V_2} = 10\ fw_4 ,$$

$$V_2 = \frac{0.005}{K} d ,$$

$$s_{V_2} = \frac{0.005^2}{K^2} s_{di} ,$$

$$= 4 \times 10^5 K^2 (fw) .$$

In the above expressions, a, b, c, and f are the settings of the recorder channels in volts per millimeter, and w_1, w_2, w_3, and w_4 are the corresponding readings in millimeters.

APPENDIX IV

INFORMATION CONTENT OF METRIC II TARGET-IDENTIFICATION PARAMETERS AND EVALUATION OF THEIR PROBABILITY DENSITY FUNCTION

INTRODUCTION

The development of Metric II (see appendix I) to obtain the probability of correct target-identification required quantative expressions of the information content and of the statistical distribution of the recognition parameters. These expressions were developed as explained below.

INFORMATION CONTENT OF SIGNATURE PARAMETERS IN RECOGNITION DECISION

Derivation of Information-Content Expression

A quantitative expression of the information contributed by a parameter to a recognition decision is obtained heuristically and corroborated experimentally in reference 16. The following analysis, based upon information theory, yields the same expression. However, the expression is modified to obtain a clearer insight into the role that a parameter plays in the making of a recognition decision. The amount of information, $I(U_{ik})$, delivered by a particular value, U_{ik}, of a signature parameter, U_i, to the recognition of a target class, A_j, is given by (reference 17, p 4)

$$I(U_{ik}) = \log \frac{P(A_j \; U_{ik})}{P(A_j)}, \tag{111}$$

or by an equivalent expression obtained from Bayes' Rule (reference 12, p 318),

$$I(U_{ik}) = \log \frac{P(U_{ik} \; A_j)}{P(U_{ik})}, \tag{112}$$

with

$P(A_j)$ = the a priori probability that a particular pattern is of class A_j,

$P(A_u \; U_{ik})$ = the conditional probability that the unknown pattern is of class A_j after a particular parameter measurement, U_{ik}, of the pattern has been made available,

$P(U_{ik})$ = the probability that the given parameter measurement is obtained, and

$P(U_{ik} \; A_j)$ = the probability that the given parameter measurement is obtained from a particular target, A_j.

If $P(A_j, U_{ik})$ represents the distribution of the target-associated parameter values over the entire sample of N_j target classes and N_k discrete parameter values, the average information, $I(U_i)$, delivered by all of these parameter values becomes, from equation 112,

$$I(U_i) = \sum_{k=1}^{k=N_k} \sum_{j=1}^{j=N_j} P(A_j, U_{ik}) \log \left[\frac{P(U_{ik}|A_j)}{P(U_{ik})} \right] . \qquad (113)$$

This expression, similar to that obtained in reference 16, is modified as follows. The log ratio is converted to a log difference and the following substitution is made,

$$P(A_j, U_{ik}) = P(A_j)P(U_{ik}|A_j) .$$

The information content of the parameter U_i then becomes

$$I(U_i) = \sum_{j=1}^{j=N_i} \sum_{k=1}^{N_k} P(A_j)P(U_{ik}|A_j) \log P(U_{ik}|A_j) -$$

$$\sum_{k=1}^{k=N_k} P(U_{ik}) \log P(U_{ik}) .$$

In terms of the familiar information theory entropy function,

$$H(x) = - \sum_x P(x) \log P(x) . \qquad (114)$$

The final expression for the information content of the parameter (U_i) is

$$I(U_i) = - \sum_{j=1}^{j=N} \left[P(A_j)H(U_i|A_j) \right] + H(U_i) . \qquad (115)$$

Thus, the average information-contributing capability of a parameter is expressed by the difference between the entropy or uncertainty of the complete across-target parameter distribution and the average entropy of the individual intratarget distributions of the parameter. Such a definition agrees with intuitive notions for desirable target recognition: that the individual intratarget distributions have as low an entropy as possible (zero-entropy, single-valued intratarget distribution functions are ideal) and that the over-all distribution functions of the parameter over all the intratarget functions be as broad as possible (have high entropy) to permit discrimination between targets.

Information Contribution of a Computed Parameter

In some cases two individual parameters may be combined to form a third

parameter. For example, the average power (Q) of a sampled signal is the quotient of the energy (E) and the number (S) of sampled points. If the parameters E and S are used, what additional information is available from the third computer parameter, Q? In a given pattern, the two measured parameter values (E_i and S_j) determine the value for a third parameter (Q_k). The resulting distribution function expressing this dependency becomes a delta function:

$$\left.\begin{aligned} P(Q_k|E_iS_j) &= 1, \text{ when } \frac{E_i}{S_j} = Q_k \\ &= 0, \text{ when } \frac{E_i}{S_j} \neq Q_k . \end{aligned}\right\} \tag{116}$$

The resulting entropy therefore is

$$H(Q|E_iS_j) = -\sum_k P(Q_k|E_iS_j) \log P(Q_k|E_iS_j) = 0 . \tag{117}$$

The joint entropy of all three parameters (from reference 18, p 5) is

$$H(QES) = H(ES) + \sum_i \sum_j P(E_iS_j)H(Q|E_iS_j) , \tag{118}$$

which, from equation 117, permits

$$H(QES) = H(ES) . \tag{119}$$

In a similar manner for every A_j target class,

$$H(QES|A_j) = H(ES|A_j) . \tag{120}$$

Therefore, from equation 115, the information content of all three parameters is equal to that of two alone, or

$$I(QES) = I(ES) , \tag{121}$$

and the third formed parameter, Q, provides no additional information.

EVALUATION OF PARAMETER PROBABILITY-DENSITY FUNCTION

Consideration of Single-Cluster Data

Experimental values of the probability density distribution, f(u), of a given parameter, u, for $u_{min} < u < u_{max}$ are available for a given target class. The distribution of these values is normalized as shown in equation 122. It is required that this data distribution, f(u), be represented by a probability density function as shown in equation 123.

$$\sum_{u = u_{min}}^{u = u_{max}} f(u) = 1 . \tag{122}$$

$$P(u) = e^{-(a + bu + cu^2)} , \tag{123}$$

with

$$\sum_{u = u_{min}}^{u = u_{max}} P(u) = 1 . \tag{124}$$

In addition, the interval between the various sampled values of u must be constant not only within a given target class function but also among all the target class functions, so that the various values of P(u) for the different values of u and for the different target classes are compatible with one another.

Consider the following relationship, D(u), between the experimental set of data, f(u), and its analytical representation:

$$D(u) = \sum_{u = u_{min}}^{u = u_{max}} f(u) \log_e \frac{f(u)}{P(u)} . \tag{125}$$

It can be shown that for $x > 0$ (this result may be obtained from formulas 601.5 and 601.6, reference 19),

$$\log_e (x) \geqq 1 - \frac{1}{x} . \tag{126}$$

Combining of equations 125 and 126 gives

$$D(u) = \sum_{u = u_{min}}^{u = u_{max}} \left[f(u)\right] \left[1 - \frac{P(u)}{f(u)}\right] \geqq \sum_{u = u_{min}}^{u = u_{max}} f(u) - \sum_{u = u_{min}}^{u = u_{max}} P(u) .$$

Because of equations 122 and 124, the above inequality becomes $D(u) \geqq 0$. The quantity D(u) is equal to zero only when for every value of u, the experimental data, f(u), and the analytical representation, P(u), are equal. Thus, the best representation, P(u), of f(u) minimizes D(u):

$$D(u) = \sum_{u = u_{min}}^{u = u_{max}} \left[f(u)\right] \left[\log_e f(u) - \log_e P(u)\right] .$$

An even more accurate representation of f(u) is obtained by minimizing the quantity S(u), which is a function of the squares of the log differences:

$$S(u) = \sum_{u = u_{min}}^{u = u_{max}} \left[f(u)\right] \left[\log_e f(u) - \log_e P(u)\right]^2 . \qquad (127)$$

Substitution of equation 123 into equation 127 gives

$$S(u) = \sum_{u = u_{min}}^{u = u_{max}} \left[f(u)\right] \left[\log_e f(u)\right]^2 + \left[f(u)\right] (a + bu + cu^2)^2 +$$

$$\left[2f(u) \log_e f(u)\right] (a + bu + cu^2) .$$

Minimization of S(u) with respect to a, b, and c provides a system of three equations:

$$\frac{\partial S}{\partial a} = 0, \frac{\partial S}{\partial b} = 0, \frac{\partial S}{\partial c} = 0 .$$

When evaluated, the system becomes

$$a \sum_{u = u_{min}}^{u = u_{max}} f(u) + b \sum_{u = u_{min}}^{u = u_{max}} uf(u) + c \sum_{u = u_{min}}^{u = u_{max}} u^2 f(u) =$$

$$- \sum_{u = u_{min}}^{u = u_{max}} f(u) \log_e f(u) , \qquad (128)$$

$$a \sum_{u = u_{min}}^{u = u_{max}} uf(u) + b \sum_{u = u_{min}}^{u = u_{max}} u^2 f(u) + c \sum_{u = u_{min}}^{u = u_{max}} u^3 f(u) =$$

$$- \sum_{u = u_{min}}^{u = u_{max}} uf(u) \log_e f(u) , \qquad (129)$$

and

$$a \sum_{u=u_{min}}^{u=u_{max}} u^2 f(u) + b \sum_{u=u_{min}}^{u=u_{max}} u^3 f(u) + c \sum_{u=u_{min}}^{u=u_{max}} u^4 f(u) =$$

$$- \sum_{u=u_{min}}^{u=u_{max}} u^2 f(u) \log_e f(u) \, . \qquad (130)$$

The solution of equations 128 through 130 provides values for a, b, and c. However, the solution is not normalized since the restraint,

$$\sum_{u=u_{min}}^{u=u_{max}} e^{-(a + bu + cu^2)} = 1 \, , \qquad (131)$$

has not been inserted into the equation system. If this were done, the resulting complexity of the equation system and its solution would be excessive. Nevertheless, since the solution is an approximation of f(u), which has been normalized, it can be assumed that the small perturbation in the value of a, necessary to achieve normalization of P(u), will not appreciably affect the values of b and c. Therefore, the values of b and c can be obtained from the equation system (equations 128 through 130) and the proper value of a for normalizing $P(u_i)$ becomes

$$a = \log_e \left[\sum_{u=u_{min}}^{u=u_{max}} e^{-(bu + cu^2)} \right] . \qquad (132)$$

Consideration of Multicluster Data

In some cases, the set of experimental data, f(u), will exhibit two or more distinct regions in which the data are clustered. Under these conditions, the form of the representation, P(u), in equation 123 is not adequate. However, if the data set is divided into two or more data subsets so that each subset will contain only one cluster of data, the representation, P(u), in equation 123 is valid. For example, a two-cluster data set with its subsets separated by boundary value u_a is represented by

$$P(u) = P_1(u_1) + P_2(u_2) \, , \qquad (133)$$

with

$$P_1(u_1) = e^{-\left(a_1 + b_1 u_1 + c_1 u_1^2\right)} \, , \text{ when } u_{min} < u_1 \leq u_a \, ,$$

$$P_1(u_1) = 0, \text{ when } u_1 > u_a ,$$

$$P_2(u_2) = e^{-\left(a_2 + b_2 u_2 + c_2 u_2^2\right)}, \text{ when } u_a < u_2 \leqq u_{max} ,$$

$$P_2(u_2) = 0, \text{ when } u_2 \leqq u_a \text{ and } u_2 > u_{max} .$$

If N_1 and N_2 represent respectively the relative portion of parameter data points that lie within regions u_1 and u_2 as defined above, the proper values of a_1 and a_2 to achieve normalization are

$$a_1 = \log_e \frac{1}{N_1} + \log_e \sum_{u = u_{min}}^{u_a} e^{-\left(b_1 u_1 + c_1 u_1^2\right)} \tag{134}$$

and

$$a_2 = \log_e \frac{1}{N_2} + \log_e \sum_{u_a}^{u = u_{max}} e^{-\left(b_2 u_2 + c_2 u_2^2\right)} . \tag{135}$$

APPENDIX V

INSTRUCTIONS TO SUBJECTS FOR TARGET-RECOGNITION EXPERIMENTS

HIGH-RESOLUTION RADAR

The purpose of this investigation is to determine whether a definable relationship exists between physical measures of imagery, such as brightness, and human target-recognition performance. The nature of this investigation requires that many interesting variables, which may affect performance but which are not specifically related to this problem, must be controlled or eliminated Hence, the task that you will be asked to perform will bear little, if any, resemblance to an operational situation. The results of this scientific study are necessary to determine perceptual requirements for target recognition. Since the task in this investigation is not similar to the operational situation, the results will not be used to rate you in any way at your job, nor will they be used to alter operational procedure.

To demonstrate the procedure we will use, I will initiate the sequence of operations by presenting on your left-hand display screen a picture of the target you will be asked to find. This picture will be the same size and in the same orientation as the target in the radar imagery. You will study this cue as long as you feel necessary and inform me when you are ready. I will then present the high-resolution radar imagery on the center screen. Some targets will be very easy to find, others will be extremely difficult. Find the target that you have studied as soon as you can. We are interested in both the speed and accuracy with which you can locate these targets. When you locate the target, press the top switch on your left. This action will cause a magnified version of the imagery right around the cross hairs to appear on the right-hand screen. Then move the cross hairs over the target. When you have laid the cross hairs, press the second switch on your left. If at some point you realize that you have erred in your identification, inform me, search again for the target, and lay the cross hairs over it. We will now have several practice trials to familiarize you with the equipment and procedure.

INFRARED AND OPTICAL IMAGERY

The purpose of our investigation is to determine if some relationship can be found between physical measures of imagery, such as brightness or variations in brightness between a target and its surrounding area, and human performance in a target recognition task. That is, is a target that is very bright in a background of moderate brightness easier or more difficult to locate than a similar target that is very dark? Does the difference between a target and its background necessary for the former to be discernible vary with the size of the target? We are trying to determine relationships of this nature using various types of imagery. In this particular phase of the investigation, we are using optical and infrared imagery.

To demonstrate the procedure, I will first show you a picture of the target you are to find. This is an exact copy of the target, with one exception. The transparent tape over the target makes the target key appear slightly darker than it will appear on the imagery. The target key will also be in the same orientation as the target in the imagery. I will tell you whether you will be

looking at infrared or optical photography and what category the target is in; that is, whether you will be looking for a shopping center, industrial complex, etc. Study the target key as long as you wish. When you are ready, I will turn over the photograph in which you are to locate the target. Find the target as quickly as you can, but be sure to be accurate. I will measure the time you take to locate the target.

I have six demonstration photographs to better acquaint you with the procedure and task. Ask any questions you like before we go on with the test photographs.

LIST OF REFERENCES

1. Birmingham, H. P., and Taylor, F. V.: "A Design Philosophy for Man-Machine Control Systems." IRE Proceedings, Vol 42, 1954.

2. Baker, C. A., Morris, D. F., and Steedman, W. C.: "Target Recognition of Complex Displays." Human Factors, Vol 2, No. 2, May 1960, p 51.

3. Steedman, W. C., and Baker, C. A.: "Target Size and Visual Recognition," Human Factors, Vol 2, No. 3, August 1960, p 120.

4. Boynton, R. M., and Bush, W. R.: "Recognition of Forms against a Complex Background." J. Opt. Soc. Amer, Vol 46, No. 9, September 1956, pp 758-764.

5. Krendel, E. S., and Wodinsky, J.: Visual Search in an Unstructured Visual Field. AFCRC-TR-59-51, Franklin Institute Report No. F-A1851, ASTIA AD-211156, 1958.

6. Miller, J. W., and Ludvigh, E.: "Time Required for Detection of Stationary and Moving Objects as a Function of Size in Homogeneous and Partially Structured Visual Fields." Visual Search Techniques, Publication No. 712, National Academy of Sciences, National Research Council, 1960.

7. Jaynes, E. T. "Information Theory and Statistical Mechanics." Phys. Review, Vol 106, No. 4, May 1957, pp 626-630; Vol 108, No. 2, October 1957, pp 171-190.

8. Tribus, M.: Maximum Entropy Estimate in Reliability. Lafayette, Ind., Purdue University, Third Conference on Decision and Information Processes, April 1961.

9. Goldman, S.: Information Theory. New York, N. Y., Prentice-Hall, Inc., 1953, pp 4-5.

10. Miller, G. A.: "Human Memory and Storage of Information." IRE Transactions on Information Theory, Vol IT-2, No. 3, September 1956.

11. Sziklai, G. C.: "Some Studies in the Speed of Visual Perception." IRE Transactions on Information Theory, Vol IT-2, No. 3, September 1956.

12. Stevens, S. S.. "Psychophysics of Sensory Functions." Symposium on Sensory Communications (W. Rosenblith, editor), Cambridge, Mass., MIT Press; New York, N. Y., John Wiley and Sons, Inc., 1961.

13. Davenport and Root: Random Signals and Noise. New York, N. Y., McGraw-Hill Book Co., 1958.

14. Pierce, B. O.: Short Table of Integrals. Boston, Mass., Ginn and Co.

15. GER-10831: First Quarterly Report for Image Quantification Program Model Department. Akron, Ohio, Goodyear Aircraft Corporation, 8 October 1962.

16. Lewis, P. M., II: "Characteristic Selection Problem in Recognition Systems." IRE Transactions on Information Theory, February 1962.

17. Goldman, S.: Information Theory. New York, N. Y., Prentice-Hall, Inc., 1953.

18. Khinchin, A. I.: Information Theory. Dover Publications, New York, N. Y., 1957.

19. Dwight, H. B.: Table of Integrals. MacMillan Co., New York, N. Y., 1961.

DOCUMENT CONTROL DATA - R&D

(Security classification of title, body of abstract and indexing annotation must be entered when the overall report is classified)

ORIGINATING ACTIVITY (Corporate author) Goodyear Aerospace Corporation Akron 15, Ohio	2a. REPORT SECURITY CLASSIFICATION UNCLASSIFIED 2b GROUP N/A

3. REPORT TITLE

MEASUREMENTS AND MODELS FOR RELATING THE PHYSICAL CHARACTERISTICS OF IMAGES TO TARGET DETECTION

4. DESCRIPTIVE NOTES (Type of report and inclusive dates)

Final report, July 1962 - September 1963

5. AUTHOR(S) (Last name, first name, initial)

Corbett, Donald G.
Diamantides, N. D.
Kause, R. H.

6. REPORT DATE	7a. TOTAL NO OF PAGES	7b. NO. OF REFS
December 1964	107	19

8a. CONTRACT OR GRANT NO. AF 33(657)-9476 b. PROJECT NO c. Program 665A Reconnaissance/Strike d.	9a. ORIGINATOR'S REPORT NUMBER(S) 9b. OTHER REPORT NO(S) (Any other numbers that may be assigned this report) AMRL-TR-64-117

10. AVAILABILITY/LIMITATION NOTICES

Qualified requesters may obtain copies of this report from DDC.
Available, for sale to the public, from the Clearinghouse for Federal Scientific and Technical Information, CFSTI (formerly OTS), Sills Bldg, Springfield, Virginia 22151

11. SUPPLEMENTARY NOTES	12. SPONSORING MILITARY ACTIVITY
	Aerospace Medical Research Laboratories, Aerospace Medical Division, Air Force Systems Command, Wright-Patterson AFB, Ohio

13. ABSTRACT

Three metrics for predicting the time required to identify targets in high-resolution radar pictures were developed. One metric, based on four automatically measured variables related to transmissivity of positive transparencies, was tested. Through multiple-regression analysis, a correlation of 0.69 between observed and predicted identification times was obtained. When these relationships were applied to a new set of radar pictures and new test subjects, the correlation coefficient was too low to be significantly different from zero with the number of pictures used. A principal reason for the low correlation was the unexpected correlation between the four transmissivity variables. The metric also had an insignificant correlation coefficient when applied to optical and infrared photographs (0.07 and 0.04, respectively). It is hypothesized that, if additional variables are utilized, the metric examined in this study may be useful as a base to develop a more effective prediction equation.

DD FORM 1 JAN 64 1473

AF-WP-8-AUG 64 480

14. KEY WORDS	LINK A		LINK B		LINK C	
	ROLE	WT	ROLE	WT	ROLE	WT
Side-looking radar						
Target recognition						
Image interpretation						
Aerial reconnaissance						
Detection						
Tracking						
Human engineering						

INSTRUCTIONS

1. ORIGINATING ACTIVITY: Enter the name and address of the contractor, subcontractor, grantee, Department of Defense activity or other organization *(corporate author)* issuing the report.

2a. REPORT SECURITY CLASSIFICATION: Enter the overall security classification of the report. Indicate whether "Restricted Data" is included. Marking is to be in accordance with appropriate security regulations.

2b. GROUP: Automatic downgrading is specified in DoD Directive 5200.10 and Armed Forces Industrial Manual. Enter the group number. Also, when applicable, show that optional markings have been used for Group 3 and Group 4 as authorized.

3. REPORT TITLE: Enter the complete report title in all capital letters. Titles in all cases should be unclassified. If a meaningful title cannot be selected without classification, show title classification in all capitals in parenthesis immediately following the title.

4. DESCRIPTIVE NOTES: If appropriate, enter the type of report, e.g., interim, progress, summary, annual, or final. Give the inclusive dates when a specific reporting period is covered.

5. AUTHOR(S): Enter the name(s) of author(s) as shown on or in the report. Enter last name, first name, middle initial. If military, show rank and branch of service. The name of the principal author is an absolute minimum requirement.

6. REPORT DATE: Enter the date of the report as day, month, year, or month, year. If more than one date appears on the report, use date of publication.

7a. TOTAL NUMBER OF PAGES: The total page count should follow normal pagination procedures, i.e., enter the number of pages containing information.

7b. NUMBER OF REFERENCES: Enter the total number of references cited in the report.

8a. CONTRACT OR GRANT NUMBER: If appropriate, enter the applicable number of the contract or grant under which the report was written.

8b, 8c, & 8d. PROJECT NUMBER: Enter the appropriate military department identification, such as project number, subproject number, system numbers, task number, etc.

9a. ORIGINATOR'S REPORT NUMBER(S): Enter the official report number by which the document will be identified and controlled by the originating activity. This number must be unique to this report.

9b. OTHER REPORT NUMBER(S): If the report has been assigned any other report numbers *(either by the originator or by the sponsor)*, also enter this number(s).

10. AVAILABILITY/LIMITATION NOTICES: Enter any limitations on further dissemination of the report, other than those imposed by security classification, using standard statements such as:

(1) "Qualified requesters may obtain copies of this report from DDC."

(2) "Foreign announcement and dissemination of this report by DDC is not authorized."

(3) "U. S. Government agencies may obtain copies of this report directly from DDC. Other qualified DDC users shall request through

_____."

(4) "U. S. military agencies may obtain copies of this report directly from DDC. Other qualified users shall request through

_____."

(5) "All distribution of this report is controlled. Qualified DDC users shall request through

_____."

If the report has been furnished to the Office of Technical Services, Department of Commerce, for sale to the public, indicate this fact and enter the price, if known.

11. SUPPLEMENTARY NOTES: Use for additional explanatory notes.

12. SPONSORING MILITARY ACTIVITY: Enter the name of the departmental project office or laboratory sponsoring *(paying for)* the research and development. Include address.

13. ABSTRACT: Enter an abstract giving a brief and factual summary of the document indicative of the report, even though it may also appear elsewhere in the body of the technical report. If additional space is required, a continuation sheet shall be attached.

It is highly desirable that the abstract of classified reports be unclassified. Each paragraph of the abstract shall end with an indication of the military security classification of the information in the paragraph, represented as *(TS), (S), (C), or (U)*

There is no limitation on the length of the abstract. However, the suggested length is from 150 to 225 words.

14. KEY WORDS: Key words are technically meaningful terms or short phrases that characterize a report and may be used as index entries for cataloging the report. Key words must be selected so that no security classification is required. Identifiers, such as equipment model designation, trade name, military project code name, geographic location, may be used as key words but will be followed by an indication of technical context. The assignment of links, rules, and weights is optional.